# ANALYSIS OF FORMATION PRESSURES ON TUNNEL AND SHAFT LININGS

Submitted in partial fulfillment of the requirements
for the degree of Master of Engineering in
Geotechnical Engineering

UNIVERSITY OF ALBERTA

December 1980

D.R. McCreath

## TABLE OF CONTENTS

## TABLE OF CONTENTS (Cont'd)

## LIST OF FIGURES

## 1.0 SUMMARY

Initially, this report was intended primarily to review currently available analytical techniques for the determination or prediction of formation pressures on shaft linings. To address this question, it has been necessary for the author to progress through a detailed mechanistic understanding of the analyses which have been developed for the prediction of formation pressures on tunnel linings. This material, presented in Section 3 of the report, provides a necessary basis and framework from which to proceed into the question of shaft analysis, presented in Section 4. A comprehensive summary of two-dimensional analyses of stresses and deformations around tunnels in a wide variety of materials has been attempted in Section 3, and is shown in two key figures (2 and 3) to which frequent reference is thereafter made. The role of gravity in the question of determining minimum required support pressures (synonymous with minimum predicted formation pressures) is addressed, as this factor is later seen to be of importance to the analysis of shafts under certain conditions. For shafts, it is shown in Section 4 that either two-dimensional or three dimensional analyses may be appropriate depending upon the conditions of the problem, notably the relationship between the horizontal to vertical field stress ratio and the formation material properties. Both types of analysis are presented, with some brief comment on the shortcomings and possible extensions to the analyses. The analytical approaches presented are used with case history data in Section 4.6 to show that reasonable predictions of formation pressure may be obtained, although the lack of available case history data for validation under a wide range of conditions is an unfortunate drawback.

Finally, some brief comments concerning additional research work which could usefully be undertaken are included in Section 5.

## 2.0 INTRODUCTION

This project was instigated to look into the problem of shaft lining design or, more precisely, the problem of adequately estimating the formation pressures for which a shaft lining must be designed. It became quickly apparent that the heart of the problem could be found in the deceptively simple question of what is the difference between a shaft and a tunnel? While the answer is obvious in the physical sense of a shaft being vertical and a tunnel being horizontal, the means by which this difference was, or could be, accounted for analytically - and indeed the need for such an accounting - were a great deal less clear. Analyses of both problems have a common root in the well known hole-in-plate analogy, and this tends to lead to a homogeneous view of the two problems as one being simply a rotation in space of the other. The question of whether or not such a view is an adequate reflection of reality might be considered as the basic theme of this report.

# 3.0 TUNNEL ANALYSIS

## 3.1 Introduction

Analytical solutions for the determination of stresses and deformations around cylindrical openings have been developed primarily for the two-dimensional plane-strain case of a tunnel cross section. These solutions provide the essential bases for all of the analyses reviewed in this report for both tunnels and shafts, and it is therefore important to derive a clear understanding of the basic model utilized, the assumptions involved, and limitations to the applicability of the results.

This section will look firstly at the model to be utilized, and the assumptions which are inherent to the model. Development of the analytical solutions for the determination of stresses and deformations will then be presented for a variety of different material characterizations, encompassing a broad range of actual materials. The physical or mechanistic meaning of the analytical results is assessed, and a brief review of areas of extension to the analyses for various phenomena not accounted for in the basic model is included.

The development given in this section draws heavily upon work by Ladanyi, 1974, Coates, 1970 and Hoek and Brown, 1980. Existing work has been extended to include the case of a purely cohesive (frictionless) material, such as the short-term response of a saturated clay. As the literature includes a wide variance in notation and in format of equations, all of the analyses have been cast in a framework which provides consistent form to the equations and parameters used, enabling ready comparison of the formulations appropriate to different cases.

## 3.2 Basic Model and Assumptions

Consider the case of a circular tunnel, to be excavated to initial radius $r_i$. The length of the tunnel is very much greater than its

diameter, with the longitudinal axis lying parallel to one principal field stress. Thus, a cross-section can be analyzed under conditions of plane-strain provided that such section is remote from the excavation face.

To analyze stress re-distribution and deformations around the tunnel as it is excavated a model as shown on Figure 1 has been selected, the essential properties of which are given below.

(1) The cross-section encompasses a region of the ground which incorporates the tunnel location and which is composed of material which is weightless.

(2) The external boundaries of the region are remote from the tunnel (i.e. $r \to \infty$) and are loaded by an in situ stress field having equal vertical and horizontal principal stresses of magnitude $p_o$, these stresses being equivalent to the in-situ stress field existing at the tunnel elevation prior to tunnel excavation. Note that this is only valid for Ko = $\sigma_H / \sigma_v = 1.0$.

(3) The tunnel boundary is defined by a cirular hole of initial radius $r_i$, initially loaded internally by a radial pressure equal to the remotely applied field stresses, $p_o$. Thus, this situation represents the virgin condition in the region, prior to any disturbance due to tunnel excavation. Stresses in the field are everywhere hydrostatic and equal to $p_o$.

(4) The effect of tunnel excavation is modelled by progressively reducing the internal pressure from $p_o$ to a lower value $p_i$, termed the support pressure, and lying in the range $p_o > p_i > o$. Thus, this model of weightless material remains radially symmetric throughout the process of tunnel excavation.

(5) No strains perpendicular to the plane of the section are generated during the process of stress redistribution resulting from the progressive reduction in internal (support) pressure, i.e. conditions of plane-strain apply.

(6) The material within the model region is assumed to behave in a linearly elastic manner until the peak strength of the material is reached. Thereafter, the post-peak or post-failure behaviour of the material is assumed to be perfectly plastic, with the transition from elastic to plastic behaviour occurring instantaneously. Any reasonable envelopes of peak and post-peak strengths may be utilized to characterize the material, and a variety of such envelopes are included in the analyses which follow.

(7) For material in the elastic range, the volumetric strains are determined by the elastic constants E and $\nu$. In the plastic range it is assumed that the plastic strain increments lie normal to the selected yield surface in principal stress space. That is, the associated flow rule of the theory of plasticity (Drucker-Prager postulate) is assumed to be valid.

(8) It is assumed, for the basic analysis, that the material does not exhibit time-dependent behaviour in either the elastic or the plastic state.

(9) Ground water pressures are neglected, i.e. all stresses are effective stresses.

## 3.3 Mechanistic Development

Mechanistically, the model selected behaves as follows:

- Initially, stresses everywhere in the region are hydrostatic and equal to $p_o$.
- As the internal (support) pressure is reduced from $p_o$ to $p_i$, simulating excavation of the tunnel, the stresses redistribute around the tunnel. Note that, from symmetry and the plane-strain condition, the principal stresses remain radial, tangential and parallel to the longitudinal axis of the tunnel respectively.
- At first, as the support pressure is reduced, the stress differences created are insufficient to cause failure and the region remains elastic. As a consequence of the stress redistribution elastic strains and deformations occur. As indicated by later analysis, the stresses within this completely elastic region are independent of the material properties, being solely a function of the geometry and the imposed boundary stresses.
- As the support pressure is further reduced, stress differences sufficient to cause failure may occur - initially at the boundary of the tunnel. Hence, a plastic zone is formed. It is important to note that in this model the onset of plasticity is governed by the radial and tangential (principal) stresses, i.e. by the principal stresses lying in the plane of the cross-section.
- The level of principal stress difference at which the onset of plasticity occurs is solely a function of the material

strength properties under consideration, and the stresses within the plastic zone are solely a function of the support pressure and the material properties.

- Upon further reduction of the support pressure, $p_i$, the plastic zone will extend outwards to a radius which is a function of the above parameters and of the level of the remotely applied stress, $p_o$.
- Once a plastic zone has formed, the stresses within the surrounding elastic zone are modified, reflecting the fact that the plastic zone has limited load carrying ability, which results in shedding of excess stresses to the elastic zone. This phenomenon has been termed "ring action".
- Deformations of the tunnel periphery now reflect both the strains within the outer elastic region, and the strains within the inner plastic region. The mode of closure deformation in the plastic zone is analogous to that of a camera shutter, and later analysis will show that movements occur along spiral slip lines in the plane of the section.

### 3.3.1 Minimum Support Pressure

The primary question which we seek to answer through analysis of this model, is the level to which the support pressure $p_i$ may be reduced while maintaining a stable and functional opening; that is, what is the minimum ground pressure for which the tunnel support system must be designed? While this question will be addressed in more detail following development of an analytical approach, the problem may be outlined mechanistically as follows:

3.3.1.1 Neglecting Gravity

As previously noted, the model selected comprises a weightless material. For this case two bounding conditions for the minimum support pressure may be postulated.

i) No Plastic Zone Formation

Clearly, the tunnel will remain stable if the peak strength of the material is not exceeded at any point in the region. Thus, if the support pressure $p_i$ is maintained at a high enough level such that the stress differences created around the tunnel are insufficient to cause the onset of plasticity, then the region will remain everywhere elastic with the stresses at every point being less than the peak strength of the material. The criterion of providing sufficient internal support pressure to avoid any onset of plasticity ("failure") has commonly been invoked in tunnel and shaft lining design. However, while this criterion is certainly sufficient to maintain stability, it may not be - and in general is not - a necessary condition.

ii) Stable Plastic Zone Formation

If the support pressure is reduced below that value indicated by (i) above, the strength of the material will be exceeded by the imposed stress difference, initially at the boundary of the tunnel, and a plastic zone will start to form, growing outwards from the tunnel wall. However, provided that the extent of the plastic zone which forms remains finite i.e. $r_e$ does not go to infinity, a zone of plastic equilibrium will form. This zone will in turn be surrounded by an outer zone which remains in elastic equilibrium, and no further stress redistribution, strain, or

deformation, will occur. Hence the tunnel may be considered stable. The minimum support pressure for which the condition of the formation of a finite plastic zone is fulfilled provides a lower bound solution to the minimum design pressure question. In this case, it is clearly necessary to maintain the support pressure at or above this level to maintain stability. However, as discussed under item 3.3.1.2, fulfillment of this condition may not be sufficient to ensure stability due to the effects of gravity.

The above two minimum support pressure conditions represent, respectively, an upper bound which is sufficient but may not be necessary to maintain stability, and a lower bound which is necessary but may not be sufficient. Note that the lower bound condition requires only that the plastic zone remain finite. In fact, if the plastic zone becomes very large in extent - even though remaining stable - the deformations of the tunnel wall may become excessive, causing a functional failure of the tunnel. Thus, between these two bounds lies a spectrum of support pressure values identified with different degrees of extension of the plastic zone and hence with different tunnel wall displacements. The relationships between support pressure and tunnel closure will be quantified analytically in Section 4.

### 3.3.1.2 Including Gravity

The model proposed above comprises weightless material acted upon by an external stress system. In reality, the self weight of the material leads to differing stability conditions between the crown and the floor of the tunnel. Given that a plastic ("failed") zone forms as the support pressure is reduced, it is necessary to assess the limit equilibrium of kinematically possible failure wedges acted upon by gravity, in order to

realistically match the stabiltity of the weightless model to the stability of a real material. The lower bound minimum support pressure necessary will then be that which is necessary to both maintain a stable zone of plastic equilibrium ($r_e < \infty$ ) and to maintain the limit equilibrium of postulated gravity block failures. While the specific manner in which this may be accounted for is explored in the next section, it is important to emphasize the need for this limit equilibrium check, as it is primarily in this factor that the difference between a shaft and a tunnel lies. In the case of a tunnel, gravity forces act within the plane of the cross-section considered in the model, and the limit equilibrium check may, therefore, be included in a two-dimensional analysis. In the case of a shaft, however, gravity forces act in a direction perpendicular to the plane of the cross-section, and a limit equilibrium check therefore invokes the third dimension.

## 3.4 Analytical Development

In order to quantify the mechanistic behaviour outlined in Section 3, we seek analytical expressions for the stresses within both the elastic and the plastic zones around the tunnel, and for the tunnel closurewhich results from the stress redistribution caused by the progressive reduction of support pressure. Utilizing such expressions, values of minimum support pressure necessary to ensure stability will be investigated. Development of the required analytical expressions is based primarily upon work by Ladanyi (1974) and Hoek (1980), extended to include a wider range of material characterizations.

The analytical material presented in the following sections is summarized in Figures 2 and 3.

For each case it is necessary to define a peak strength envelope within which the material behaves elastically, and a post-peak envelope defining the plastic behavior of the material. While the four cases outlined below have been selected to cover a fairly wide range of combinations of elastic and plastic material behaviour, any reasonable combination of elastic and plastic failure envelopes is, of course, perfectly admissible.

3.4.1 Material Characterizations

See Figures 2 and 3 for a summary of the following material.

Case 1: Coulomb

(A) Elastic Behavior

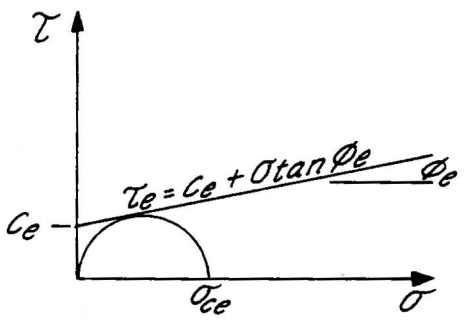


$\tau_e$ = Shear strength
$\sigma$ = Normal stress
$C_e$ = Cohesion (elastic)
$\phi_e$ = Angle of internal friction in elastic range.

The material displays a linear Coulomb failure criterion on a Mohr envelope ($\tau$ vs $\sigma$) plot. For convenience in maintaining a consistent format between the various cases considered, the following parameters are defined:

- Terzaghi's flow value in the elastic range:

$$N_{\phi e} = \tan^2\left(45 + \frac{\phi_e}{2}\right)$$

- Intercept on $\sigma$ axis in elastic range:

$$S_{Ce} = C_e / \tan \phi_e$$

- An empirical parameter, M, giving a relationship between field stress $p_o$ and material strength:

$$M_{COULOMB} = M_c = [1 + (N\phi_e - 1)\, P_o/\sigma_c]/(N\phi_e + 1)$$

(B) Plastic Behavior

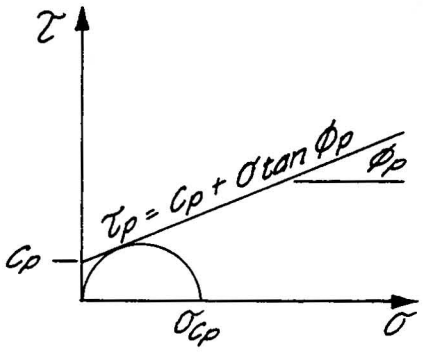


$c_p$ = Cohesion (plastic)

$\phi_p$ = Angle of internal friction in plastic range.

This material also displays a linear Coulomb criterion on a Mohr envelope plot, with the parameters modified to reflect post-peak behaviour. Analogous to the elastic behaviour, we define the parameters:

$$N\phi_p = \tan^2(45 + \phi_p/2)$$
$$S_{cp} = c_p/\tan\phi_p = \sigma_{cp}/(N\phi_p - 1)$$

This Case 1 model would generally be expected to have applicability to soils displaying both cohesive and frictional behaviour, and could also be utilized for a reasonable approximation of rock mass behaviour. Clearly, the choice of the governing values for the basic cohesion and friction parameters is of critical importance, as with all such material characterization models.

Case 2: Fairhurst - Coulomb

Ladanyi (1974) has suggested that a rock mass may be more adequately characterized by a Fairhurst parabolic failure envelope in the elastic ("intact rock") range, and a linear Coulomb envelope in the plastic ("broken rock") range.

(A) Elastic Behaviour

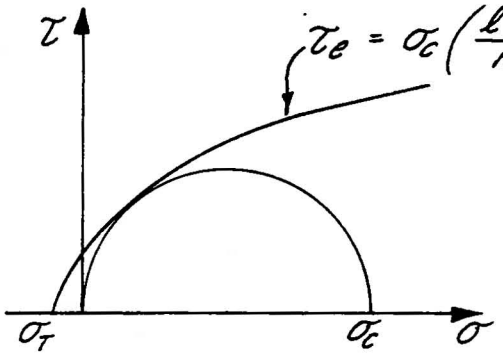


Once again, we define a parameter M giving the relationship between field stress $p_o$ and material strength as:

$$M_{FAIRHURST} = M_F = \left[1+\frac{nP_o}{\sigma_c}-\frac{1}{4}(\ell-1)^2\right]^{\frac{1}{2}}/(\ell+1)$$

(B) Plastic Behaviour

Identical to Case 1, a linear Coulomb criterion of the form:

$$\tau_p = c_p + \sigma\tan\phi_p$$

and for which; $N\phi_p = \tan^2(45+\phi_p/2)$

$$s_{cp} = c_p/\tan\phi_p$$

Case 3: Hoek-Brown Parabola

Hoek and Brown (1980) have suggested that a failure envelope for rock may be appropriately drawn on a principal stress ($\sigma_1$ vs $\sigma_3$) plot. The equation of the envelope is defined in terms of two empirically derived constants and the uniaxial compressive strength.

(A) Elastic Behaviour

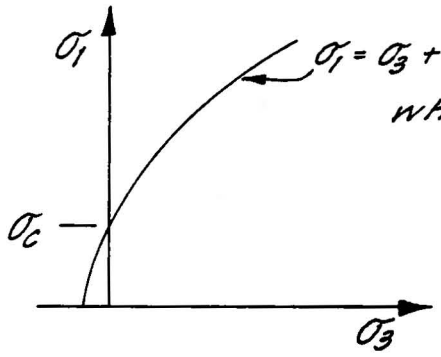

In this case, the parameter M is defined as:

$$M_{HOEK} = M_H = \frac{1}{2}\left[\left(\frac{m_e}{4}\right)^2 + \frac{m_e P_o}{\sigma_c} + s_e\right]^{\frac{1}{2}} - \frac{m_e}{8}$$

(B) Plastic Behaviour

An envelope of the same general form as that for the elastic region is used, but the constants m and s are modified to reflect plastic behaviour, i.e. $m_p$ and $s_p$.

Case 3: Purely Cohesive Material

Whereas the special case of a cohesionless material may be extrapolated directly from Case 1, the case of a frictionless material (purely cohesive) is somewhat less evident. The model used is that of an elastic perfectly plastic material with no post-peak strength reduction. Hence, the elastic and plastic envelopes are identical and, on a Mohr envelope plot, are simply a horizontal ($\phi = 0$) line as shown.

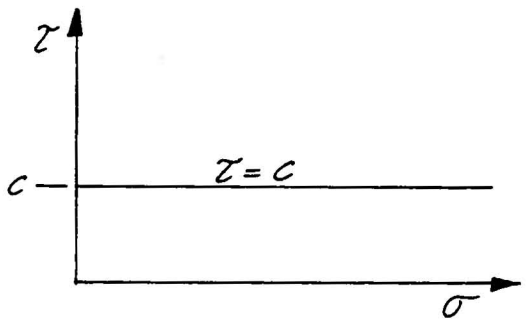


3.4.2 Analysis of Stresses and Deformations

Development of the analytical expressions for stresses and displacements are well covered in the literature for Cases 1 and 2 (Ladanyi,

1974) and Case 3 (Hoek and Brown, 1980). Case 4 is a relatively simple extension, based upon the same steps used for the other cases. As an example, and for clarity, the expressions for Case 1 are developed in this section, with the resulting expressions for all four cases summarized in Figure 2. As the logical sequence of the steps is identical in all four cases, detailed development of each case may be readily undertaken.

3.4.2.1 Stresses

For the case of cylindical symmetry, the differential equation of equilibrium in polar coordinates is:

$$\frac{d\sigma_r}{dr} + \frac{(\sigma_r - \sigma_\theta)}{r} = 0 \qquad (1)$$

Assuming linear-elastic response and satisfying Eq. (1) for the boundary conditions $\sigma_r = p_i$ at $r = r_i$ and $\sigma_r = p_o$ at $r = \infty$ gives:

$$\sigma_r = P_o - (P_o - P_i)(r_i/r)^2 \qquad (2)$$

$$\sigma_\theta = P_o + (P_o - P_i)(r_i/r)^2 \qquad (3)$$

These two equations give the radial and tangential stresses within an elastic medium loaded by a stress $p_o$ at infinity and containing a circular hole at the origin of radius $r_i$ with an internal pressure of $P_i$. If a plastic zone of radius $r_e$ forms around the central hole, then the stresses in the surrounding elastic region are found by satisfying Eq. (1) for the boundary conditions $\sigma_r = \sigma_{re}$ at $r = r_e$ and $\sigma_r = p_o$ at $r = \infty$, giving:

$$\sigma_r = P_o - (P_o - \sigma_{re})(r_e/r)^2 \tag{4}$$

$$\sigma_\theta = P_o + (P_o - \sigma_{re})(r_e/r)^2 \tag{5}$$

It is readily seen that Eq. (4) and (5) are exactly analogous to Eq. (2) and (3), but with the hole of radius $r_i$ replaced by the radius of the plastic zone, $r_e$, and the internal support pressure, $p_i$, replaced by the radial stress at the elastic-plastic interface, $\sigma_{re}$ . Note that the stresses within the elastic zone are independent of the material strength properties.

Within the plastic or "failed" zone, the failure criterion defined for Case 1 must be satisfied. As noted in Section 4.1, the plastic behavior of the material for Case 1 is governed by the Coulomb failure criterion:

$$\tau_p = c_p + \sigma \tan \phi_p = \tfrac{1}{2}(\sigma_1 - \sigma_3)$$

which may be rewritten as:

$$(\sigma_1 + S_{cp}) / (\sigma_3 + S_{cp}) = N\phi_p$$

where:

$$S_{cp} = c_p / \tan \phi_p \tag{5a}$$

$$N\phi_p = \tan^2(45 + \phi_p/2) \tag{5b}$$

as defined under Case 1 in Section 4.1. Recognizing that, for the model under consideration, $\sigma_1 = \sigma_\theta$ and $\sigma_3 = \sigma_r$, we may write;

$$(\sigma_\theta + S_{cp}) / (\sigma_r + S_{cp}) = N\phi_p \tag{6}$$

Substituting the failure criterion from Eq. (6) into Eq. (1), integrating Eq. (1), and applying the boundary conditions that $\sigma_r = p_i$ at $r = r_i$ gives the radial and tangential stresses in the plastic zone as:

$$\sigma_r = (p_i + S_{cp})(r/r_i)^{(N\phi_p - 1)} - S_{cp} \tag{7}$$

$$\sigma_\theta = N\phi_p (p_i + S_{cp})(r/r_i)^{(N\phi_p - 1)} - S_{cp} \tag{8}$$

Note that the stresses in the plastic zone are solely a function of the strength properties of the material and the internal support pressure.

At the boundary between the elastic and plastic zones the failure criterion for the original material i.e. the elastic material, must also be satisfied. For Case 1, the elastic behaviour failure criterion may be written as:

$$(\sigma_1 - \sigma_3) = \sigma_c + \sigma_3 (N\phi_e - 1)$$

or: (9)

$$(\sigma_{\theta e} - \sigma_{re}) = \sigma_c + \sigma_{re} (N\phi_e - 1)$$

The principal stress difference within the elastic zone may also be written, from Eq. (4) and (5) as:

$$(\sigma_{\theta e} - \sigma_{re}) = 2 (p_o - \sigma_{re}) \tag{10}$$

Substitution of Eq. (10) into Eq. (9) gives:

$$\sigma_{re} = p_o - M_c \sigma_c \tag{11}$$

where, as previously defined;

$$M_c = [1 + (N\phi_e - 1) p_o / \sigma_c] / (N\phi_e + 1) \tag{11a}$$

At the transition interface between the elastic and plastic zones, there must be continuity of the radial stress. Thus, the expression for radial stress in the plastic zone, Eq. (7), and the expression for radial stress in the elastic zone, Eq. (4) must both be valid. Solving these two equations simultaneously, the extent of the plastic zone, $r_e$, may be determined as:

$$r_e = r_i \left[ \frac{(p_o + S_{cp} - M_c \sigma_c)}{(p_i + S_{cp})} \right]^{1/(N\phi_p - 1)} \tag{12}$$

The value of internal support pressure, $p_i$, at which the onset of plasticity occurs, and the minimum value of support pressure necessary to maintain a stable plastic zone around the tunnel may be determined as follows.

A plastic zone will exist when the radius of the elastic - plastic interface, $r_e$, is greater than the radius of the tunnel, $r_i$. Thus, the onset of plasticity will occur when $r_e = r_i$ for which, from Eq. (12), plasticity will occur when:

$$P_i \leq P_o - M_c \sigma_c \tag{13}$$

Comparing Eq. (13) and (11) shows them to be identical. In other words, for a condition of plasticity to be generated at the tunnel boundary, the internal support pressure is, of course, identical to the radial stress at the plastic - elastic interface. It is of some interest to note that the onset of plasticity for the two bounding cases of purely frictional (cohesionless) and purely cohesive (frictionless) materials will occur at:

Cohesionless material; $P_i \leq 2P_o/(N\phi_e + 1)$

Cohesive materaial; $P_i \leq P_o - \sigma_c/2$

In order to maintain a stable plastic zone around the opening, the radius of the plastic zone must be maintained at less than infinity. From Eq. (12) it may be seen that $r_e < \infty$ for any positive value of internal support pressure, even for a cohesionless material (i.e. $S_{cp} = 0$). For a material displaying some cohesion in the plastic state the plastic zone will theoretically stabilize even if the support pressure is reduced to zero, although the zone may be of very large extent and the consequent deformations may be quite unacceptable.

Finally, the nature of the deformations which will occur within the plastic zone is governed by the system of sliplines which develop.

Jaeger, 1969 (p. 192) shows that the plastic slip lines form a family of equiangular spirals of the form;

$$r = r_i e^{(\pm \theta / \sqrt{N\phi_p})} \qquad (14)$$

and the existence of such slip lines give rise to the type of "camera-shutter" closure movements referred to previously. Analytical expressions for the amount of closure occurring are included in the next section.

Referring back to the mechanistic discussion of Section 3, the above analytical development allows determination of the radius of the plastic zone which forms as the internal support pressure is reduced (Eq. 12); the radial stress at the elastic - plastic boundary (Eq. 11); the principal stresses within the elastic zone (Eq. 4 and 5) and within the plastic zone (Eq. 7 and 8), and gives values of the minimum required support pressure based either on the criterion that no plastic zone is allowed to form (upper bound; Eq. 13), or that the plastic zone which does form reaches a stable limit (lower bound; Eq. 12 $<\infty$). However, the lower bound solution, which is really the one of primary interest, is of relatively little value as it tells us that the support pressure may be reduced to zero for all but cohesionless materials, and even for this case any positive value of $p_i$ will suffice to stabilize the plastic zone. To obtain a more realistic assessment of minimum support pressures, it is necessary to assess the closure deformations, and to assess the effect of gravity. This is undertaken in following sections.

An example which demonstrates the nature of the change in formation stresses around a tunnel due to reduction of the internal support pressure is shown in Figure 4. A material obeying linear Coulomb failure criteria in both the elastic and plastic states was selected (Case 1) and

the analysis is outlined below. The material properties have been chosen to emphasize the mechanisms of interest.

Elastic Behavior

Let: $\phi_e = 35°$

$\sigma_c = 0.5 p_o$ i.e. uniaxial compressive strength equals 1/2 the remotely applied field stress.

Hence:

$$N_{\phi e} = \tan^2(45 + \phi_e/2)$$
$$N_{\phi e} = 3.69$$

As; $\sigma_c = 2 c_e \cos\phi_e / (1 - \sin\phi_e)$

Then $c_e = 0.13 p_o$ $\qquad c_e = \frac{\sigma_c}{2 \cdot \cos\phi_e} \cdot (1 - \sin\phi_e)$

And $M_c = [1 + (N_{\phi e} - 1) p_o / \sigma_c] / (N_{\phi e} + 1)$
$M_c = 1.36$

Plastic Behavior

The strength parameters have been arbitrarily reduced to:

$$\phi_p = 30°$$
$$c_p \sim 1/10\, c_e = 0.01 p_o$$

Thus:

$$S_{cp} = c_p / \tan\phi_p = 0.017 p_o$$
$$N_{\phi p} = \tan^2(45 + \phi_p/2) = 3.0$$

Prior to excavation, the internal support pressure, $p_i$, is equal to the field stress, $p_o$, and thus the field stresses are given by

$$\sigma_r = \sigma_\theta = p_o$$

as shown by (1) on Figure 4.

As the support pressure is progressively reduced, modelling the excavation process, the material initially behaves elastically, redistributing the field stresses according to Eq. (2) and (3). From these it may be

seen that the tangential stress near the hole is progressively increased, with radial stress decreasing as $p_i$ is reduced. Eventually, a sufficient stress difference is generated to cause failure (onset of plasticity) at the tunnel wall. The value to which $p_i$ may be reduced before plasticity is generated is, by Eq. (13), equal to 0.32 $p_o$.

At this point, shown as (2) on Figure 4, the tangential stress at the tunnel wall has increased to a value of 1.68 $p_o$, with the radial stress being equal to $p_i$ i.e. 0.32 $p_o$.

As the internal support pressure is further reduced, a plastic zone grows outwards from the tunnel. The maximum extent of the plastic zone is reached when the support pressure is reduced to zero for which, from Eq. (12), the plastic zone extends to a distance of 4.45 times the tunnel radius. Thus, for points located closer to the tunnel than (4.45) $r_i$, the stresses are given by Eq. (7) and (8), with the radial stress at the elastic - plastic boundary being given by Eq. (11). For points beyond the elastic - plastic boundary, the stresses are given by Eq. (4) and (5). The results are shown as (3) on Figure 4.

From this example, the meaning of the upper and lower bound minimum support pressures discussed in Section 3.1 is indicated. Growth of the plastic zone first commences at the upper bound value, in this case when $p_i$ is reduced from its initial value of $p_o$ to 0.32 $p_o$. Growth of the plastic zone ceases, having reached its maximum extent, when the lower bound support pressure is reached, in this case when $p_i$ is reduced to zero. As previously noted, the fact that a stable plastic zone is achieved even when $p_i$ is reduced to zero is due to the small cohesion which was assumed to exist for the material in the plastic state. Once again it is emphasized that this analysis deals with a weightless material,

and more realistic minimum support pressure assessment requires the inclusion of gravity effects.

Similar analyses could be undertaken for any of the different material characterizations represented by Cases 1 to 4. The relevant analytical expressions for all four cases, derived using the same framework as given in this section, are summarized on Figure 2.

3.4.2.2 Deformations

While this report is concerned primarily with the formation pressures developed on tunnel or shaft linings, it is obvious from the foregoing section that the formation pressures which develop are related to the closure deformations which occur. We have seen that there is no unique value of internal support pressure - a reduction in support pressure is accompanied by a stress redistribution in the elastic material and a growth in the extent of plastic zone, if such a zone has formed. These changes will give rise to closure deformations. Conversely, one might state that as more closure of the tunnel is allowed to occur, the necessary support pressure is reduced. This section outlines an analytical approach, based on the work of Ladanyi, 1974, which relates the closure deformations to the material properties and the internal support pressure. As with the previous section, only Case 1 (linear Coulomb material) is explicitly considered, as the derivations for the other three cases follow identical logic. All cases are summarized on Figure 3.

Consider first the radial displacement, $u_e$ , of the elastic - plastic interface at $r = r_e$. The elastic tangential strain at this interface, $\varepsilon_\theta$, may be written:

$$\varepsilon_\theta = \frac{1}{E}\left[\Delta\sigma_\theta - \nu(\Delta\sigma_r + \Delta\sigma_z)\right] \qquad (15)$$

Where $\sigma_z$ is the normal stress parallel to the longitudinal axis of the tunnel and $\nu$ is Poisson's Ratio. For the two-dimensional model and loading system selected, it may be readily shown that, in the elastic region, the change in longitudinal stress is zero for conditions of plane-strain (or, in fact, plane stress).

Hence; $\varepsilon_\theta = \frac{1}{E}[\Delta\sigma_\theta - \nu\Delta\sigma_r]$

As; $\varepsilon_\theta = u_e/r_e$

Thus; $u_e/r_e = \frac{1}{E}(\Delta\sigma_\theta - \nu\Delta\sigma_r)$ (16)

From consideration of Eq. (4) and (5) we may write that;

and $\Delta\sigma_\theta = [P_o + (P_o - \sigma_{re})(r_e/r)^2] - P_o$

$\Delta\sigma_r = [P_o - (P_o - \sigma_{re})(r_e/r)^2] - P_o$

Substituting the above into Eq.(16) and simplifying gives the Lamé equation:

$$u_e/r_e = (P_o - \sigma_{re})(1+\nu)/E$$

Substituting Eq. (11) into the above gives;

$$u_e = \frac{(1+\nu)}{E}(M_c\sigma_c)r_e \quad (17)$$

which is the radial displacement of the elastic - plastic interface and is valid under conditions of either plane stress or plane strain.

In addition to the elastic radial displacement above, the radial displacement of the plastic zone (if any) must be considered. If it is possible to determine the average plastic dilation (volumetric strain) of the material within the plastic zone, $e_{av}$, then for plane strain conditions we may determine the radial closure associated with a given extent (radius) of plastic zone. Ladanyi, 1974 undertakes this task based upon the concept of the associated flow rule of the theory of plasticity which

implies that the plastic strain increments are normal to the yield surface in principal stress space (Drucker-Prager postulate).

For Case 1 (linear Coulomb) the yield function may be written

$$F = 0 = (\sigma_1 - \sigma_3) - \sigma_c - \sigma_c (N\phi_e - 1) \tag{18}$$

As noted, Drucker's postulate states that:

$$d\varepsilon_{ij} = \lambda \, \delta F / \delta \sigma_{ij} \tag{19}$$

where $\lambda$ is a constant of proportionality, F is the yield function and $d\varepsilon_{ij}$ refers to a plastic strain increment. From (18) and (19), the ratio of the plastic dilation to the plastic shear strain increment is;

$$\frac{de}{d\gamma} = \frac{d\varepsilon_1 + d\varepsilon_3}{d\varepsilon_1 - d\varepsilon_3} = -\sin\phi_e = D_c \tag{20}$$

and, for small increments of strain, we may assume a direct proportionality between plastic dilation, $e$ , and plastic shear strain, $\gamma$ .

Thus, $$e \cong D_c \gamma \tag{21}$$

The average plastic dilation, $e_{av}$, is determined by dividing the total volume change of the plastic zone, dVp, by the original volume of the plastic zone, Vp.

$$e_{av} = dV_p / V_p \tag{22}$$

While the volume of the plastic zone is readily calculated as:

$$V_p = \pi (r_e^2 - r_i^2) \tag{23}$$

the total volumetric change must be calculated from

$$dV_p = \int_{r_i}^{r_e} 2\pi e(r) r \, dr \tag{24}$$

To express the plastic dilation, e, as a function of radius, r, use is made of approximate relationships (Ladanyi, 1974) which allow the integration of Eq. (24) and thus the determination of $e_{av}$ from Eq. (22) as;

$$e_{av} = \frac{2(u_e/r_e)(r_e/r_i)^2}{[(r_e/r_i)^2 - 1][1 + 1/R_c]} \tag{25}$$

where $e_{av}$ is negative for volume increase.

The parameter $R_c$ (the subscript referring to the Coulomb model of Case 1) reflects a concern over the range of validity of Druckers postulate. Ladanyi argues that the volume change rate can only be assumed to obey the associated flow rule within a limited portion of post failure strains and hence, for a thick plastic zone, Eq. (24) should only be integrated over a portion of the zone. Ladanyi suggested that:

For a thin plastic zone, i.e. $r_e/r_i < \sqrt{3}$

Then: $$R_c = 2 D_c \ln r_e/r_i \tag{26}$$

For a thick plastic zone, i.e. $r_e/r_i > \sqrt{3}$

Then: $$R_c = 1.1 D_c \tag{27}$$

Having obtained an expression for the average plastic dilation, the tunnel closure, $U_i$, may be calculated. Comparing the volume of the plastic zone before and after its formation;

$$\pi(r_e^2 - r_i^2) = \pi[(r_e + u_e)^2 - (r_i + u_i)^2](1 - e_{av})$$

Simplifying, gives;

$$u_i = r_i\left[1 - \left(\frac{1 - e_{av}}{1 + A}\right)^{\frac{1}{2}}\right] \tag{28}$$

Where:

$$A = (2 u_e/r_e - e_{av})(r_e/r_i)^2 \tag{29}$$

The equations derived from the foregoing development, which may be followed in similar fashion for Case 2 (Ladanyi, 1974), Case 3 (Hoek and Brown, 1980) and Case 4, are summarized on Figure 3.

Using the foregoing analysis, displacements may be calculated for the example presented in the previous section and shown on Figure 4. To

calculate displacement, Poisson's Ratio and Young's Modulus are required. For illustrative purposes, the following values have been chosen:

$$\nu = 0.30$$
$$E = 100\, p_o$$

We wish to calculate the closure associated with progressively decreasing values of internal support pressure, $p_i$. As previously shown, the material will remain fully elastic until the support pressure is reduced to 0.32 $p_o$, at which point a plastic zone is instigated at the tunnel wall. Thus the tunnel closure to this point is elastic and may be calculated from Eq. (17) replacing $r_e$ by $r_i$, which shows a closure of 0.009 times the original radius, $r_i$. This point is shown on Figure 5 as ②, corresponding to the equivalent stress distribution shown on Figure 4. As the support pressure is further reduced the radius of the plastic zone grows according to Eq. (12), and hence the ratio $(r_e/r_i)$ increases. Knowing the values of $(U_e/r_e)$ from Eq. (17); of Dc from Eq. (20), and of $(r_e/r_i)$ Eq. (12), the appropriate values of R may be calculated from Eq. (26) or (27), giving values of $e_{av}$ from Eq. (25), A from Eq. (29) and hence of radial closure $U_i$ from Eq. (28). The results are plotted on Figure 5 in the form of a dimensionless closure versus support pressure curve.

The results show that maintenance of the upper bound support pressure (onset of plasticity, point ②) allows a radial closure of 0.009 $r_i$, whereas reduction of the support pressure to its theoretical lower bound allows closure of 0.28 $r_i$, which would generally be completely unrealistic. To maintain a more realistic closure, a support pressure greater than the lower bound (zero in this case) is normally installed. The analysis of the interaction between support reaction curves and ground

reaction curves is well covered in the literature (Lombardi, 1973; Kaiser, 1980; Hoek and Brown, 1980, Ladanyi, 1974 and others) and will not be repeated here. A question of primary interest to this report is the determination of the actual minimum support pressure which will maintain the tunnel in a stable condition. To determine this value we must now move away from the weightless model which has been used, and invoke the effect of gravity, thus differentiating between the crown of the tunnel and the floor - a distinction which has not been present so far.

3.4.2.3 Gravity Effect - Limit Equilibrium

In the preceding analyses, we have seen that progressive reduction in support pressure leads to the development of plasticity in the material surrounding the tunnel. In a manner somewhat analogous to a slope stability or retaining wall problem, we now seek to analyze kinematically possible failure mechanisms to determine what minimum support pressure must be installed to stabilize such mechanisms. In other words, the approach of limiting equilibrium can be utilized.

According to Eq. (14), there exists an infinite family of spiral slip lines in the plastic zone of the form:

$$r = r_i \cdot e^{\left(\pm \theta / \sqrt{N_{\phi p}}\right)}$$

for a Case 1 material. For the example which has been utilized in the last two sections, typical slip lines are shown in Figure 6, for the limiting case of $p_i = 0$ when the plastic zone has reached its maximum extent ($r_e = 4.45\ r_i$). The existence of such slip lines, in a homogeneous material, has been well demonstrated by the model tests of York and Reed, 1953. As shown on Figure 6, it is possible to define blocks or wedges of material, bounded by plastic slip lines, which could provide kinematically

possible failure mechanisms. Clearly, there are an infinite number of such blocks, as there are an infinite number of slip lines. The stability of a given block is a function of the weight of material contained within the block, the plastic shear strength of the material (which is fully mobilized along the slip lines) and the existence of any internal support pressure. In general, the internal support pressure required to stabilize a block may be found by summing forces in the direction of potential movement, which is parallel to the axis of symmetry of the block. Hence, for the block shown, the general expression;

$$\int (P_i)_{vert.} = W - \int S_{vert.}$$

would be valid.

It is readily seen, by inspection, that a block with a vertical axis of symmetry is most critical, as the driving force (W) is in the direction of potential movement. For a wall block, the driving force is zero in the direction of potential movement, and is opposed to the direction of movement for a floor block. Thus, some minimum value of support pressure, (Pi) min, may be required to stabilize the tunnel crown due to gravity effects, whereas the sidewalls require no such support, and the floor stability is actually enhanced by gravity.

To determine the value of the minimum required support pressure on the basis of seeking out the most critical failure block bounded by slip lines as shown on Figure 6 is analytically feasible. However, such an approach would be somewhat cumbersome. More seriously, determination of minimum support pressure on such a basis would be placing an unwarranted confidence in the highly idealized model of a perfectly homogenous, perfectly plastic etc. material which we have utilized. For material such as rock, the plastic zone represents a zone of broken rock, which will have

been greatly affected by geological detail and will certainly not produce the idealized slip lines shown in Figure 6. To obtain a simple and conservative value for the effect of gravity blocks in the crown it is generally assumed that the full weight of the failed material i.e. the material in the plastic zone $r_i < r < r_e$, must be carried by internal support (Hoek and Brown, 1980). This is equivalent to assuming a vertically bounded prismatic failure block with zero shear resistance along its boundaries, and extending from the tunnel crown to the limit of the plastic zone. As previously noted, the gravity destabilizing effect is fully active at the crown, irrelevant at the side walls, and of a negative sense (i.e. stabilizing) at the floor. These effects may therefore be simply, although crudely, accounted for by adjustment of the closure support curve shown in Figure 6 by the term $\gamma (r_e - r_i)$, where $\gamma$ is the unit weight of rock, increasing the support pressure by this amount in the crown, and decreasing it in the floor, as shown schematically in Figure 7. Thus, as experience clearly tells us, there exists a difference in the support requirements of the crown compared to the sidewalls or floor. Although this difference, which is the effect of gravity, has been rather crudely accounted for in this analysis, it is important to recognize that the fundamental step which enabled the gravity effect to be accounted for in the context of a weightless material model was the use of a limit equilibrium check on potential gravity failure blocks. Although the limit equilibrium analysis was greatly simplified, the validity of the logic remains, and is important in the analysis of formation pressures on shaft linings.

### 3.4.3 Minimum Internal Support Pressures

From the foregoing analyses, it is seen that the minimum internal support pressure - which essentially corresponds to the design pressure of the formation upon the tunnel supports - may be defined in several ways which have quite different physical meanings. There are really four basic definitions which are outlined below in quantitatively descending order.

(1) Maintain Material in Elastic Range

This refers to the internal support pressure required to avoid any failure of the material around the tunnel i.e. no onset of plasticity. Widely suggested as design criterion for use in tunnel and shaft analyses (Dixon and Mahtab, 1976). Referred to herein as the upper bound value of minimum support pressure.

(2) Limit Closure of Tunnel

Referring to the characteristic closure - support curve of Figure 6, a support system may be installed to provide a reaction which is sufficient to limit the closure deformation to a pre-determined, acceptable, value. This design support value would in general be less than 1) above. Methods of treating analysis of support reaction are covered by Lombardi, 1973; Hoek and Brown, 1980.

(3) Maintain Limiting Equilibrium of Gravity Blocks

Referring to the (schematic) modified characteristic curves of Figure 7, a minimum support value is required in the crown of the tunnel to maintain the equilibrium of gravity blocks. This, realistically, is the lower bound value for internal support pressure in the crown.

(4) Maintain Stable Plastic Zone

This is the absolute minimum support pressure. For values less than this the radius of the plastic zone expands to infinity, giving rise to infinite closure movements. This parameter has relatively little meaning, as the analytical equations show that for a material displaying any cohesion in the plastic state - however small - a stable plastic zone is always achieved, albeit at the cost of extremely large displacements. For a material which is cohesionless in the failed (plastic) state, a stable plastic zone can theoretically be achieved provided some positive value of internal support, no matter how small, is maintained. In reality, requirements (2) or (3) will generally control.

### 3.4.4 Extensions to Analysis

While it is not the intention herein to undertake an exhaustive review of tunnel analysis criticisms and extensions, some comments are in order for purposes of completeness and clarity.

#### 3.4.4.1 Face Effect

It was noted in Section 2 that the model utilized was for conditions of plane strain, and hence existed remote from the three-dimensional effects of the tunnel excavation face. It was further stated that the process of tunnel excavation would be modelled by reducing the internal support pressure from an initial value, $p_o$, equal to the virgin field stress, to progressively smaller values. In reality, excavation of the tunnel does not occur gradually, but results in an instantaneous reduction of the internal support due to removal of the rock core. Nevertheless, work by Lombardi, 1973 and by Panet, 1974, indicates that the restraining effect

of the tunnel face upon closure deformations of the tunnel in the proximity of the face is reasonably modelled by the approach of progressively reducing the internal support pressure in the analytical model. Thus, a fictitious internal support is presumed to exist within the tunnel near to the face. Panet, 1974, compared a 3-D axisymmetric numerical analysis with the results of the type of 2-D analytical analysis outlined in the previous sections. He found that, for a material in the elastic range, the radial closure immediately behind the face was in the order of 0.3 to 0.4 times the closure which ultimately occurred when the tunnel face, and hence its restraining effect, were advanced more than 2 diameters from the point in question. This may be viewed as equivalent to maintaining an initial fictituous internal support pressure of between 0.7 $p_o$ and 0.6 $p_o$ at the face. Thus, the restraining effect of the face may be approximately modelled in the 2-D analysis by assuming that the (fictitious) internal support pressure is equal to (say) 2/3 $p_o$ when the face is at the point in question, and reduces to zero when the face is a distance of 4 $r_i$ from the point in question. Thus, artificial support which is intended to maintain a minimum internal support pressure as discussed previously must be installed between the time of excavation and the time at which the face has advanced a distance of four times the tunnel radius.

More detailed analysis of the stress-deformation response near the tunnel face requires 3-D analysis - most readily undertaken by numerical analysis of an axisymmetric model. Nevertheless, the 2-D model with a fictitious internal support pressure which is progressively reduced does provide a most useful analytical method which provides excellent insight to the mechanisms of stress redistribution and deformation.

3.4.4.2 Time Dependent Behavior

The model utilized is independent of time. Ladanyi, 1974, proposes a simple method of utilizing "isochrone" lines to modify the support-closure diagram derived from the foregoing analysis consisting, in essence, of arbitrarily reducing the material strength parameters as a function of time. More recently, Ladanyi, 1980 and Hanafy, 1980 have utilized creep relationships based on a power law to account for time dependence. The thesis by Da Fontura, 1980 provides a useful review.

3.4.3.3 Non-Hydrostatic Field Stresses

All of the foregoing analysis has been based upon a hydrostatic state of stress in the virgin condition. This may be a serious restriction with regard to the analysis of tunnels. Muir-Wood, 1975, and more recently Pender, 1980 have extended the characteristic line method to include non-hydrostatic loading. This restriction is not as serious for the problem of shaft analysis for which the condition of hydrostatic loading will generally be closely met.

3.4.5 Summary

This section has outlined the basic derivation of an analytical approach to the analysis of the stress-deformation response of a tunnel section. Four cases of different elastic and plastic material properties have been presented, and an attempt has been made to explain, qualitatively, the mechanisms at work during the process of stress redistribution and deformation. While the approach is strictly valid only for a two-dimensional problem in plane-strain, it is able to provide useful insight to the process of tunnel excavation by the device of progressively reducing a fictitious

internal support pressure. It is emphasized that the onset of plasticity or failure around the tunnel is due to the difference between the major and minor stresses in the plane of the cross-section i.e. the tangential and radial stresses, giving rise to a "camera-shutter" type of closure along an infinite family of equiangular spiral slip lines. Because the model is weightless, it is necessary to check the limit equilibrium under gravity loading of potential failure blocks bounded by the spiral slip lines in order to determine the minimum support pressure required. This limit equilibrium check is approximated by simply considering the full weight of the material in the plastic zone to require support, and this approach succeeds in differentiating between the crown, sidewalls and floor of a tunnel.

In essence, the well known hole-in-a-plate model has been utilized for the basic analytical approach, modified for the special conditions of a tunnel by including a limit equilibrium check of potential gravity failure blocks. An exactly analogous approach may be followed for the analysis of the formation pressures acting on a shaft lining, with the primary modifications being due to the nature of the stresses causing plasticity and to the fact that gravity effects act perpendicular to the plane of the hole-in-a-plate cross-section.

## 4.0 SHAFT ANALYSIS

### 4.1 Introduction

After extensive review of the literature pertaining to the analysis of formation pressures on shafts, one is struck by several factors. Firstly, there is a surprising paucity of material. Secondly, it is commonly argued that whereas the simple hole-in-a-plate model may be questionable for a tunnel due to non-hydrostatic loading and due to differences in the effects of gravity at different points around the tunnel periphery, these deficiencies are not generally present for a shaft. As a consequence, simple hole-in-a-plate models are almost universally invoked for shaft analysis, and the result is then idential to the basic characteristic support-closure curve outlined in the last section, but neglecting any gravity corrections. In short, a shaft is viewed simply as a two-dimensional tunnel problem around which gravity may be neglected. To quote Lombardi, 1973 "In the centrosymmetrical case, as perhaps for a vertical shaft sunk in a homogeneous rock, the problem is simpler in so far as every displacement points towards the centre and thus exhibits only radial components. In the same way the forces and stresses are only directed radially or tangentially". As we shall see, this convenient and simple two-dimensional approach is reasonably valid, but only under cerain conditions, depending primarily upon the ratio of horizontal to vertical field stresses, $k_o$. Terzaghi, 1942, had already recognized that the problem of shaft design in soils was not as simple as merely rotating a tunnel in a weightless medium through ninety degrees, and undertook an elegant engineering solution to a three-dimensional shaft problem. This section will endeavour to reconcile both approaches by outlining the ranges of validity of each.

Finally, it should be noted that attempts to determine the current state-of-the-art basis for assessment of formation pressures around shafts were remarkably unproductive. Mayo, 1968, in a state-of-the-art report refers to the rule of thumb of "one inch of concrete (liner) per foot of diameter" as still being the most acceptable. Virtually all of the more analytical approaches which were found were simply based on provision of sufficient support pressure to avoid the onset of plasticity - identical to the upper bound minimum support pressure from the previous section - although most authors emphasize that this is really only an approximate method for controlling deformations (Weehuizen, 1959; Ostrowski, 1972). In private communication with several consultants and contractors currently involved in shaft design or construction, little additional insight was gained. Indeed, in two cases the view was expressed that supports capable of resisting pressures equal to the virgin state of stress, po, should generally be provided. Such a view cannot in general be defended, and would place an unnecessary penalty on the cost of shaft supports.

## 4.2 Mechanisms of Shaft Behaviour

The two basic shaft models referred to briefly above may be thought of as essentially two-dimensional (hole-in-a-plate model, weightless material) and essentially three-dimensional (Terzaghi, 1942) respectively. The applicability of each model may be understood in terms of the mechanics of behaviour of the material around the shaft, notably the manner in which failure (plasticity) of the surrounding material is generated.

Consider the excavation of a vertical shaft as shown in Figure 8. As with the tunnel analysis, the excavation of the shaft at any particular section (depth) may be modelled by considering the progressive relaxation

of the internal support pressure starting from an initial value equal to the in situ horizontal stresses appropriate to the depth being considered. We will consider the horizontal stress field to be hydrostatic and of magnitude $p_o = k_o \sigma_v$, where $k_o$ is the ratio of the virgin horizontal to vertical stresses. The vertical stress is initally equal to the overlying weight of material i.e. $\sigma_v = \sigma_z = \gamma z$. The internal support pressure prior to excavation is equal to the remotely applied stress, i.e. $p_i = p_o$. As excavation proceeds $p_i$ is progressively reduced.

As $p_i$ is reduced, the material initially responds elastically with the tangential stress increasing above $p_o$ near the shaft, the radial stress deceasing, and the longitudinal stress remaining constant, vertical and equal to $\gamma z$. For this axisymmetrical case, as long as the material remains in the elastic range, the equations governing the stress distribution in the plane of the section are identical to those derived for the two-dimensional tunnel case (Poulos and Davis, 1971), given by Eq. (2) and (3).

$$\sigma_r = P_o - (P_o - P_i)(r_i/r)^2 \tag{2}$$

$$\sigma_\theta = P_o + (P_o - P_i)(r_i/r)^2 \tag{3}$$

Thus, as $p_i$ is reduced, a stress difference is generated at the shaft wall due to the increasing $\sigma_\theta$ and decreasing $\sigma_r$. Provided that no plasticity occurs, the closure of the shaft in the elastic medium may also be calculated by the same equations as those utilized for the tunnel case.

If the process of decreasing the internal pressure could be continued, without the onset of plasticity, to the point where the internal pressure is equal to zero, we see from Eq. (2) and (3) that the tangential stress would rise to a value of twice the field stress at the shaft wall,

the radial stress would drop to zero, and the vertical stress would remain equal to the gravity load, all three stresses being principal.

$$\text{i.e.} \quad \sigma_\theta \rightarrow 2P_o = 2K_o\gamma z$$
$$\sigma_r \rightarrow 0$$
$$\sigma_z = \gamma z$$

As the potential for the onset of plasticity depends upon the maximum principal stress difference, we see that there are actually three possible alternatives for which pair of stresses initiates failure. Plasticity could be generated in the plane of the cross-section by the difference between the tangential and radial stresses, or it could be generated in the vertical plane by the difference between either the vertical and radial stresses or the vertical and tangential stresses. The latter case, although possible, has been neglected in the following analysis. Which of the remaining two mechanisms occurs first, depends upon whether the vertical or the tangential stress is the larger. This in turn depends upon the value of $k_o$.

Consider first, as an example, a case for which the value of $k_o$ is equal to or greater than unity as shown diagrammatically on Figure 9. As $p_i$ is reduced, $\sigma_\theta$ rises to values always greater than $\sigma_z$, and $\sigma_r$ falls rapidly below $\sigma_z$ (except for extremely high values of $k_o$), and thus the maximum stress difference lies in the plane of the section and is due to $(\sigma_\theta - \sigma_r)$. If, during this process, the strength of the material is insufficient to sustain the stress difference - which may, of course, occur before $p_i$ is reduced to zero - then plasticity will be generated at the shaft wall. The nature of this plastic zone is to form spiral slip lines, exactly as in the tunnel case previously investigated. Plastic closure of the shaft will occur in "camera-shutter" form, with the surfaces of sliding

causing movements only in the horizontal plane. Shear stresses in the vertical direction remain zero, and the vertical stress will remain unchanged, as no failure has occurred in the vertical plane. This statement implies that failure in the horizontal plane does not affect the material strength in the vertical plane, which is true only for an ideal material. While this is clearly a simplification, it allows the mechanistic difference to be clearly seen between the cases of horizontally generated plasticity, $(\sigma_\theta - \sigma_r)$ and vertically generated plasticity, $(\sigma z - \sigma_r)$. Thus, the situation described closely resembles the two-dimensional tunnel case, with the minor change that a condition of constant longitudinal stress prevails $(\Delta \sigma z = 0)$ compared to the constant longitudinal strain $(\Delta \varepsilon_z = 0)$ assumed for the tunnel case. It is this case, which we may refer to as "horizontal plasticity" that has been referred to as the two-dimensional case, and it is intuitively obvious that use of the simple 2-D hole-in-plate model may be used to give approximately correct solutions to the stress - deformation response, as outlined in following sections.

The above case contrasts with that shown diagrammatically in Figure 10 where, for illustration, a value of $k_o < 1/2$ has been assumed. In this case, even if the internal pressure is reduced to zero, the tangential stress never reaches a value as great as the vertical stress. Thus, as $p_i$ is progressively reduced, the maximum stress difference is always governed by $(\sigma z - \sigma_r)$. If, at some stage of this process, the strength of the material is exceeded, plasticity will be generated in the vertical plane by the $(\sigma z - \sigma_r)$ stress difference. Failure generated in this mode will create a family of inclined slip lines in the vertical plane, as illustrated in the lower part of the figure, requiring downwards and inwards movement of the material. As a consequence of the relative vertical

movement, shear stresses will act vertically in the r - z plane, and excess vertical stress (due to further reduction of $p_i$ or due to the higher initial vertical stresses at sections deeper in the shaft) is thereby shed to surrounding material, causing a rotation of principal stresses in the vertical, $(\sigma_z - \sigma_r)$, plane. At the same time, the wedging action of the inward movement will cause an increase in tangential stresses to a limiting value equal to the major (near-vertical) principal stress. Thus, principal stresses are no longer radial, tangential and vertical, the problem ceases to be two-dimensional and the direct use of the 2-D tunnel model to determine the stress-deformation response is no longer justified. Terzaghi, 1942, and later Coates, 1970 addressed this problem of "vertical plasticity" with a view to determining the minimum support pressure required for stability i.e. the minimum design formation pressure.

Before proceeding further with the analysis of these two cases, it is worthwhile to develop a means of identifying the general range of applicability of each model i.e. the two-dimensional model of horizontal plasticity and the three-dimensional model of vertical plasticity.

### 4.2.1 Conditions of Validity for 2-D and 3-D Models

The simple mechanistic arguments of the previous section suggest that a 2-D hole-in-a-plate "tunnel" model is reasonably applicable to a shaft if the onset of plasticity is generated by stresses in the horizontal plane i.e $(\sigma_\theta - \sigma_r)$, whereas a 3-D model must be invoked if plasticity is generated in the vertical plane by the $(\sigma_z - \sigma_r)$ stress difference. By inspection of the illustrative examples in Figures 9 and 10, plasticity will generally be of the horizontal $(\sigma_\theta - \sigma_r)$ type for $k_o < 1.0$ [excluding the unusual case of the $\sigma_\theta - \sigma_z$ stress difference generating plasti-

city], and of the vertical ($\sigma_z - \sigma_r$) type for $k_o < 1/2$. Between these two bounds, the determination of which mechanism will occur for a particular case may be analytically solved as follows.

As the internal support pressure is reduced, the material redistributes stresses elastically, and the tangential-radial stress difference at the shaft wall may be written from Eq. (2) and (3) as:

$$(\sigma_\theta - \sigma_r) = 2(p_o - p_i) = 2(k_o \sigma_z - p_i) \tag{30}$$

Assuming a linear Coulomb material (Case 1 from the tunnel analysis section), the maximum stress difference which may be sustained may be written

$$(\sigma_1 - \sigma_3) = \sigma_c + \sigma_3 (N\phi e - 1) \tag{31}$$

As, for elastic response, $\sigma_\theta$ and $\sigma_r$ are principal stresses, we may equate Eq. (30) and (31) and simplify to give;

$$p_i = (2k_o \sigma_z - \sigma_c)/(N\phi e + 1) \tag{32}$$

Eq. (32) thus indicates that, once $p_i$ is reduced to the value given by the above expression, horizontal plasticity due to the ($\sigma_\theta - \sigma_r$) stress difference will occur.

Similarly, we may write an expression for the ($\sigma_z - \sigma_r$) stress difference in the vertical plane at the shaft wall from Eq. (2) as:

$$(\sigma_z - \sigma_r) = (\sigma_z - p_i) \tag{33}$$

Once again, in the elastic range, $\sigma_z$ and $\sigma_r$ are principal stresses and, equating Eq. (33) and (31) gives, upon simplification;

$$p_i = (\sigma_z - \sigma_c)/N\phi e \tag{34}$$

Eq. (34) indicates that, if $p_i$ is reduced to the above value, vertical plasticity will occur due to the ($\sigma_z - \sigma_r$) stress difference.

Comparing Eq. (32) and (34) we may deduce that the equation which gives the larger value of $p_i$ will determine which form of plasticity will first occur, as it is the larger value of $p_i$ which will first be

encountered during the progressive reduction of the internal support pressure. From this comparison, by equating Eq. (32) and (34) we may define a critical value of $k_o$ - the ratio of horizontal to vertical field stresses - as follows;

$$(k_o)_{crit.} = \frac{1}{2} + 1/(2N\phi e) - \sigma_c/(2N\phi e\,\sigma_z) \qquad (35)$$

If the actual value of $k_o$ at the depth of the particular shaft section being considered is greater than $(k_o)$ crit, then horizontal plasticity will first be generated. Note that this expression does not indicate that plasticity <u>will</u> be generated - only that if plasticity does occur, then it will be in the horizontal plane. Conversely, for $(k_o)$ actual < $(k_o)$ crit, any onset of plasticity will be in the vertical plane due to the $(\sigma_z - \sigma_r)$ stress difference.

Referring to the illustrative examples previously used, we see that the use of Eq. (35) agrees with the previous conclusions of potential horizontal plasticity for $k_o > 1.0$, and potential vertical plasticity for $k_o < 1/2$. From Eq. (35), the maximum possible positive value which $(k_o)$ crit can attain is equal to 1.0. Thus, any in situ value of $(k_o)$ actual > 1 will always be greater than $(k_o)$ crit, and any plasticity generated will therefore be of the horizontal mode. It can also be shown that no plasticity can occur if the value of $(k_o)$ crit is less than 1/2, as the uniaxial compressive strength, $\sigma_c$, must then be greater than the vertical stress, $\sigma_z$, and no vertical plasticity can occur even if $p_i$ $(= \sigma_r)$ is reduced to zero. Thus, the minimum value of $(k_o)$ crit with which we need be concerned is 1/2.

Equations similar to Eq. (35) could be developed for other material characteristics, such as Cases 2, 3 and 4 on Figure 2, and would provide a means of determining the type of shaft analysis appropriate to the

particular section under consideration, provided that in situ values of $k_o$ are known. However, values of $k_o$ are difficult to obtain. Nevertheless, precedent data and knowledge on the likely ranges of $k_o$ in different formations provides some insight to distinguishing the type of shaft analysis most probably appropriate.

i) For: $(k_o)$ actual > $(k_o)$ crit.

If plasticity occurs under these conditions it will be of the horizontal mode due to the stress difference in the plane of the cross-section ($\sigma_\theta - \sigma_r$), and a 2-D hole-in-a-plate analysis is appropriate (see Section 3). This situation would be expected where $(k_o)$ actual is relatively high compared to conventional at rest earth pressure coefficients, and in all situations where $(k_o)$ actual is greater than unity. Published data on measured $k_o$ values (e.g. Hoek & Brown, 1980) suggests that most rock formations would fall into this category, particularly at relatively shallow depths (say less than 1000 m) where $k_o$ is commonly greater than unity. Thus, as a broad but reasonable generalization, we may state that for shafts in rock;

$$(k_o) \text{ actual} > (k_o) \text{ crit.}$$

is likely to occur. Thus, if actual field data is not obtainable, it would be generally reasonable to proceed with a 2-D hole-in-a-plate type of shaft analysis in rock. This conclusion indicates that the hole-in-a-plate analytical shaft approach taken by many workers in rock mechanics does, in fact, have justification, although this justification has not been explicitly stated.

ii) For: $(k_o)$ actual < $(k_o)$ crit.

If plasticity occurs under these conditions, it will be of the vertical mode due to the stress difference in the vertical plane $(\sigma_z - \sigma_r)$, and a 3-D Terzaghi type analysis is appropriate (See Section 4). As noted previously, this situation is valid for all cases where $(k_o)$ actual is less than 1/2, which covers most soil deposits. For normally consolidated soils the at-rest earth pressure may be approximated by;

$$(k_o)_{actual} \cong (1 - \sin\phi_e) \tag{36}$$

Manipulating Eq. (36) in conjunction with the inequality above (based on Eq. (35)) shows that the condition of vertical plasticity will govern for all cases where plasticity is possible (i.e. exluding cases for which $\sigma_c > \sigma_z$) in a normally consolidated soil.

Theoretically, the value of $(k_o)$ actual may rise to the limit of the passive earth pressure coefficient for overconsolidated soils, and thus achieve values greater than $(k_o)$ crit within a soil deposit. Practically, however, it is unlikely that $k_o$ will lie above the range 0.5 - 1.0 in most soil deposits. Lacking specific field data, it would be reasonable to assume in soil deposits that;

$$(k_o) \text{ actual soil} < (k_o) \text{ critical}$$

is likely to occur, giving rise to vertical plasticity and the need for a 3-D shaft analysis.

From the foregoing discussion, a simple and convenient division arises between the analysis of shafts in rock (or, perhaps, very heavily overconsolidated soils) and in soils (normally consolidated to moderately overconsolidated). The former (rock) case may be treated in essentially two-dimensions due to the "horizontal" mode of $(\sigma_\theta - \sigma_r)$ plasticity engendered, while the latter (soils) case requires a three-dimensional treatment due to the "vertical" mode of $(\sigma_z - \sigma_r)$ plasticity which dominates. It is

of interest to note that Coates, 1970, derives an analysis for shafts in rock based upon the 3-D Terzaghi analysis, justified by the statement "... where the ground around the shaft has failed, the vertical stress for the elastic condition before failure might have been the major principal stress and thus greater than the horizontal tangential stress. In this case, the stress initiating failure would be the vertical stress". As shown by the foregoing analysis, however, this situation is, in fact, very unlikely to arise in rock, due to the generally high values of $k_o$ encountered.

The two basic analytical models, two-dimensional and three-dimensional, are reviewed in the following sections.

## 4.3 Two-Dimensional Analysis

As long as the material surrounding the shaft in the axisymmetrically loaded model remains elastic as the internal support pressure is decreased, the equations for stress redistribution and deformations derived in Sections 3.4.2.1 and 3.4.2.2 for the tunnel case are valid for the shaft case. As further support pressure reduction causes horizontal $(\sigma_\theta - \sigma_r)$ plasticity to be generated, Eq. (7) and (8) will govern the stresses within the plastic zone (for a Coulomb material), provided that the onset of horizontal plasticity has not caused a change in the vertical stress i.e. the material strength in the vertical plane remains unchanged, leaving the vertical stress as an intermediate principal stress.

However, the analyses of plastic closure deformations presented previously are no longer precisely applicable to this case of shaft analysis. It will be recalled that Ladanyi, 1974, computed the closure due to the plastic zone around a tunnel based on the assumption of plane-strain, which allowed the volume of material in the plastic zone before and after

its formation to be compared while ignoring volume changes parallel to the tunnel axis. In the case of a shaft, the condition of plane-strain must be replaced by a condition of constant vertical stress (i.e. $\Delta\sigma_z = 0$). If such a modification were made, values of plastic shaft closure could be determined to produce a support pressure - closure characteristic curve such as that utilized in the previous analyses of tunnels. Lacking such an extension, the direct use of the tunnel analysis equations (see Figures 2 and 3 for different material characterization) will result in some error when applied to a shaft. It would be of interest to undertake the necessary analytical modifications to determine the significance of the errors. Despite several attempts, this extension has not been adequately derived within the scope of this work. Nevertheless, as a first approximation, the tunnel formulae may be used to derive a support pressure - closure characteristic curve for a shaft in rock (high $k_o$).

With regard to the minimum support pressure applicable to this case, we see that the situation is analogous to that of a tunnel side wall as indicated on Figure 7. The question of limiting equilibrium of gravity blocks is irrelevant for this case, as the vertical stress remains everywhere equal to the gravity stresses and thus the weight of any vertically bounded block is supported at its base by the in situ vertical stress (recalling that the spiral plastic slip lines in the horizontal plane are sections through vertical planes). Unlike a tunnel, for which the gravity block limiting equilibrium condition creates different characteristic lines for the crown, sidewalls and floor, only a single characteristic curve is applicable to this shaft case. Minimum support pressure may thus be variously defined as that required to avoid the onset of any plasticity, or as

that required to maintain a stable plastic zone, or as that pressure associated with some desired limit of radial closure.

In short, the foregoing case of a shaft in rock - or in any material for which $(k_o)$ actual > $(k_o)$ crit. as defined by Eq. (35) - may be approximately analyzed by using the two-dimensional tunnel equations previously derived and summarized in Figures 2 and 3, although with some degree of error due to the deviation from plane-strain conditions. This is precisely the approach taken classically by many investigators (Ostrowski, 1972, Weehuizen, 1959, Galanica, 1959), who have considered a shaft as a vertical tunnel in weightless material.

An interesting approach to the problem of predicting the formation pressure which will develop on a rigid liner placed at or near the shaft face has been suggested by Abel et al, 1979, in analyzing the results from an instrumented shaft at the Mt. Taylor mine. As this case history is analyzed in further detail in Section 4.6, the original paper has been included as an Appendix for reference purposes. In this section, the approach suggested by Abel is presented in more generalized form than in the original reference.

The problem under consideration is that of a concrete lined shaft in rock, for which the relatively rigid concrete lining is placed right up to the shaft face as soon as possible after excavation. The question is to predict the formation pressures which will develop against the liner as the shaft face is further advanced. The case is appropriate to a two-dimensional analysis on the basis of $k_o$ considerations.

From the 2-D tunnel equations previously developed, the radius of plastic zone which develops may be written, Eq. (12), as

$$r_e = r_i \left[ \frac{(P_o + S_{cp} - M_c \sigma_c)}{P_i + S_{cp}} \right]^{1/(N\phi p - 1)} \qquad (12)$$

for a Coulomb material. Thus, the formation pressure which develops on the lining, $p_i$, may be written in terms of the plastic zone radius, as;

$$P_i = (P_o + S_{cp} - M_c \sigma_c)(r_i/r_e)^{(N\phi p - 1)} - S_{cp} \qquad (36)$$

Note that this equation is analogous to that given in Abel's paper as Eq. (1), but is generalized to account for the difference between the plastic properties of the rock ($S_{cp}, N\phi p$) and the elastic properties of the rock ($M_c, \sigma_c$ ). If the material is considered as elastic perfectly plastic such that the plastic envelope is identical to the elastic peak strength envelope, then the above equation becomes identical with Abel's Eq. (1), given below in conforming notation;

$$P_i = \frac{2}{(N\phi+1)}\left[P_o + \frac{\sigma_c}{(N\phi-1)}\right](r_i/r_e)^{(N\phi-1)} - \frac{\sigma_c}{(N\phi-1)}$$

A variety of expressions similar to Eq.(36) may be readily developed for different material characterizations. For the four cases shown in Figures 2 and 3, the equations for the radius of plastic zone may simply be rewritten to express ($p_i$) as a function of ($r_e$). Abel quotes an additional expression based on a material characterization suggested by Talobre, 1957 (not reviewed - in French) which is essentially the same as Eq. (36) with the cohesion of the material in the plastic state set equal to zero. From any such expression which is selected as appropriate to the material involved, the formation pressure could be determined if the radius of plastic zone which develops is known. The key problem, therefore, is to assess the likely thickness of the plastic zone which develops.

Abel argues that (for this "rigid" lining case) the plastic zone will develop to that distance at which the radial stress, as determined from an elastic analysis of the zero internal pressure case, is just sufficient to provide the confinement necessary to resist the tangential stress, also determined from an elastic, $p_i = 0$, analysis. Thus, this limiting value of radial stress may be calculated, according to Abel, from knowledge of the elastic stress distribution for $p_i = 0$ and the failure criterion of the material. This is shown schematically on Figure 11, taken from Figure 5 of Abel's paper. The extent of plastic zone which has been determined in this manner must be associated with a specific value of internal support pressure or formation pressure as required by Eq. (36). Thus, the value of formation pressure, $p_i$, which will act on the lining may be directly predicted from Eq. (36) based on this assessment of plastic zone extent. Plotting the curves shown in Figure 11 is somewhat tedious, and Abel's approach may be undertaken analytically quite simply as follows.

As previously derived, the radial stress at the plastic - elastic boundary is given by Eq. (11) as:

$$\sigma_{re} = (p_o - M_c \sigma_c) \tag{11}$$

(Reference to Figure 2 will give other expressions for $\sigma_{re}$ for other material characterizations). Thus, $\sigma_{re}$ may be directly calculated from knowledge of the field stress, $p_o$, and the elastic material properties $M_c$ and $\sigma_c$. Then, for a purely elastic material, the radial stresses are given by Eq. (2) as:

$$\sigma_r = p_o - (p_o - p_i)(r_i/r)^2 \tag{2}$$

for zero internal pressure, this reduces to

$$\sigma_r = p_o [1 - (r_i/r)^2] \tag{37}$$

(Given as Eq. 4 in Abel's paper).

The radial stresses given by Eq.(37) and Eq.(11) are equated at $r = r_e$ to give;

$$r_e = r_i \Big/ \left(\frac{M_c \sigma_c}{p_o}\right)^{\frac{1}{2}} \tag{38}$$

The value of $r_e$ from Eq. (38) may then be substituted in Eq. (36) to determine the predicted value of formation pressure, $p_i$. Knowing this value for $p_i$, the actual distribution of radial and tangential stresses in the plastic zone may then be calculated if desired.

Conceptually, the justification for Abel's approach is somewhat difficult to see - the best argument seems to be as follows. Abel argues that, at a section just above the shaft face, the radial stresses are those which would occur for an elastic medium and zero support pressure i.e. Eq. (37). The tangential stresses which are generated, however, are much less than those predicted by an elastic analysis, due to the supporting or "stress shielding" action of the face. A lining is then placed up to the face, and the face is further advanced. As the face advances, removing the stress-shielding effect, the tangential stresses increase towards their maximum possible value, as given by the elastic analysis for the $p_i = 0$ case. However, the value which the tangential stress can actually reach is limited by the material strength, which is dictated by the value of the confining (radial) stress at any point. Hence, plasticity may be generated, commencing at the shaft wall and moving outwards until a sufficient radial stress value is reached to stop the process. During this process, deformations occur and the lining causes a reaction i.e. the value of support pressure $p_i$ increases. As the support pressure increases, the plastic zone growth is inhibited, and a balance is reached when the plastic zone

just extends to the point at which the radial stress is equal to the specific value of elastic - plastic interface stress appropriate to the material properties and remote stress field under consideration (Eq. 11). The support pressure associated with this balance is the predicted formation pressure.

The approach taken by Abel has two significant advantages - it is simple and, at least for the case analyzed by Abel, it appears to give very satisfactory results compared to measured values of formation pressures.

The specific analysis undertaken by Abel is summarized in Section 4.6, and is compared to an analysis of the same data based upon use of the two-dimensional "tunnel" equation to derive a support pressure - closure characteristic line diagram.

## 4.4 Three-Dimensional Analysis

The case for which plasticity of the material surrounding a shaft is initially generated by the vertical and radial stress difference, $(\sigma z - \sigma r)$, is treated by Terzaghi, 1942 and later by Coates, 1970. However, as previously demonstrated, this case is really only applicable to soils, rather than to rocks as assumed by Coates.

Referring to Figure 12, let us assume that, at a given depth in a shaft, plasticity has been generated by the $(\sigma z - \sigma r)$ stress difference, causing downwards and inwards movement of the material. Vertically acting shear stresses, $\tau_{rz}$, will thus be generated on cylindrical surfaces as shown in Figure 12 and the principal stresses will rotate by an amount, $\delta$, such that the state of stress upon an element near the shaft will be as shown in Figure 12. For ease of computation, a cohesionless Coulomb material will be considered, and the state of stress on an element may then be

represented in the Mohr diagram shown in the figure. We see that the principal stresses in the vertical plane have changed from $(\sigma_z - \sigma_r)$ to $(\sigma_1 - \sigma_3)$, due to the onset of plasticity.

For a case in which the principal stresses in the plastic zone remain parallel to the shaft (or tunnel) axis, tangential, and radial respectively, we see from Eq. (7) and (8) (see also Figure 2) that for a cohesionless Coulomb material the plastic zone stresses are given by:

$$\sigma_r = (P_i)(r/r_i)^{(N\phi p - 1)} \tag{37}$$

and

$$\sigma_\theta = N\phi p\,(P_i)(r/r_i)^{(N\phi p - 1)} \tag{38}$$

for the case shown in Figure 12, Terzaghi argues as follows. Due to the downwards and inwards movement of the shaft wall, wedging action will cause the (intermediate) tangential stress to increase to its maximum value compatible with the Mohr theory, which will be when it is equal to the major principal stress, $\sigma_1$. Thus, in the plastic zone,

$$\sigma_1 = \sigma_2 = \sigma_\theta \tag{39}$$

From the Mohr diagram, we see that the maximum ratio of vertical to radial stress which the material can sustain is given by:

$$(\sigma_z/\sigma_r) = N\phi_1 = \tan^2(45 + \phi_1/2) \tag{40}$$

We also note that $\phi_1 < \phi_p$.

If we undertake to analyze a horizontal section through the shaft, the maximum ratio of tangential to radial stress which could exist in the plastic zone is, from Eq. (39) and reference to the Mohr digram, given by:

$$(\sigma_\theta/\sigma_r) = (\sigma_1/\sigma_r) \tag{41}$$

However, from the Mohr diagram, it is clear that the ratio $(\sigma_1/\sigma_r)$ is always greater than the ratio $(\sigma_z/\sigma_r)$. Thus, if we analyze the section on the assumption that a stress ratio of only $(\sigma_z/\sigma_r)$ can be sustained, de-

fined by the flow value $N\phi_l$, this will give conservative answers as the actual stress ratio which can be sustained is greater than this, equal to $(\sigma_\theta/\sigma_r)$ as defined by the flow value $N\phi_p$. Thus, as a reasonable approximation, the stresses in the plastic zone may be determined from the 2-D equations Eq. (37) and (38) by replacing the value of $N\phi_p$ by $N\phi_l$, giving;

$$\sigma_r = p_i (r/r_i)^{(N\phi_l - 1)} \tag{42}$$

and

$$\sigma_\theta = N\phi_l (r/r_i)^{(N\phi_l - 1)} \tag{43}$$

Although the ratio $(\sigma_\theta/\sigma_r)$ is somewhat greater than $(\sigma_z/\sigma_r)$, Terzaghi assumes that, for purposes of analysis,

$$\sigma_\theta \cong \sigma_z \tag{44}$$

Similarly, an expression for the radius of the plastic zone, $r_e$, may be determined by replacing $N\phi_p$ by $N\phi_l$ in Eq. (12) which, for a cohesionless material, results in:

$$r_e = r_i \left[ \frac{p_o - M_c \sigma_c}{p_i} \right]^{1/(N\phi_l - 1)} \tag{45}$$

Equations (42), (43) and (44) thus give an approximate analysis of the stresses in the plastic zone, based upon modification to the two-dimensional tunnel analysis equations to account (approximately) for the rotation of principal stresses.

The primary goal of Terzaghi's analysis is to determine the minimum internal support pressure, $p_i$, which must be sustained. Just as in the tunnel analyses outlined previously, an upper bound value of $(p_i)_{min.}$ could be defined as that value necessary to avoid the onset of any plasticity, given by;

$$(p_i)_{min.} = 2p_o/(N\phi_e + 1) \tag{46}$$

A lower bound value, defined as that required to ensure that a stable plastic zone is formed ($r_e < \infty$) is satisfied for any value of $p_i$ greater than zero, from Eq. (45). However, to determine if this lower bound value can in fact be reached without instability, it is necessary to check the limiting equilibrium of potential gravity failure blocks. Terzaghi undertakes this check by considering a cylindrical potential failure block of radius r as shown in Figure 13. Due to the shear stresses acting on the vertical plane, $\tau_{rz}$, the vertical stress $\sigma_z$ is less than the gravity stress $\gamma z$, and hence the block is not held in simple equilibrium between the weight of the block and the vertical stresses at its base - unlike the previous two-dimensional case. For the block shown,

$$W = Q + S \tag{47}$$

were:

$$W = \pi(r^2 - r_i^2)\gamma z \tag{48}$$

$$Q = \int_{r_i}^{r} 2\pi r \sigma_z dr \tag{49}$$

$$S = 2\pi r z (\tau_{rz})_{AVG} \tag{50}$$

Using Eq.'s (42), (43), and (44) to determine the stresses acting, and Eq. (47) to check the limit equilibrium of the gravity block, it is then possible to determine the minimum support pressure which must be maintained in the shaft, as follows.

From the Mohr diagram, Figure 12, the value of the shear stress at given depth Z and radius r is given by:

$$\tau_{rz} = \sigma_r \tan \phi_2 \tag{51}$$

Assuming a linear increase in $\sigma_r$ with depth, the average shear resistance available along the cylindrical surface of radius r extending from ground surface to depth Z may be written

$$\tau_{rz} = (\tfrac{1}{2}\sigma_r) \tan \chi \tag{52}$$

Note that this is conservative, as the actual average value of the radial stress will be greater than $(1/2\sigma_r)$. Hence, from Eq. (50), we may write;

$$S = (2\pi rz)(\tfrac{1}{2}\sigma_r \tan\chi) \tag{53}$$

Thus, from Eq. (47), (48), (49) and (53),

$$\pi(r^2 - r_i^2)\gamma z - \int_{r_i}^{r} 2\pi r \sigma_z dr = (2\pi rz)(\tfrac{1}{2}\sigma_r \tan\chi) \tag{54}$$

Utilizing the stresses determined from Eq. (42), (43) and (44) we may write;

$$\tan\chi = \frac{n^2-1}{m_\sigma n^{N\phi_1}} - \frac{2N\phi_1}{N\phi_1+1}\ \frac{r_i}{z}\ \frac{n^{(N\phi_1+1)}-1}{n N\phi_1} \tag{55}$$

where: $$n = r/r_i \tag{56}$$

and $$m_\sigma = P_i/\gamma r_i \tag{57}$$

The location of the critical failure surface will be that for which the average shear stress reaches a maximum i.e at location $r_1 = n_1 r$ on Figure 13. For this, we set $d(\tan\chi)/dn = 0$ in Eq. (55) giving;

$$m_\sigma = \frac{z}{r_i}\ \frac{N\phi_1+1}{2N\phi_1}\ \frac{N\phi_1 - (N\phi_1-2)n_1^2}{N\phi_1 + n_1(N\phi_1+1)} \tag{58}$$

We also see, from Figure 13, that the maximum possible value that tan $\chi$ could achieve at a radius $r_1$ is equal to tan $\phi_2$, and thus, from Eq. (55);

$$\tan\phi_2 = \frac{n_1^2-1}{m_\sigma n_1^{N\phi_1}} - \frac{2N\phi_1}{N\phi_1+1}\ \frac{r_i}{z}\ \frac{n_1^{(N\phi_1+1)}-1}{n_1 N\phi_1} \tag{59}$$

The minimum required support pressure, embodied in the parameter $m_\sigma$, and the location of the critical surface of sliding, represented by $r_1 = n_1 r$

may be calculated for any depth from Eq. (58) and (59), provided values of $\phi_1$ and $\phi_2$ are known.

To assess the values of $\phi_1$ and $\phi_2$, Terzaghi utilizes an ingenious numerical analysis which results in the conclusion that, under conditions of minimum internal support;

$$\phi_1 \cong \phi_2 = (\phi_p - 5°) \text{ for } 30° < \phi_p < 40° \qquad (60)$$

Thus, for a material of known angle of internal friction in the plastic state, $\phi_p$, values of $N\phi_1$ and $\tan \phi_2$ may be calculated. For selected values of the depth ratio, $Z/r_i$, the parameter $m_\sigma$ may then be expressed as a function of the distance to the failure surface, $n_1$, from Eq. (58). Substituting in Eq. (59) then allows calculation of the value of $n_i$ and hence of $m_\sigma$, giving the required value of $(p_i)$ min. The results of this calculation, for the case of a cohesionless Coulomb material, are presented in the U.S. Department of the Navy Design Manual NAVFAC DM-7 and are reproduced as Figure 14. The results show, for materials of $\phi_p > 30°$ that a maximum value of the minimum support pressure is reached at a depth ratio $Z/r_i$ of approximately 4, whereas materials weaker than this will show a continued increase in required support pressure to depth ratios of about 10. As most shafts extend to depths of at least ten times their radius, it may be concluded that a limiting maximum value of required minimum support pressure is generally reached beyond which, for further advances of the shaft face, no increase in the necessary minimum support pressure occurs.

Thus, Terzaghi's approximate three-dimensional analysis may be viewed, in its essence, as a method of accounting for the necessary limit equilibrium check of potential failure blocks under the action of gravity. In both the tunnel and the shaft analyses stress distributions are ini-

tially calculated assuming a model of weightless material. For a tunnel, this model is corrected for gravity (in terms of the minimum support pressures required) by accounting for the limit equilibrium of the gravity blocks existing in the broken zone above the crown of the tunnel. For a shaft in which it is assumed that no vertical plasticity occurs ($k_o$ actual > $k_o$ critical), no correction is required as the vertical stresses in the walls remain equal to the gravity stresses. For a shaft in which vertical plasticity is generated ($k_o$ actual < $k_o$ critical), the Terzaghi approach provides the necessary correction for the support pressure required to resist the failure of vertical cylindrical gravity blocks in the shaft walls.

The limit equilibrium of gravity blocks which are not vertically sided provides the basis for the minimum support pressure predictions reviewed by Prater, 1977. Full assessment of Prater's paper would require a project of its own, as the work refers to a series of German language publications. However, several serious shortcomings are evident in Prater's paper. He refers to a shortcoming of Terzaghi's work in "its unrealistic prediction of the shape of the plastic zone which according to Terzaghi increases in radius with increasing depth reaching a limiting value asymptotically". This is not predicted by the Terzaghi approach. Whereas the minimum support pressure, based on limit equilibrium, does reach a limiting value, this is by no means a prediction of the radius of the plastic zone. It simply reflects the fact that, within a plastic zone of some unspecified extent, the location of the critical (vertical) slip surface reaches a limiting distance from the shaft wall. Terzaghi does, however, utilize a calculation of the stresses in the plastic zone to define the stresses acting upon the potential failure surface - chosen to

be a vertical cylindrical annulus with a horizontal base. This step is ignored by Prater, and apparently by the German work which he reviews, giving rise to a serious error. Without regard to the effect of shedding of excess vertical stress away from the plastic zone around the shaft, Prater et al go directly to a limit equilibrium analysis of a potential truncated cone failure block, shown in Figure 15. In assessing the equilibrium of the block, it is assumed that the tangential stress (and hence the tangential force, T) is related to the vertical stress by an earth pressure coefficient (variously assumed as $k = 1$; $k = (1 - \sin \phi)$; etc.) and that the vertical stress is equal to the overburden stress ($\gamma z$). As the tangential force has an outward acting wedging component, F, which tends to stabilize the block, this wedging component is thus related linearly to the overburden depth. Hence, as the shaft depth increases to infinity;

$$\sigma_z = \gamma z \rightarrow \infty$$
$$T = k(\gamma z) \rightarrow \infty$$
$$F = f(T) \rightarrow \infty$$

As the wedging force goes to infinity, the block cannot fail, and the result is thus predicted that the support pressure required decreases to zero at an infinite shaft depth - a result which hardly seems likely. This deficiency is noted by Walz, 1978, in his discussion of Prater's paper. However, as all of the significant referenced work is in German, notably in a Ph.D. thesis by Walz, this material has not been accessed for the current project. The work refers to the case of shafts in soil, and may provide useful additional insights to this problem.

## 4.5 Criticisms, Extensions and Comments

Two basic approaches to the analysis of formation pressures around shafts have been presented in the foregoing sections. Firstly, a two-dimen-

sional approach was presented, generally applicable to shafts in rock and based upon the same analytical expressions as those applicable to the analysis of a tunnel under plain strain conditions. Secondly, a three-dimensional approach was reviewed, generally applicable to shafts in soil and based upon approximate modifications to the two-dimensional stress analysis equations combined with an assessment of limit equilibrium conditions around the shaft. Both methods are approximate in many areas, and some criticisms, extensions and comments to the methods are briefly outlined in this section.

### 4.5.1 Field Stresses

For all analyses presented it has been assumed that the field stresses in the plane of the cross-section are hydrostatic. In general, this is a reasonable assumption for shaft analysis. If specific data are available to indicate a non-hydrostatic state of stress the analyses may be modified, although at the cost of increased complexity. Muir-Wood, 1975, and Pender, 1980 indicate methods by which unequal field stresses may be accounted for in analysis.

### 4.5.2 Horizontal and Vertical Plasticity

In differentiating between the cases appropriate to two-dimensional and three-dimensional analysis respectively (Section 4.2.1), it was implicitly argued that creation of horizontal plasticity due to a tangential - radial stress difference would not significantly alter the elastic material properties in the vertical plane. As shown in Abel's paper (see Appendix,

Figure 4) the cracking around a shaft in rock (a two-dimensional, horizontal plasticity case) tends to form vertically sided cylinders, and it may thus be argued that the material strength in the vertical direction remains essentially intact. However, large scale disruption of the material due to the $(\sigma_\theta - \sigma_r)$ stress difference is in fact likely to affect the vertical strength. Thus, if determination of the absolute minimum support pressure (formation pressure) is being sought, it would generally be prudent to assume that the Terzaghi model of limit equilibrium under conditions of vertical plasticity may apply, and the stability of the lining checked for this value. As the minimum pressures given by this approach are small (see Figure 14), they will generally not control the lining design.

### 4.5.3 Material Characteristic

The four cases of different elastic and plastic material characterizations presented on Figures 2 and 3 cover a very wide range, and should provide an adequate basis for most situations. Additional characterizations have been presented by Talobre, 1957 and Rabcewicz, 1964. However, these characterizations are in fact special cases of the more general characterizations given in the four cases presented.

### 4.5.4 Failure Criteria

The failure criteria embodied in the four cases presented include both shear stress criteria and principal stress criteria (Hoek-Brown envelope). Trollope, 1970 suggests that a criterion of maximum effective tensile stress may be more appropriate for shafts in hard rock than a Mohr-Coulomb criterion. His argument rests on the observation that a failure generated by a $(\sigma_z - \sigma_r)$ stress difference around a shaft cannot occur

unless the failed element of rock is freed from the surrounding rock (by joints, for instance) and thus able to move downwards and inwards along the inclined shear surface. Note, however, that the discussion in Section 4.2.1 implies that such a failure is very unlikely in a hard rock shaft. Nevertheless, Trollope defines an effective tensile stress criterion as:

$$\overline{\sigma_t} = \sigma_3 - \nu(\sigma_1 + \sigma_2)$$

This criterion may be introduced to the analysis of stresses around the shaft to give a critical depth of shaft at which such failure will first initiate. Trollope suggests that structural support sufficient to avoid such failure should be installed. As previously noted, however, the provision of internal support sufficient to avoid any failure (plasticity) is unnecessarily stringent. The above failure criterion could readily be utilized within the analytical framework presented, and would modify the calculated support pressure at which failure first initiates, the radius of plastic zone etc., and may be valid for brittle rocks which tend to display strain-extension fracturing under low confining stresses. In essence, this is simply a modification to the material characterization chosen.

### 4.5.5 Deformations

For the two-dimensional analysis of a shaft section, it was noted that use of the plane-strain tunnel formulation to determine radial deformation is not strictly valid, although the errors are likely to be small. For the Terzaghi type of three-dimensional model, no reference material is available concerning deformation analyses. While such a task might be fruitful, the use of numerical analysis techniques by computer modelling world generally be preferable. As a very approximate guide, the shaft wall movements necessary to allow the full mobilization of shear strength along

the limiting equilibrium surface selected could be roughly deduced from the strains measured at peak strength in testing the material. Coates, 1970, indicates this approach.

### 4.5.6 Face Effect

As discussed in Section 3.4.4.1 with reference to tunnels, the face of the excavation provides a supporting or stress-shielding effect. Panet, 1974, suggests that the effect of the face upon the deformations of a section immediately behind the face is equivalent to maintaining a fictitious internal support pressure of about 2/3 the field stress, with this effect reducing to near zero at a distance of about four radii from the face. Galle, 1962, suggests that the stresses in the elastic walls of a vertical well are equal to those calculated by two-dimensional analysis at any distance greater than about 3 radii from the face. However, both of the above analyses are based upon elastic models, and could usefully be extended to compare numerical 3-D elastic - plastic models with 2-D elastic - plastic models.

### 4.5.7 Thickness of Plastic Zone

Ostrowski, 1972, in one of the more interesting papers available on the analytical design of shafts, used the theory of the strain energy of distortion to predict the thickness of plastic zone. The apparent advantage of such an approach is that it deals with volumetric and shear stress invariants, thus including the effect of the intermediate principal stress. Unfortunately, derivation and application of the relevant equations is only briefly presented in Appendices, making them difficult to follow. Abel, 1979, has found that the use of Ostrowski's approach gives values which are

not compatible with field data, and there would therefore seem to be little advantage in its use.

### 4.5.8 Time Dependence

No consideration has been given to the effects of time dependence of material properties in the foregoing analyses, and reference should be made to the comments on this topic under Section 3.4.4.2.

### 4.5.9 Face Stability

An additional stability phenomenon which is well known during shaft sinking, particularly in soils, is that of heave of the face. The question of face stability has not been reviewed herein, although this does not imply that it is of minor importance. Indeed for many shafts it is the critical stability concern, and its omission here is due solely to lack of time. Some interesting work was instigated by Broms, 1967, and extended by Attewell, 1971, on the question of stability ratios in saturated clays (i.e. the determination of critical values of the ratio of undrained shear strength to overburden stress at which intrusion of the clay into the shaft or tunnel face would occur). Review and extension of this work to provide guidance for shaft design in a wider variety of materials including both soils and rocks would be a useful undertaking.

## 4.6 Case History Analysis

In order to provide validation for the analytical approaches outlined in this report, the literature was surveyed to obtain case history data which could be analyzed. Unfortunately, only a single paper - that by Abel et al, 1979 - was found which contained data which was at all adequate

to provide a case history. This scarcity of published case history data on shaft analyses and field measurements is a serious deficiency in trying to assess the most appropriate analytical approaches for various shafting conditions. The author is grateful to Dr. Morgenstern for uncovering the paper by Abel.

Most published reports on shaft sinking projects contain data on advance rates and shaft excavation techniques, but with only fragmentary information (if any) on the properties of the formations being penetrated, the basis of design of the shaft linings, and the field performance of the linings in terms of stresses or deformations. Such papers include those by Pack and Skinner, 1976; Barron and Toews, 1963; Gooch and Conway, 1976; Redpath, 1971; Collins and Deacon, 1972; Hulshizer et al, 1976; Lambert, 1968; Grieves, 1974; Sibson, 1968;' and Zahary and Unrug, 1972. According to Zahary "Interesting results were obtained recently in Poland and Russia using dynamometer and strain gauges installed in the shaft lining. Lateral pressures measured showed wide variations, particularly in competent rocks". Unfortunately, the results are not presented, with reference being made to the Russian language publications of Krupiennkow, 1963 and Unrug, 1970.

The paper by Abel, Dowis and Richards, 1979, is, therefore, a particularly useful contribution, containing adequate data on the formation properties and field stress, the concrete lining, and the results of lining stress measurements at the 14 foot diameter Mt. Taylor mine shaft. This paper has been attached for reference as an Appendix to this report.

In his paper, Abel suggests an interesting approach to the problem of predicting the formation pressures which develop upon a rigid concrete liner cast close to the excavation face as the face advances. The basis of

the analysis has been presented in Section 4.3. Sufficient data is presented in Abel's paper to provide a quantitative example and validation of the analytical approaches suggested in this report. In this section, the data applicable to the 3032 foot level of the Mr. Taylor shaft is analyzed both by the method suggested by Abel, modified somewhat to allow the analysis to be undertaken in a more general form, and by the support pressure - closure characteristic line method. An interesting and worthwhile comparison emerges.

While reference may be made to the attached paper for more detail, the critical elements of the data necessary for analysis are summarized below, with notation conforming to that used in this report.

Field Stresses

$\sigma_v$ = 2906 psi, based on overburden load
$p_o$ = 2150 psi, based on hydrofracture stress measurements
$k_o$ = 2150/2906 = 0.74

Shaft Geometry

$r_i$ = 7 ft.
Depth = 3032 ft.

Material Characterization

Linear Mohr-Coulomb

i) Elastic Properties:

$\sigma_c$ = 500 psi (uniaxial compressive strength), based upon reduction of intact specimen strengths by a factor of about 5
$\phi_e$ = 29°. Hence $N_{\phi e} = \tan^2 (45 + \phi_e/2) = 2.90$
E = 60,000 psi.

ii) Plastic Properties:

$\sigma_{cp}$ assumed to vary linearly from 0 psi at the shaft wall to 500 psi at the elastic-plastic interface ($r = r_e$). Therefore, $(\sigma_{cp})$ AVG. = 250 psi.

$\phi_p = \phi_e$ = 29°. Hence $N_{\phi e} = N_{\phi p}$ = 2.90

Liner Properties

$t_c$ = 24 inches (thickness of concrete)
$E_c$ = 4.03 x $10^6$ psi
$f'_c$ = 5,000 psi (uniaxial compressive strength)

Abel proceeds directly to utilize two-dimensional analyses, which implicitly assumes that the stress difference which governs formation of a plastic zone is the tangential - radial stress difference. Following Section 4.2.1, this assumption may be checked explicitly as follows:

$$(k_o)_{crit.} = \frac{1}{2} + 1/(2 N\phi_e) - \sigma_c/(2 N\phi_e \sigma_z) \quad (35)$$

Substituting the relevant figures gives:

$$(k_o)\text{crit.} = 0.64$$

As: $$(k_o)\text{actual} = 0.74$$

we see that $(k_o)$ actual > $(k_o)$ critical, which defines a condition for which plasticity will occur in the horizontal plane, generated by the $(\sigma_\theta - \sigma_r)$ stress difference. As argued in Section 4.2.1, this condition allows use of a 2-D analysis.

As outlined in Section 4.3, Abel criticizes the equation relating support pressure to plastic zone radius derived from Terzaghi's work on the basis that it applies to an elastic - perfectly plastic material. The more general form of equation for a linear Coulomb material having different elastic and plastic properties may be substituted, as given by Eq. (12), where:

$$r_e = r_i \left[ \frac{(P_o + S_{cp} - M_c \sigma_c)}{P_i + S_{cp}} \right]^{1/(N\phi_p - 1)} \quad (12)$$

While other material characterizations could be used, see Figure 2, the test data on the formation materials is not presented by Abel in sufficient

detail to allow this. The relevant terms for the above, and following, equations may be readily determined from the data as:

$$P_o = 2150 \text{ psi}$$

$$S_{cp} = C_p / \tan\phi_p = 132 \text{ psi}$$

$$M_c = [1 + (N\phi_e - 1) P_o/\sigma_c]/(N\phi_e + 1)$$

$$M_c = 2.35$$

From Eq. (11), the radial stress at the elastic-plastic interface is given by:

$$\sigma_{re} = (P_o - M_c \sigma_c) \qquad (11)$$

from which;

$$\sigma_{re} = 975 \text{ psi}$$

Note that this simply derived value agrees exactly with the value determined by Abel using a more complex iterative procedure (Eq. 11 in Abel's paper).

For a purely elastic material, the radial stress distribution under conditions of zero internal support pressure (i.e. immediately upon excavation and before a lining reaction has developed) are given from Eq. (2) as:

$$\sigma_r = P_o[1 - (r_i/r)^2]$$

Hence, at r = a distance, $r_e$,

$$\sigma_{re} = P_o[1 - (r_i/r_e)^2]$$

From which, $r_e = 1.35\ r_i$

which agrees with Abel's value. Abel then suggests that the lining pressure which will develop is that which is appropriate to the above value of plastic zone radius. Abel uses a formulation for elastic material given by Talobre, 1957, and obtains a predicted value of support pressure as:

$$p_i = 506 \text{ psi}$$

Using the general Coulomb material representation given in Eq. (12), with the parameters determined from the given data gives;

$$p_i = 494 \text{ psi}$$

which is seen to agree very closely with Abel's predicted value. The actual measured support pressure which developed at the 3032 foot level was 548 psi giving agreement within 10 per cent of the above predicted values. Considering the many major assumptions which have been made concerning the material properties (for instance, the lineal increase of unconfined compressive strength from 0 to 500 psi over the thickness of the plastic zone) and the approximate nature of the 2-D approach, this agreement may reflect a considerable degree of good fortune. Nevertheless, the agreement does exist and suggests that Abel's approach, generalized to the form given here, may provide a very rapid, simple and reasonably accurate prediction of rigid lining stresses.

Production of a complete support pressure - closure diagram is a good deal more cumbersome. We proceed by calculating the radial closure of the shaft, $U_i$, according to the equations summarized on Figures 2 and 3 for progressively decreasing values of internal support pressure, $p_i$. The steps are as follows.

For each value of $p_i$, the radius of plastic zone is calculated from Eq. (12)

$$r_e = r_i \left[ \frac{(P_o + S_{cp} - M_c \sigma_c)}{(P_i + S_{cp})} \right]^{1/(N\phi p - 1)} \qquad (12)$$

from which the value of $r_e$ first becomes greater than $r_i$ (onset of plasticity) at $p_i$ = 975 psi. Note that this may also be determined from Eq. (11);

$$\sigma_{re} = (p_o - M_c \sigma_c) \tag{11}$$

Starting at $p_i$ = 975 psi, for each further reduction in $p_i$, the displacement of the elastic-plastic interface, $U_e$, is calculated from Eq. (17)

$$u_e = \frac{(1+\nu)}{E} (M_c \sigma_c) r_e \tag{17}$$

A value of $\nu$ = 0.20 was assumed (Not given in Abel's paper). The calculated thickness of plastic zone, Eq. (12) is assessed to see whether it is a thin zone (i.e. $r_e/r_i < \sqrt{3}$) or thick zone ($r_e/r_i > \sqrt{3}$) and the appropriate value of the parameter $R_c$ calculated by:

Thin zone; $R_c = 2 D_c \ln(r_e/r_i)$ (26)

Thick zone; $R_c = 1.1 D_c$ (27)

where Dc is the ratio of plastic dilation to plastic shear strain,

$$D_c = -\sin\phi_e \tag{20}$$

The average plastic dilation, $e_{av}$, may then be calculated for each step from Eq. (25) as:

$$e_{av} = \frac{2(u_e/r_e)(r_e/r_i)^2}{[(r_e/r_i)^2 - 1][1 + 1/R_c]} \tag{25}$$

Note that negative values are obtained for $e_{av}$, indicating volume increase of the plastic zone. Finally, the total closure (elastic plus plastic) of the shaft wall is calculated from Eq. (28) as:

$$u_i = r_i \left[1 - \left(\frac{1 - e_{av}}{1 + A}\right)^{\frac{1}{2}}\right] \tag{28}$$

where the parameter A is equal to:

$$A = (2u_e/r_e - e_{av})(r_e/r_i)^2 \qquad (29)$$

The resulting characteristic line of support pressure versus closure is given for the 3032 foot level of the Mt. Taylor shaft in Figure 16.

In order to predict the lining pressure, it is necessary to calculate the lining stiffness. Following Hoek and Brown, 1980, the stiffness of the concrete lining, kc, is given by;

$$k_c = \frac{E_c[r_i^2-(r_i-t_c)^2]}{(1+\nu_c)[(1-2\nu_c)r_i^2+(r_i-t_c)^2]}$$

Note that $r_i$ refers to the excavated radius of the shaft and not to the internal radius of the concrete lining as incorrectly shown in the reference. Choosing a value of Poisson's Ratio for the concrete of $\nu_c = 0.2$, gives

$$k_c = 1.48 \times 10^6 psi = \Delta P_i/\Delta(u_i/r_i)$$

As discussed in Section 3.4.4.1 and Section 4.5.6, the effect of the shaft face, according to Panet, 1974, is to provide a "fictitious" internal support pressure of roughly (2/3) $p_o$. Thus, if the lining is assumed to be poured right up to the excavation face, the liner installation will have taken place at a closure appropriate to a support pressure of $p_i$ = (2/3) $p_o$. If no further factors were involved, the lining would then deform according to its stiffness to produce an equilibrium support pressure of about 1100 psi as shown on Figure 16. However, Abel calculates that the combined effects of concrete shrinkage and creep give rise to a radial closure of about 0.25 inches. Shifting the lining reaction curve by this amount, gives an equilibrum support pressure of about 740 psi. This has been referred to as $(p_i)$ max., as it represents the maximum possible formation pressure which could develop upon the lining

if the lining were poured right up to the excavation face and in perfect contact with the rock. In reality, some gap will exist between the end of the lining and the shaft face, allowing some additional inwards deformation of the rock to occur before the lining is placed. A rough approximation to the amount of additional closure occurring due to this gap might be obtained by assuming that the full shaft closure of approximately 4 inches would occur with an unsupported gap of about 4 radii from the face (Panet, 1974), and simply pro-rating this closure according to the unsupported gap actually left. By this very crude method, a gap of about 1-1/2 ft. would account for an additional wall closure of 0.2 inches, shifting the origin of the lining reaction curve by this amount and producing an equilibrium support pressure of 550 psi, as measured in the field. Even without this refinement - more properly considered as fiddling - the results of the characteristic line analysis are very encouraging. The analysis indicates a predicted upper limit to the formation pressure which could be expected of 740 psi. Design of the liner to resist this stress could justifiably be undertaken with a reduced factor of safety, in the knowledge that the actual liner will not be installed flush to the excavation face. On this basis the factors of safety for the 24 inch concrete liner, based on a 5,000 psi concrete compressive strength are, from use of Lame's thick-walled cylinder equation,

$$\text{for } (p_i)\ \text{max.} = 740 \text{ psi, F.S.} = 1.35$$
$$\text{for } (p_i)\ \text{actual} = 548 \text{ psi, F.S.} = 1.82$$

Thus, use of the characteristic line method to determine a maximum formation pressure, and use of this pressure to design the liner on the basis of a factor of safety of 1.3 to 1.4 appears justified as the actual factor of safety will then be higher than this, depending upon how much gap is left between the shaft face and the lining. The advantage of the

characteristic line method is that it provides a fairly complete picture of the shaft lining response, such that the effects of changes in construction sequence or modifications to the lining stiffness can be reasonably assessed, providing a rational basis for decisions. Abel's method has the advantage of simplicity, but provides only a "single-point" answer, for which prudence would suggest that a somewhat more generous factor of safety be used.

## 5.0 FURTHER WORK

It is not intended in this section to provide an exhaustive listing of possible extensions to the question of shaft analysis which could be undertaken. Numerous areas of deficiency are undoubtedly evident upon reading of this report. However, during the progress of this work two major concerns were persistently encountered which would benefit greatly from further investigation.

The greatest single deficiency is the lack of well documented case histories on shafts. Considering the antiquity of shaft sinking, the vast number of shafts which have been sunk, and the high cost of the substantial linings which are normally placed, this is a somewhat surprising lack. As with any area of geotechnical engineering, it cannot be presumed that any analytical methodology provides an adequate model of reality until such methods have been tested against the actual performance of structures. The lack of published data on shaft performance, including adequate detail on formation material properties, in situ stresses, and lining response represents a serious stumbling block to the validation of appropriate predictive techniques for formation pressures. Research field programs aimed at gathering such data must be considered a high priority if we are to advance to a state of rational lining design for shafts.

A second area within which research work would provide significant benefits is the utilization of numerical techniques capable of including the three-dimensional effects occurring near a shaft face for the purpose of calibrating or correcting the more simply based two-dimensional analytical techniques. The latter have the benefit of relative simplicity and speed, and hence may be inexpensively utilized. However, analysis of the stresses, deformations and generation of plastic zones at or near the shaft

face cannot be undertaken by simple models, and require that the 2-D models be corrected for 3-D effects based upon a more complete understanding derived from numerical modelling. The work of Panet, 1974, while useful in this regard, deals only with very limited cases. Recent numerical models suggested by Hanafy and Emery, 1980, appear useful as a basis for a comprehensive assessment of 3-D effects, time-dependence, liner placement sequence etc. which would provide considerable benefit to the correction and calibration of 2-D analytical approaches.

The above two areas are viewed as high priority research needs. Beyond these, many areas of fruitful and important research may be envisaged. The question of shaft lining design for drilled shafts utilizing stabilizing muds and jacked-in liners is becoming of increasing importance as drilling equipment becomes available for the provision of large diameter shafts. The increasing use of subsurface space for housing a wide variety of facilities, often at considerable depth and with stringent operating or safety requirements, is evident in such schemes as radioactive waste storage, compressed air energy storage, and underground mining of tar sands deposits. In all such projects shafts will provide the lifeline link to the surface, and the assurance of adequate methods of designing such shafts will be an important responsibility of the geotechnical community.

## LIST OF REFERENCES


Abel, J.F., Dowis, E. and Richards, P. "Concrete Shaft Lining Design" 20th U.S. Symp. on Rock Mech., Austin, Texas, 1979

Attewell, P.B. and Boden, J.B. "Development of Stability Ratios for Tunnels Driven in Clay" Tunnels and Tunnelling pp. 195-198 Vol. 3, No. 3, May 1971

Barron, K and Toews, N.A. "Deformation Around a Mine Shaft in Salt" Proc's. 2nd Can. Symp. on Rock Mechanics, pp. 115-134, Kingston 1963

Brockenbrough, R.L. "Steel Linings for Deep Mine Shafts" Trans. Soc. Min. Engs. AIME Vol 258 pp. 132-136, 1975

Broms, B.B. and Bennermark, H. "Stability of Clay in Vertical Openings" Proc's. ASCE Soil Mech. and Fndtn. Eng. Div., Vol. 193 Part 1, 1967

Coates, D.F. "The Effect of Stress Concentrations on the Stability of Tunnels" Proc. 1st Congr. ISRM Vol. 2, 1966

Coates, D.F. "Rock Mechanics Principles" Dept. Energy Mines & Resources, Mines Branch", Monograph 874 Revised 1970

Collins, S.P. and Deacon, W.G. "Shaft Sinking by Ground Freezing: Ely Ouse-Essex Scheme, U.K." Proc. Inst. Civ. Engrs. Suppl. No. 7506S, 1972

Collins, S.P. "The Three Valley Aqueductin Tunnel" Tunnels and Tunnelling Vol. 4 No. 5 pp. 441-445, 1972

Curtis, D.J. and Rock, T.A. "Tunnel Linings-Design?" in: Computer Methods in Tunnel Design, Inst. Civ. Engrs., 1978. Symposium on Shafts and Shaft Sinking. The Chem. Metall. and Min. Soc. of South Africa, 1948/1949

da Fontura, S.A.B. "Time-Dependent Response of Rock Masses During Tunnelling" Ph.D. Thesis, Univ. of Alberta, 1980

Daeman, J.J.K. "Problems in Tunnel Support Mechanics" Underground Space, Vol. 1 pp. 163-172, 1977

Dahl, D. and Voight, B "Isotropic and Anisotropic Plastic Yield Associated with Cylindrical Underground Excavations". Proc's Int. Symp. on Large Underground Openings, Oslo 1969

Deere, D.U. et al. "Design of Tunnel Liners and Support Systems" Nat. Tech. Inf. Service PB183799, 287 pp.

Deere, D.U., Peck, R.B. et al. "Design of Tunnel Support Systems" Highway Research Record No.339, Transp. Res. Board, Washington, 1970

Desai, C.S. and Reese, L.C. "Stress-Deformation and Stability Analyses of Deep Boreholes" Proc's 2nd Congr. ISRM paper 4-13, pp.475-484, Belgrade, 1970

Dixon, J.D. and Mahtab, M.A. "A Method for Computing Stabilization Pressures for Excavations in Incompetent Rock" U.S. Bureau of Mines. Report of Investigation RI8128, 1976

Dschandshgawa, J. et al. "The Results on Rock Pressure of Deep Mines of Tkibuli-Shaori (USSR) Coal Deposits" Proc. 2nd Congr. ISRM, Theme 4 No.10, Belgrade, 1970

Fairhurst, C. and Daemen, J.J.K. "Practical Inferences from Research on the Design of Tunnel Supports" Underground Space Vol. 4 No. 5, pp. 297 -311, 1980

Florence, A.L. and Schwer, L.E. "Axisymmetric Compression of a Mohr-Coulomb Medium Around a Circular Hole" Int. Journal for Numerical and Analytical Methods in Geot. Eng. Vol. 2, pp. 367-379, 1978

Galanka, J. "Problems of Shaft Sinking in Poland" Op. cit.

Galle, E.M. and Wilhoit, J.C. "Stresses Around a Wellbore Due to Internal Pressure and Non-Symmetrical Geostatic Stresses" Soc. Petrol. Eng's Journ. Vol. 2, No. 2, pp. 145-155, 1962

Golder Associates and J.F. Maclaren Ltd. "Tunnelling Technology: An Appraisal of the State of the Art for Application to Transit Systems" Publ. Ontario Ministry Trans. and Comm., 1976

Gooch, A.E. and Conway, J.P. "Field Measurements and Corresponding Finite Element Analysis of Closure at the Lucky Friday Mine in the Coeur D'Alene District, Idaho" U.S. Dept. Interior, Bureau of Mines, Research Report R18193, 1976

Grieves, M. "Shaft Sinking at Boulby Mine" Tunnels and Tunnelling pp. 32 - 34, July 1974

Hanafy, E.A. and Emery, J. "Advancing Face Simulation of Tunnel Excavations and Lining Placement" Proc's 13th Can. Symp. on Rock Mechanics, Toronto, 1980

Hebblewhite, B.K., Miller, H.D.S., Potts, E.L.J. "A Method for Predicting Time Dependent Deformations in Evaporite Around a Vertical Shaft" Proc's Conf. Rock Eng. Brit. Geot. Soc. Vol. 1, pp. 529-539, 1977

Hoek, E and Brown, E.T. "Underground Excavations in Rock" Restricted Circulation Draft: to be published by Inst. Min. & Met., London, 1980

Horvath, J. "Calculation of Rock Pressure in Shafts and Roadways of Circular Section" Int. Journal Rock Mech. and Min. Sci. Vol. 8, pp. 239-276, 1971

Hulshizer, A.J., Desai, A.J., Dave, B.J. "Drilling and Lining of Ocean Shafts - Seabrook Power Project" Proc's RETC, pp. 148-168, Las Vegas, 1976

Jacobsen, S. "Pressure Distribution in Steel Lined Rock Tunnels and Shafts" Int. Water Power and Dam Const. Vol. 29 No. 12, pp. 47-51, 1977

Jaeger (1969) p 192
Jaeger, J.C. "Elasticity, Fracture and Flow" J. Wiley and Sons, 1956

Kaiser, P.K. "Effect of Stress History on the Deformation Behavior of Underground Openings". Proc. 13th Can. Symp. on Rock Mechanics, Toronto, 1980

Kitamura, I. (ed.) "Tunnelling Under Difficult Conditions" Proc's Int. Tunns. Symp. Tokyo, 1978

Ladanyi, B. "Use of the Long-Term Strength Concept in the Determination of Ground Pressure on Tunnel Linings" Proc's 3rd Congress ISRM. Vol. II Part B, Denver, 1974

Ladanyi, B. "Direct Determination of Ground Pressure on Tunnel Lining in a Non-Linear Viscoelastic Rock" Proc's 13th Can. Symp. on Rock Mechanics, Toronto, 1980

Lambert, R.N. "High Speed Shaft Sinking in South Africa" Proc's Tunnel and Shaft Conf. Ed. D.H. Yardley, pp. 195-214, Minnesota, 1968

Lombardi, G. "The Influence of Rock Characteristics on the Stability of Rock Cavities" Tunnels and Tunnelling Vol. 2 No. 2, pp. 19-22 and Vol. 2 No. 3, pp. 104-109, 1970

Lombardi, G. "Dimensioning of Tunnel Linings" Tunnels and Tunnelling, pp. 340-351, Vol. 5 No. 4, July 1973

Longden, H.A. "Current Techniques in Deep Shaft Sinking and Development" Can. Min. Journ. V. 90 No. 3, pp. 61-65, 1969

Mayo et al. "Tunneling - The State of the Art. A Review and Evaluation of Current Tunneling Techniques and Costs with Emphasis on Their Application to Urban Rapid Transit Systems in the U.S.A." U.S. Dept. Housing and Urban Devel., Contract H-766 NTIS: PB178036, 263 pp., 1968

Morrison, R. and Coates, D. "Soil Mechanics Applied to Rock Failure in Mines" Trans. CIM Vol. 58, 1955

Muir-Wood, A. "The Circular Tunnel in Elastic Ground" Geotechnique Vol. 25 No. 1, pp. 115-127, 1975

Onischev, U. "Ground Stress in Vertical Shafts" Ugul, Dec. 1959 (in Russian)

Ostrowski, W.J.S. "Design Considerations for Modern Shaft Linings" Can. Min. and Met., Trans. CIM, Vol. LXXV, pp. 184-198, 1972

Pack, P.D. and Skinner, E.H. "Design Review of a Rectangular Shaft In Alluvium" Proc's 17th U.S. Symp. on Rock Mech., Utah 1976

Panet, M. "Contribution to the Design of Tunnel Support Behind the Face" proc's 3rd Cong. ISRM Vol. II Part B, pp. 1163-1168 (in French), 1974

Peck, R.B. "Deep Excavations and Tunnelling in Soft Ground" State of the Art Report, Proc's 7th Int. Conf. Soil Mech. Fndtn. Eng., Mexico 1969

Pender, M.J. "Simplified Analysis for Tunnel Supports - Discussion" ASCE Journ. Geot. Eng. Div., Vol. 106 No. GT-7, pp. 833-835, July 1980

Poulos, H.G. and Davis, E.H. "Elastic Solutions for Soil and Rock Mechanics" J. Wiley and Sons, 1975

Prater, E.G. "An Examination of Some Theories of Earth Pressure on Shaft Linings" Can. Geot. Journal Vol. 14 No. 1, pp. 91-106, 1977

Redpath, J.S. "Sinking the Creighton No. 9 Shaft at Sudbury" Min. Congr. Journal Vol. 57 No. 3, pp. 66-70, 1971

Shtein, M.S. "The State of Stress Near the Bottom of a Mine Shaft" Soviet Mining Science Vol. 9, pp. 123-128, 1973

Sibson, J.N.S. "Photoelastic Investigation of Shaft Stress Changes Due to Mining" Trans. Inst. Min. & Metall. Section A. Min. Ind. V. 77 No. 1, pp. A34-A36, 1968

Swaisgood, J.R. and Versaw, R.E. "Geotechnical Investigations for Mine Shafts" Mining Engineering Vol. 26 No. 6, pp. 37-40, 1974

Terzaghi, K. "Theoretical Soil Mechanics" J. Wiley and Sons, 1942

Trollope, D.H. "The Stability of Deep Circular Shafts in Hard Rock" Proc's 2nd Cong. ISRM Vol. 2 paper 4-39, Belgrade 1970,

U.S. Department of the Navy. "Design Manual: Soil Mechanics Foundations and Earth Structures" NAVFAC DM-7, March 1971

Wagner, H. "The Application of Rock Mechanics Principles to Strata Control in South African Gold Mines" Proc. 10th Can. Rock Mech. Symp., pp. 247-280, 1975

Walz, B. "Discussion" Can. Geot. Journ. Vol. 15 No. 3, pp. 438-440, 1978

Weehuizen, J.M. "New Shafts of the Dutch State Mines" Symp. on Shaft Sinking and Tunnelling, Inst. Min. Eng., London 1959

Westergaard, H.M. "Plastic State of Stress Around a Deep Well" Jour. Boston Soc. of Cw. Eng. Vol. XXVII No. 1, Jan. 1940 in Contributions to Soil Mechanics, 1925-1940

Wichur, A. "Rock Pressure on the Shaft Circumference as a Normal Stationary Probability Function Archiwum Gornictwa 6.1, 1970

Wilson, J.W. "Shaft Sinking Technology and the Future Needs of the Mining Industry" Proc's RETC, pp. 103-125, Las Vegas, 1976

York, B. and Reed, J.J. "An Analysis of Mine Opining Failure by Means of Models" Trans. AIME Mining Branch V. 196, pp. 705-710, 1953

Zahary, G. and Unrug, K. "Reinforced Concrete as a Shaft Lining" Proc. 8th Can. Rock Mech. Symp., pp. 265-282, 1972

## ADDITIONAL REFERENCE MATERIAL (Sought But Not Obtained)


Buchanan, J. "The Load Cell Installation in No. 3 Mine, Dominion Wabana Ore Ltd. Bell Island, Nfld" Mines Branch PM 194, 1955

Krupiennikow, G.A. "Some Methods, Results and Investigations of the Co-operation Between Rock Masses and a Shaft Lining" In volume Rock Mass Pressure Acting on the Lining of Vertical Shafts, Moscow 1963 (in Russian)

Kyoto University, Memoirs of Faculty of Engineering, Vol. 21, Part II, 1959; Vol. 23 Part I, 1961; Vol. 25, Part II, 1963

Murty, N.P.L. "Earth Pressure on Shafts" Journ. Soil Mech. Fndtn. Eng. India, Vol. 9, No. 4, pp. 435-443, 1970

Talobre, J. "La Mechanique des Roches" Dunod, Paris 1957

Unrug, K.F. "The Measurement of Strains, Stresses and Rock Mass Pressure Applied in Mining Openings" Budownictwo Gornicze No. 2, 1970 (in Russian)

U.S. Army Corps of Engineers "Tunnels and Shafts in Rock" Engineer Manual EM 1110-2-2901, 1978

Walz, B. "Active Soil Pressure on a Cylindrical Caisson Compared with Model Measurements" Proc's. 6th Conf. on Soil Mech. and Intn. Eng. Vienna, Austria. Vol. III, pp. 669-672, 1976

Walz, B. Ph.D. Thesis, No. D83, Univeristy of Berlin, 1976

# FIGURES

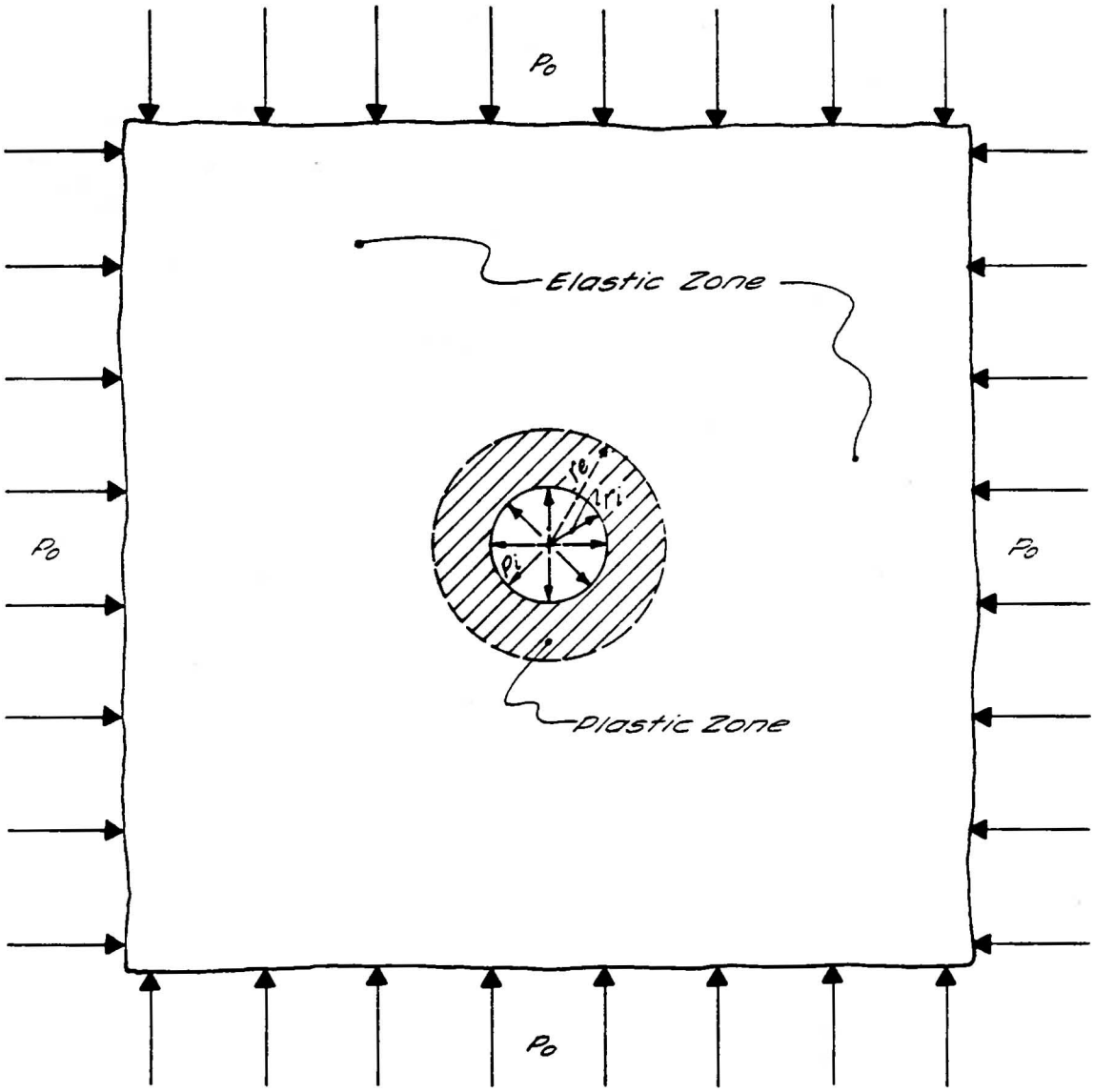


$P_o$ = In-situ stress at elevation of tunnel ℄ ($K_o = 1.0$).

$P_i$ = Internal support pressure.

$r_i$ = Initial radius of tunnel.

$r_e$ = Radius to boundary between elastic and plastic zones.

Figure 1 **BASIC TUNNEL MODEL: 2D.**

| MATERIAL CHARACTERIZATION | | EXTENT OF PLASTIC (BROKEN) ZONE | RADIAL STRESS AT ELASTIC-PLASTIC INTERFACE | STRESSES IN ELASTIC ZONE | STRESSES IN PLASTIC ZONE |
|---|---|---|---|---|---|
| ELASTIC (INTACT) ZONE | PLASTIC (BROKEN) ZONE | $-r_e$ | $-\sigma_{re}$ | $r_e \le r \le \infty$ | $r_i \le r \le r_e$ |
| **CASE 1** 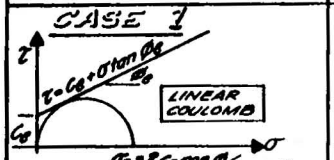  $\sigma_c = 2C_e\cos\phi_e/(1-\sin\phi_e)$ $S_{Ce} = \frac{C_e}{\tan\phi_e} = \frac{2C_e\sqrt{N\phi_e}}{N\phi_e - 1} = \frac{\sigma_c}{N\phi_e - 1}$ $N\phi_e = \tan^2(45 + \phi_e/2)$ $M_c = [1+(N\phi_e-1)P_o/\sigma_c]/(N\phi_e+1)$ | LINEAR COULOMB 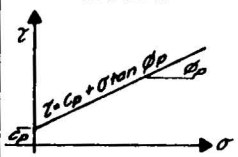  $S_{Cp} = \frac{C_p}{\tan\phi_p} = \frac{\sigma_{cp}}{N\phi_p - 1}$ $N\phi_p = \tan^2(45 + \phi_p/2)$ $= 1 + \sin\phi_p/1 - \sin\phi_p$ | $r_e = r_i\left[\frac{(P_o + S_{cp} - M_c\sigma_c)}{(P_i + S_{cp})}\right]^{1/N\phi_p - 1}$ | $\sigma_{re} = (P_o - M_c\sigma_c)$ | $\sigma_r = (P_i + S_{cp})(r/r_i)^{N\phi_p - 1} - S_{cp}$ $\sigma_\theta = N\phi_p(P_i + S_{cp})(r/r_i)^{N\phi_p - 1} - S_{cp}$ | |
| **CASE 2** 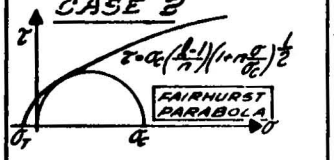  $n = \sigma_c/-\sigma_T$ $l = \sqrt{n+1}$ $M_F = [1 + nP_o/\sigma_c - \frac{1}{2}(l-1)^2]^{1/l}/(l+1)$ | 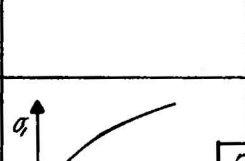  $\sigma_1 = \sigma_3 + (m_p\sigma_c\sigma_3 + s_p\sigma_c^2)^{1/2}$ $(m_p, s_p)$ = coefficient for broken rock | $r_e = r_i\left[\frac{(P_o + S_{cp} - M_F\sigma_c)}{(P_i + S_{cp})}\right]^{1/N\phi_p - 1}$ | $\sigma_{re} = (P_o - M_F\sigma_c)$ | $\sigma_r = P_o - (P_o - \sigma_{r\theta})(r_e^2/r^2)$ $\sigma_\theta = P_o + (P_o - \sigma_{r\theta})(r_e^2/r^2)$ | |
| **CASE 3** 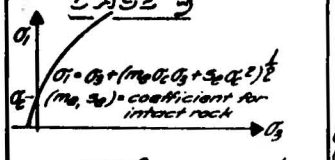  $M_H = \frac{1}{2}\left[\left(\frac{m_\sigma}{4}\right)^2 + m_\sigma P_o/\sigma_c + s_\sigma\right]^{1/2} - \frac{m_\sigma}{8}$ HOEK-BROWN PARABOLA | 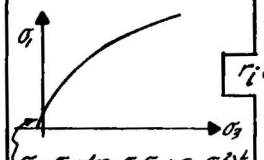  | $r_e = r_i e\left[N - \frac{2}{m_p\sigma_c}(m_p\sigma_c P_i + s_p\sigma_c^2)^{1/2}\right]$ where: $N = \frac{2}{m_p\sigma_c}(m_p\sigma_c P_o + s_p\sigma_c^2 - m_p\sigma_c^2 M_H)^{1/2}$ | $\sigma_{re} = (P_o - M_H\sigma_c)$ | $\sigma_r = \frac{m_p\sigma_c}{4}\left[\ln\left(\frac{r}{r_i}\right)\right]^2 + P_i + \ln\left(\frac{r}{r_i}\right)(m_p\sigma_c P_i + s_p\sigma_c^2)^{1/2}$ $\sigma_\theta = \sigma_r + (m_p\sigma_c\sigma_r + s_p\sigma_c^2)^{1/2}$ | |
| **CASE 4** PURELY COHESIVE (FRICTIONLESS) (Elastic - perfectly plastic) 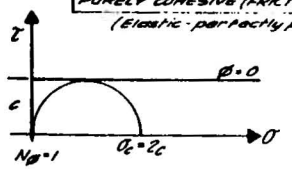  | | $r_e = r_i e^{\left(\frac{P_o - P_i}{\sigma_c} - \frac{1}{2}\right)}$ | $\sigma_{re} = (P_o - \frac{1}{2}\sigma_c)$ | $\sigma_r = P_i + \sigma_c \ln\left(\frac{r}{r_i}\right)$ $\sigma_\theta = P_i + \sigma_c\left[1 + \ln\left(\frac{r}{r_i}\right)\right]$ | |

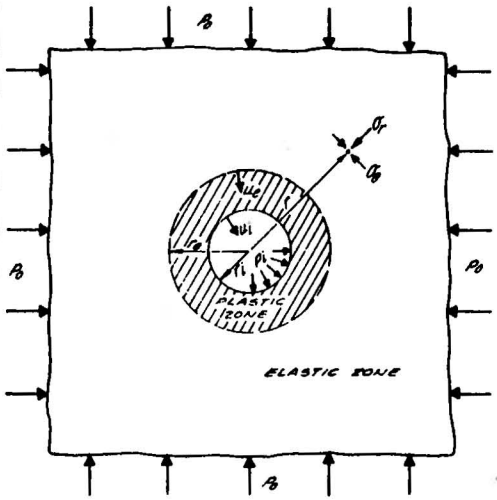


Figure 2 MATERIAL CHARACTERIZATIONS AND STRESS ANALYSIS EQUATIONS FOR TUNNELS - SUMMARY.

| MATERIAL CHARACTERIZATION | | RADIAL DISPLACEMENT AT ELASTIC, PLASTIC INTERFACE $-u_e-$ | RATIO OF PLASTIC DILATION TO PLASTIC SHEAR STRAIN $D$ | AVERAGE PLASTIC DILATION $e_{av} = d V_p / V_p$ | RADIAL DISPLACEMENT AT WALL OF CAVITY $-u_i-$ |
|---|---|---|---|---|---|
| ELASTIC (INTACT) ZONE | PLASTIC (BROKEN) ZONE | | | | |
| **CASE 1**<br>$\tau = c_p + \sigma \tan \phi_p$<br>LINEAR COULOMB<br>$\sigma_c = 2c_p \cos\phi_p/(1-\sin\phi)$<br>$S_{cp} = \frac{c_p}{\tan\phi_p} = \frac{2c_p\sqrt{N_{\phi p}}}{N_{\phi p}-1} = \frac{\sigma_c}{N_{\phi p}-1}$<br>$N_{\phi p} = \tan^2(45+\phi_p/2)$<br>$M_c = [1+(N_{\phi p}-1)P_o/\sigma_c]/(N_{\phi p}+1)$ | LINEAR COULOMB<br>$\tau = c_p + \sigma \tan\phi_p$<br>$S_{cp} = \frac{c_p}{\tan\phi_p} = \frac{\sigma_{cp}}{N_{\phi p}-1}$<br>$N_{\phi p} = \tan^2(45+\phi_p/2)$<br>$= 1+\sin\phi_p/1-\sin\phi_p$ | $u_e = \frac{(1+\nu)}{E} r_e M_c \sigma_c$ | $D_c = -\sin\phi_p$ | $e_{av} = \frac{2(u_e/r_e)(r_e/r_i)^2}{[(r_e/r_i)^2-1][1+1/R_{(C,F,M)}]}$<br>where.<br>For thin plastic zone<br>i.e $r_e/r_i < \sqrt{3}$<br>$R_{(C,F,M)} = 2D_{(C,F,M)} \ln(r_e/r_i)$<br>For thick plastic zone<br>i.e $r_e/r_i > \sqrt{3}$<br>$R_{(C,F,M)} = 1.1 D_{(C,F,M)}$ | $u_i = r_i\left[1-\left(\frac{1-e_{av}}{1+A}\right)^{\frac{1}{2}}\right]$<br>where:<br>$A = (2u_e/r_e)-e_{av})(r_e/r_i)^2$ |
| **CASE 2**<br>$\tau = \sigma_c\left(\frac{n-1}{n}\right)\left(1+n\frac{\sigma}{\sigma_c}\right)^{\frac{1}{2}}$<br>FAIRHURST PARABOLA<br>$n = \sigma_c/-\sigma_T$<br>$l = \sqrt{n+1}$<br>$M_F = [1+nP_o/\sigma_c - \frac{1}{2}(l-1)^2]^{\frac{1}{2}}/(l+1)$ | | $u_e = \frac{(1+\nu)}{E} r_e M_F \sigma_c$ | $D_F = \frac{-(l-1)}{2(1+n\sigma_{re}/\sigma_c)^{\frac{1}{2}}+l-1}$ | | |
| **CASE 3**<br>$\sigma_1 = \sigma_3 + (m_o\sigma_c\sigma_3 + s_o\sigma_c^2)^{\frac{1}{2}}$<br>$(m_o, s_o)$ = coefficient for intact rock<br>$M_N = \frac{1}{2}\left[\left(\frac{m_o}{4}\right)^2 + m_o P_o/(\sigma_c+s_o)\right]^{\frac{1}{2}} - m_o/8$ | $\sigma_1 = \sigma_3 + (m_p\sigma_c\sigma_3 + s_p\sigma_c^2)^{\frac{1}{2}}$<br>$(m_p, s_p)$ = coefficient for broken rock | $u_e = \frac{(1+\nu)}{E} r_e M_N \sigma_c$ | $D_N = \frac{-m_p}{m_p + 4(m_p\sigma_{re}/\sigma_c + s_p)^{\frac{1}{2}}}$ | | |
| HOEK-BROWN PARABOLA | | | | | |
| **CASE 4**<br>PURELY COHESIVE (FRICTIONLESS)<br>(Elastic perfectly plastic)<br>$\phi = 0$<br>$N_\phi = 1$<br>$\sigma_c = 2c$ | | $u_e = \frac{(1+\nu)}{E} r_e\left(\frac{\sigma_c}{2}\right)$ | $D = 0$ | $e_{av} = 0$ | $u_i = r_i\left[1-\left(\frac{1}{1+A}\right)^{\frac{1}{2}}\right]$<br>where<br>$A = (2u_e/r_e)(r_e/r_i)^2$ |

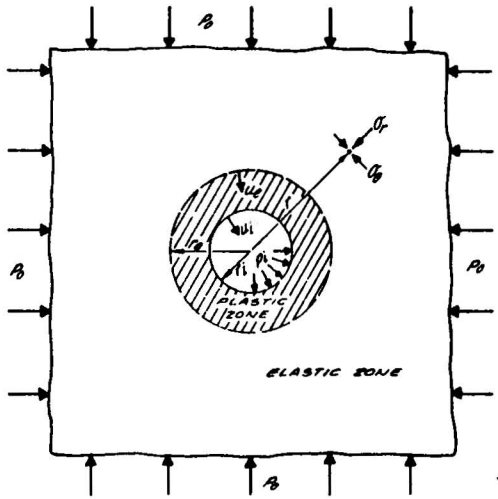


Figure 3 MATERIAL CHARACTERIZATIONS AND DEFORMATION ANALYSIS EQUATIONS FOR TUNNELS - SUMMARY.

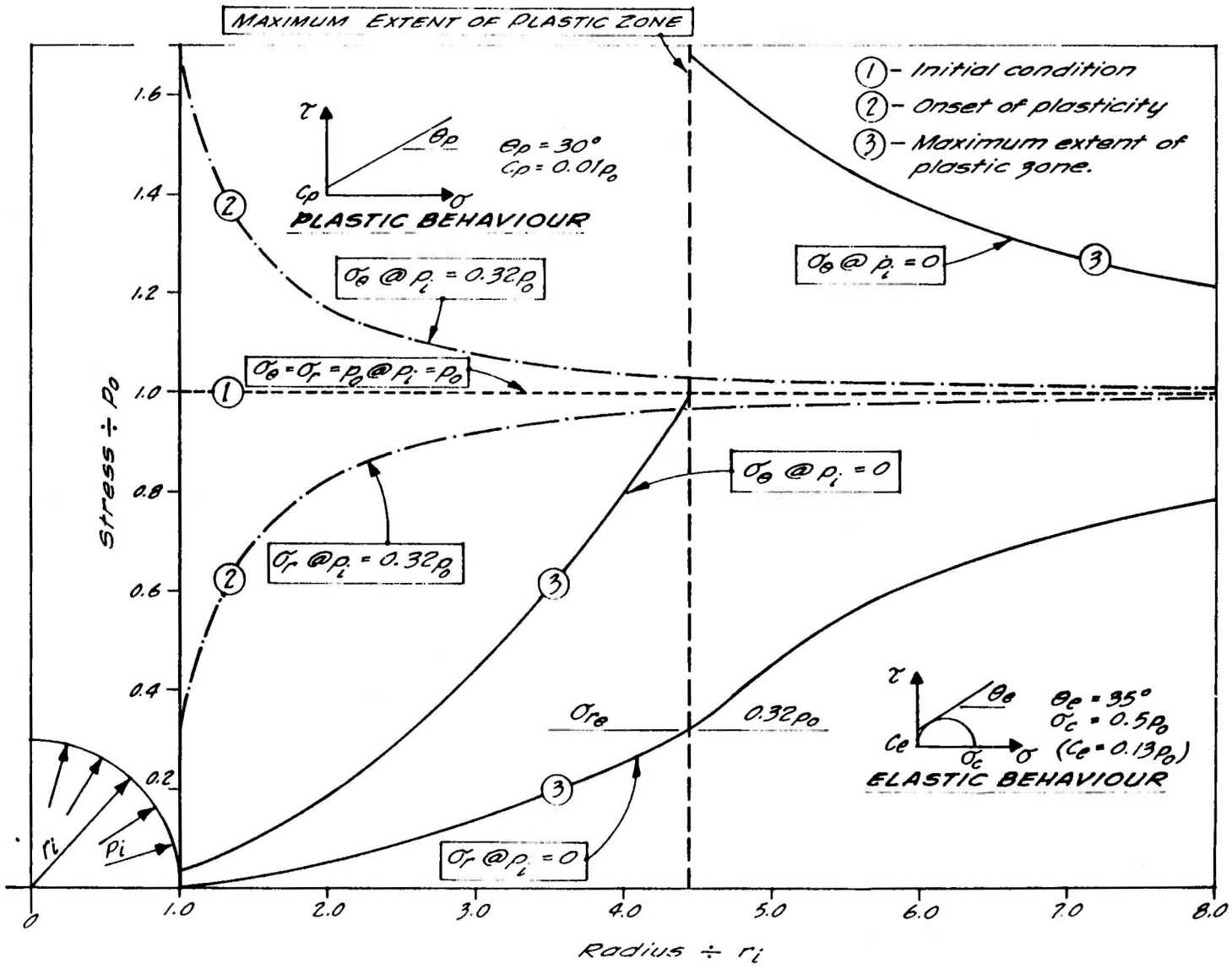


Figure 4 EXAMPLE OF STRESS DISTRIBUTIONS WITH REDUCING INTERNAL SUPPORT.

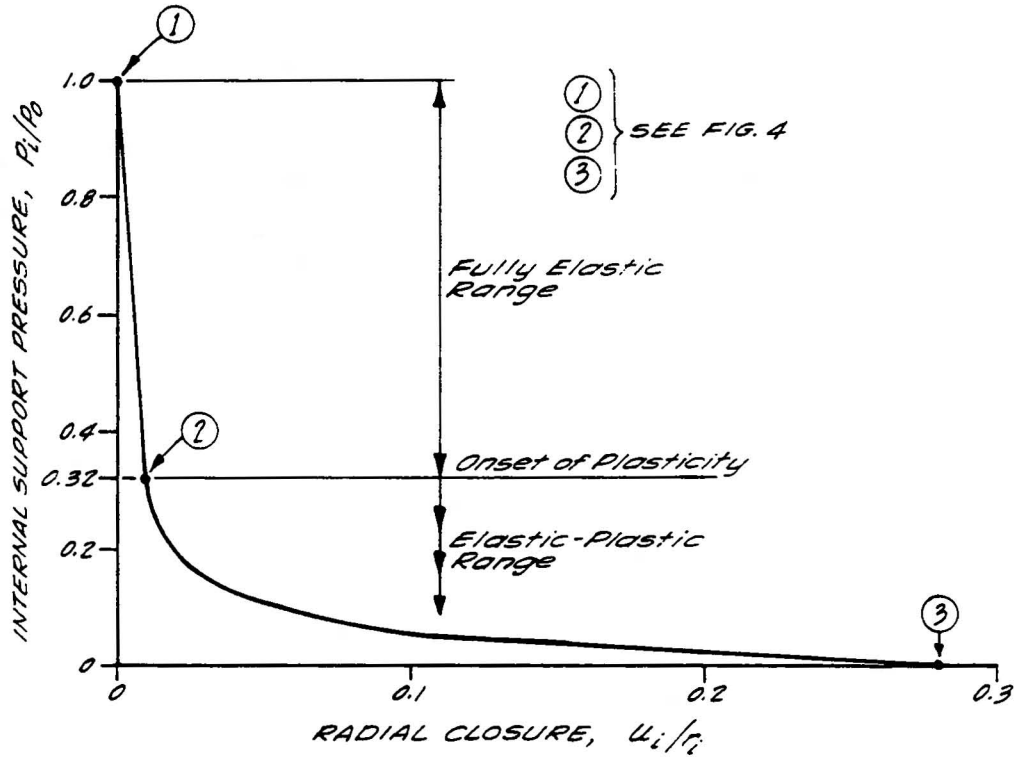


Figure 5 - **TYPICAL CLOSURE - SUPPORT CURVE.**

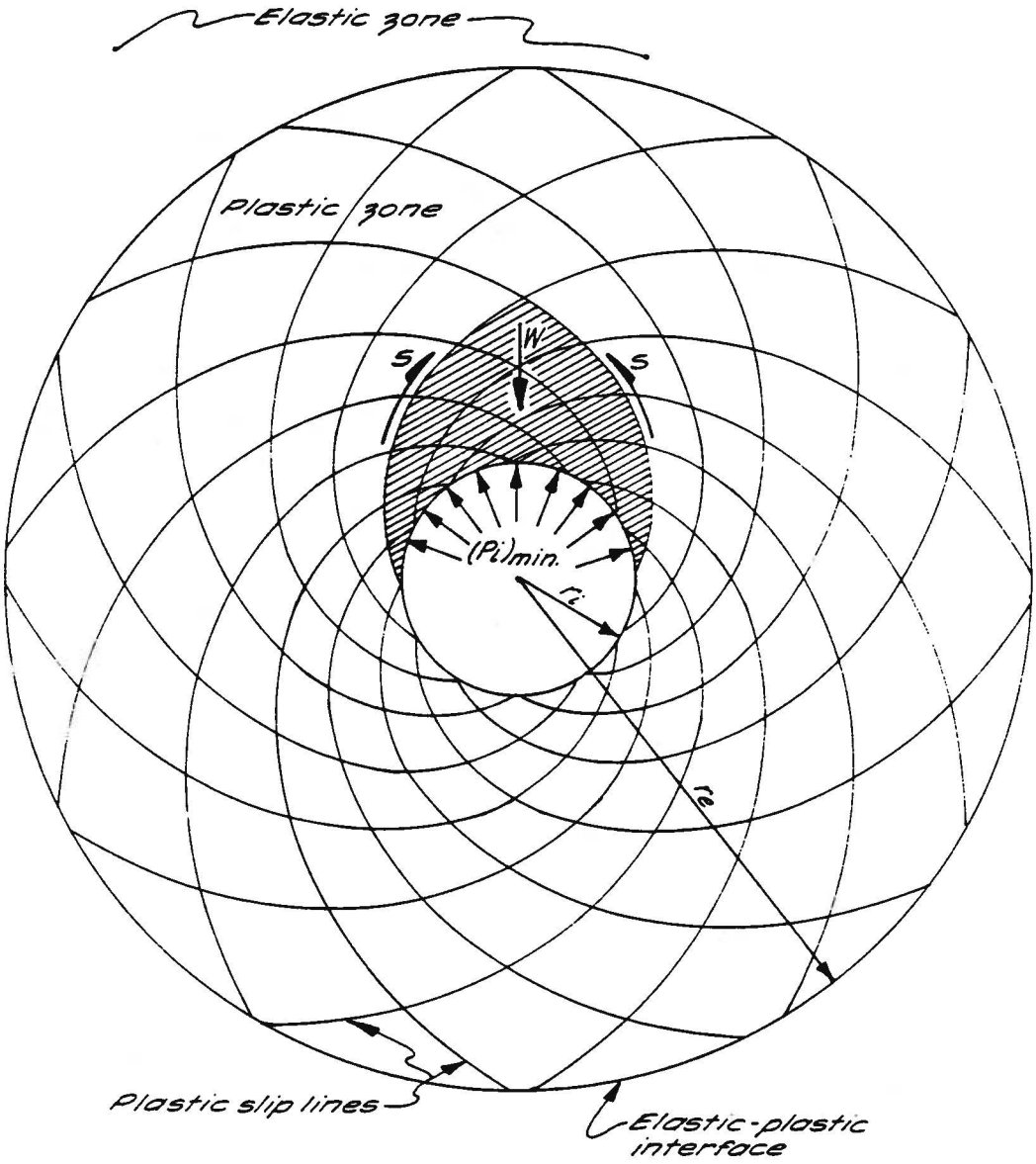


Figure 6 **LIMIT EQUILIBRIUM OF GRAVITY BLOCKS.**

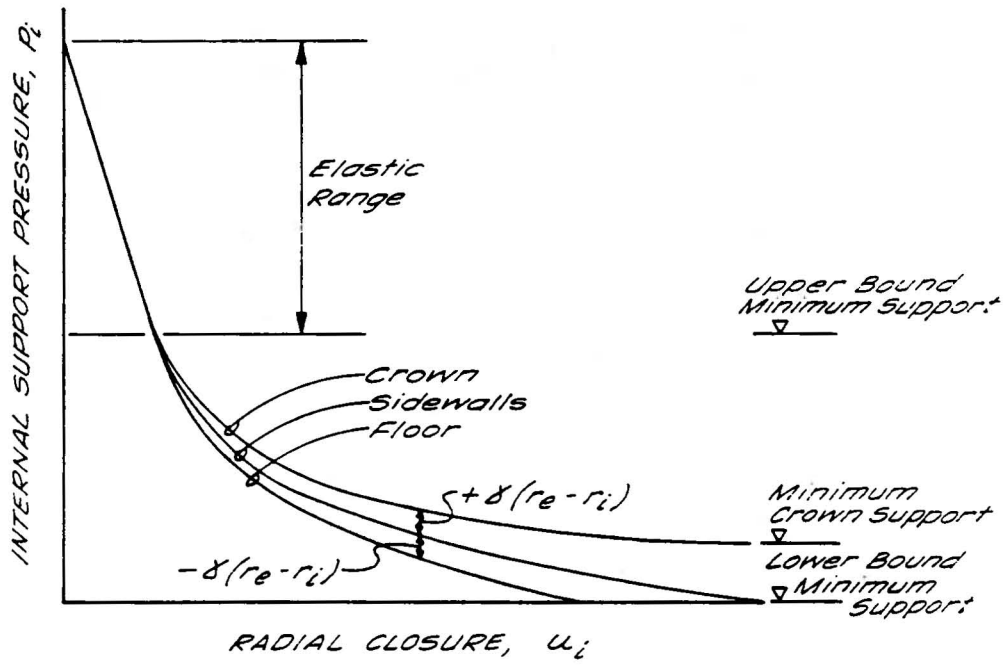


Figure 7 **CHARACTERISTIC LINES FOR TUNNEL.**

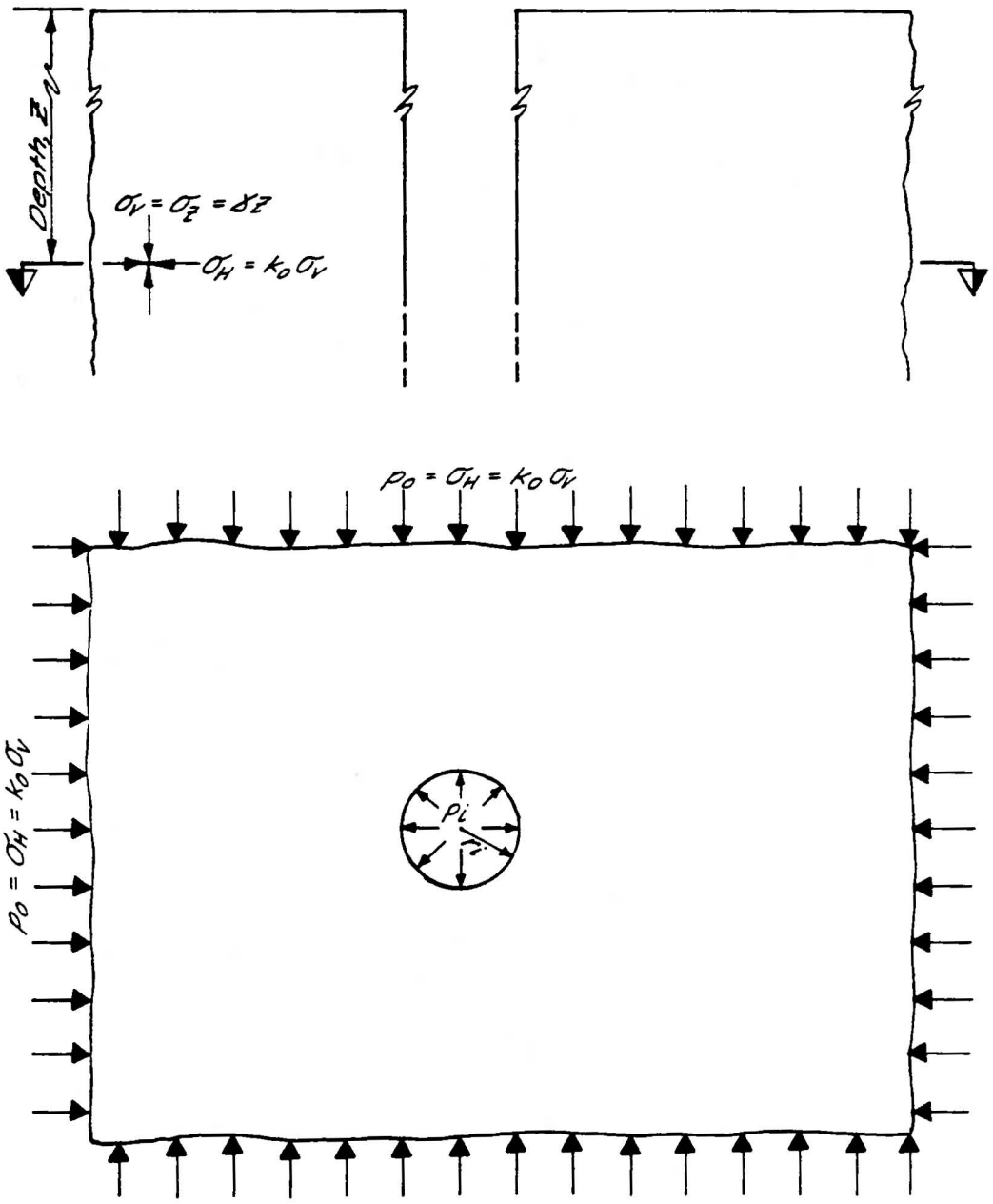


Figure 8 - SHAFT MODEL

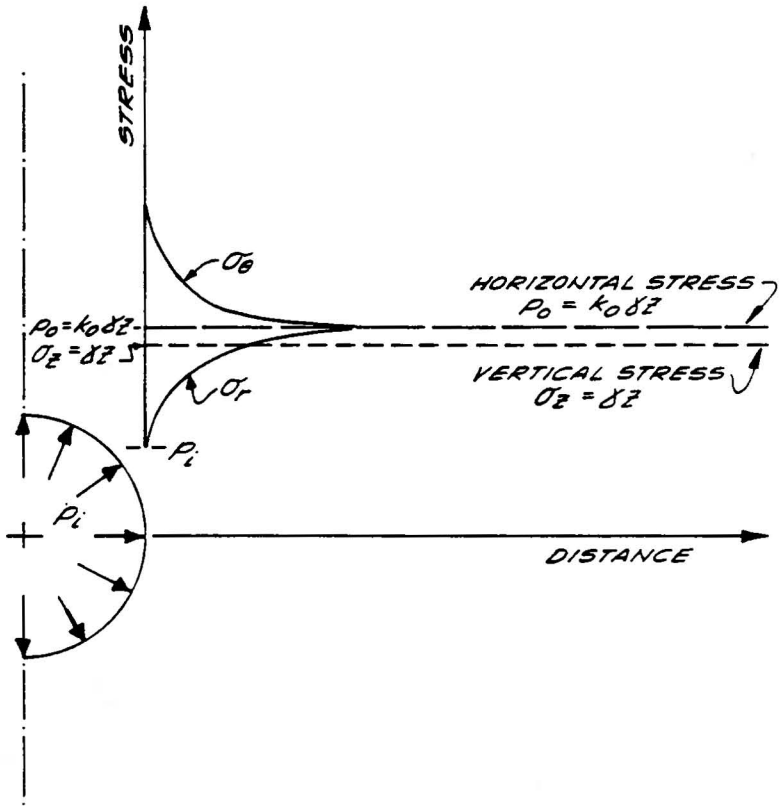


Figure 9 STRESSES AROUND SHAFT; $k_o \geq 1$

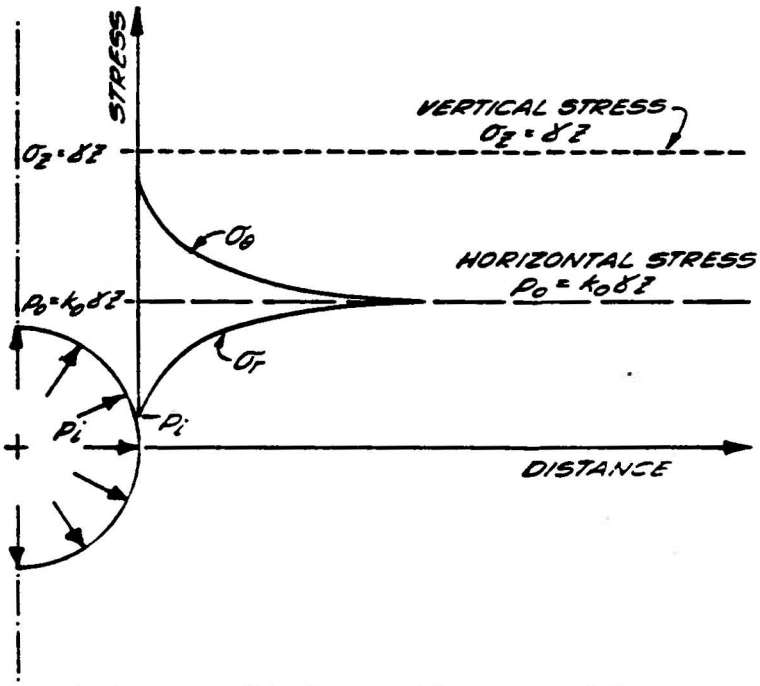


ELASTIC STRESSES AROUND SHAFT;
$k_o \leq \frac{1}{2}$

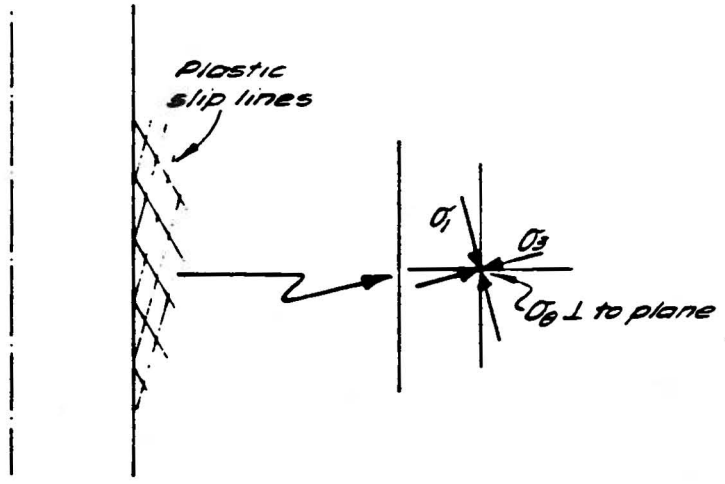


PLASTICITY IN VERTICAL PLANE

Figure 10 **STRESSES AROUND SHAFT;**
$k_o \leq \frac{1}{2}$.

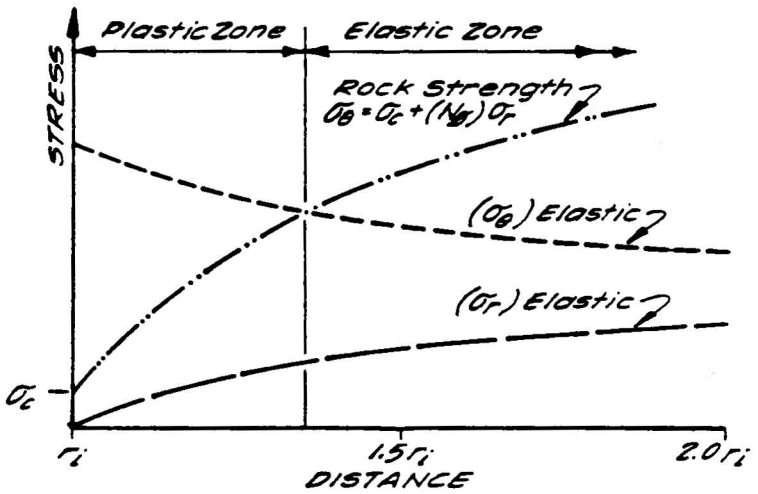


After : Abel et al, 1979.

Figure 11 DETERMINATION OF PLASTIC ZONE.

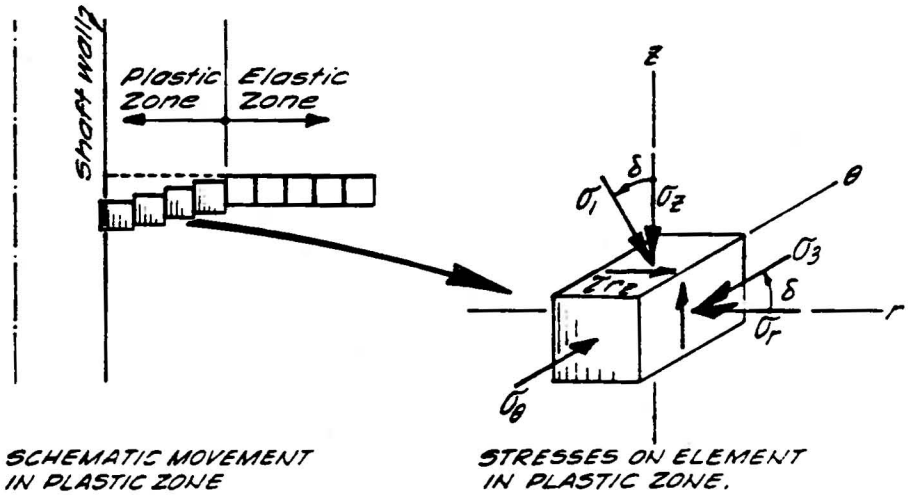


SCHEMATIC MOVEMENT IN PLASTIC ZONE

STRESSES ON ELEMENT IN PLASTIC ZONE.

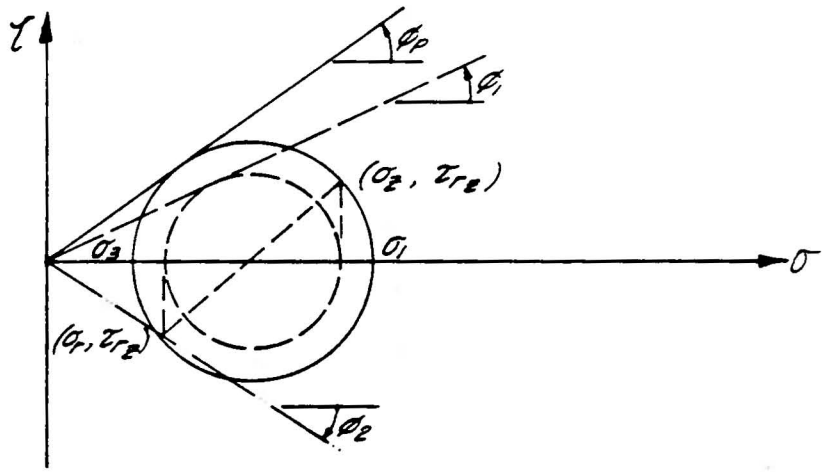


Figure 12 STRESSES IN ZONE OF VERTICAL PLASTICITY NEAR SHAFT.

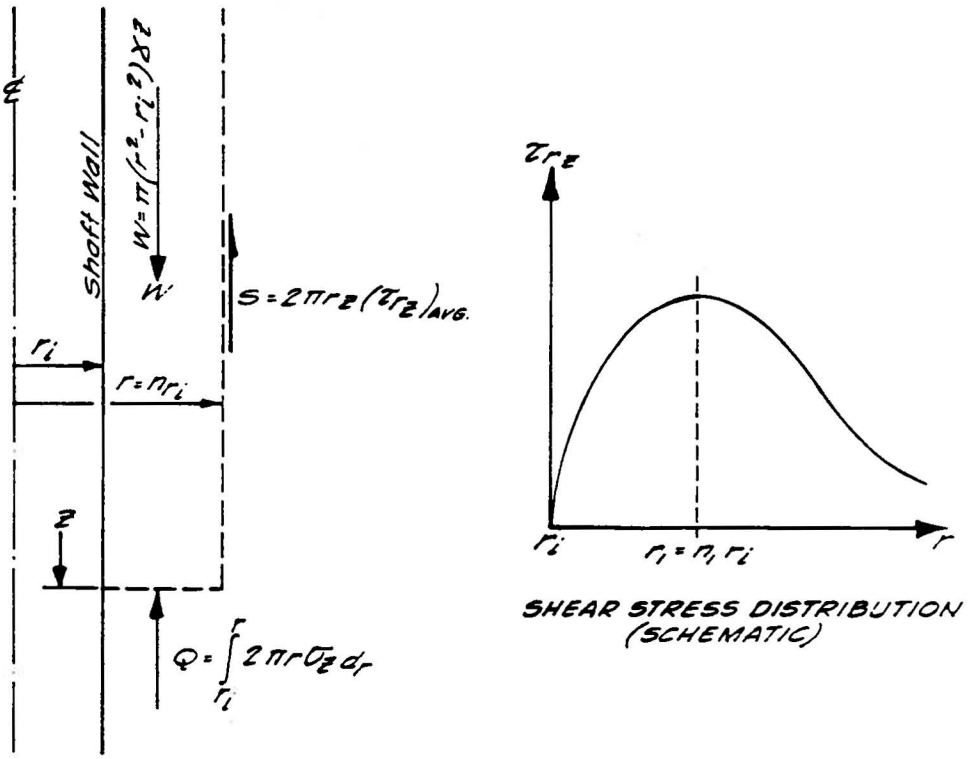


Figure 13 LIMIT EQUILIBRIUM OF GRAVITY BLOCK.

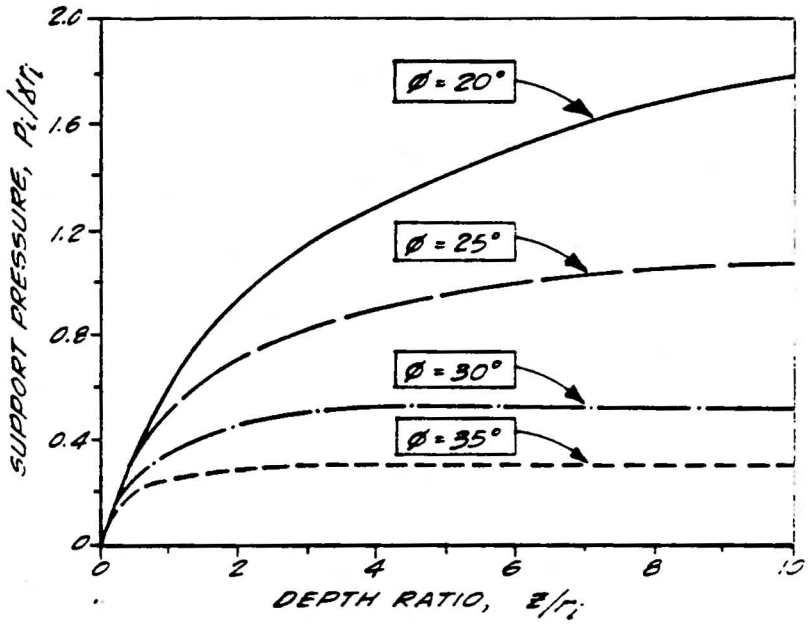


Ref. U.S. Dep.t of Navy
NAVFAC DM-7, 1971.

Figure 14: MINIMUM SUPPORT PRESSURES: SHAFT IN COHESIONLESS MATERIAL.

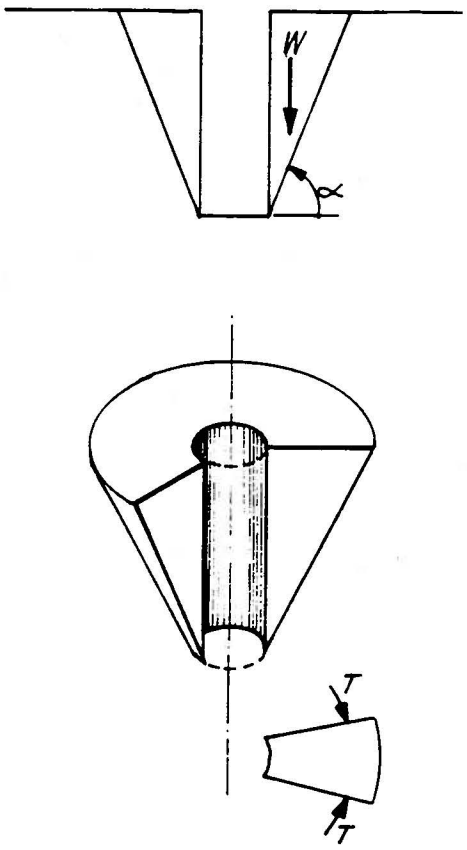


After: Prater, 1977

Figure 15 CONICAL POTENTIAL FAILURE SURFACE.

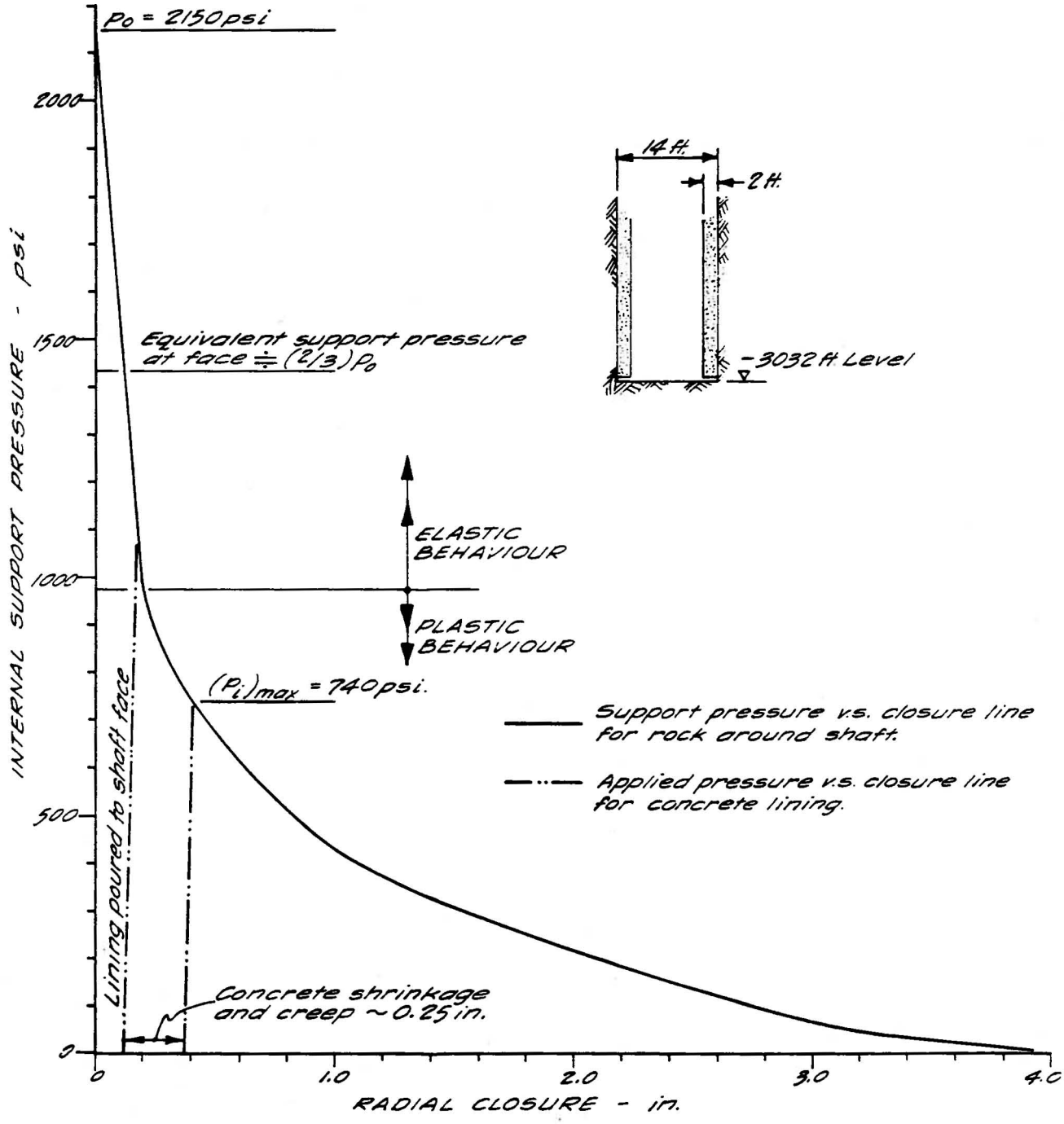


Figure 16 CHARACTERISTIC LINE FOR 3032 ft. LEVEL, MT. TAYLOR MINE SHAFT.

## APPENDIX

PAPER BY ABEL, J.F; DOWIS, E. AND RICHARDS, P. - "CONCRETE SHAFT LINING DESIGN" 20th U.S. SYMPOSIUM ON ROCK MECHANICS, AUSTIN, TEXAS, JUNE 4th - 6th, 1979

# NCRETE SHAFT LINING DESIGN

J.F. Abel Jr., Colorado School of Mines;
. Dowis, Gulf Mineral Resources Co.; and
. Richards, Jenny Engineering Corp.

is paper was presented at the 20th U.S. Symposium on Rock Mechanics, held in Austin, Texas, June 4-6, 1979. The material i ject to correction by the author. 

BSTRACT

Instrumentation placed at three levels in the concrete lining of the 14-ft I.D. shaft at the Mt. Taylor Mine permitted checking which lining pressure equation best fit the particular geologic conditions. Jobre's (1957) lining pressure prediction equation for clastic rock most closely approximated the measured results. The Mohr-Coulomb strength criteria appeared to best describe the strength/confinement conditions outward into rock adjacent to the 14-ft Mt. Taylor shaft.

INTRODUCTION

Traditional shaft support has been with either timber or steel sets or a cast concrete lining. Steel and timber sets are much more flexible than concrete. This results from (1) the low compressive strength, typically 250 psi across the grain, of the timber blocking which braces the sets against the rock, and (2) the high elastic flexibility of steel or timber sets. The stiffness of concrete, after curing, is much higher than any composite structure of timber blocking and steel sets. It is this feature of concrete which complicates the understanding of concrete lining design.

Irrespective of whether steel, timber or concrete is used for shaft support, the very nature of the shaft sinking cycle generally results in the support being installed fairly close to the shaft bottom. In North American sinking practice concrete lining is seldom more than 20 ft away from the shaft bottom. A zone of "stress shielding" occurs near the shaft bottom which benefits sinking in weak ground.

The elastic analysis of Galle and Wilhoit (1961) demonstrated that the elastic stresses in the wall "as close as 2.9 radii from the bottom agreed well with those calculated by the plane strain solution". They also show that the tangential stresses at the shaft wall within 2.9 radii above the shaft bottom are less than predicted by the plane strain solution. The 2.9 radii interval above the shaft bottom represents the elastic "shielded zone". They state, "Therefore, the plane strain solution may be used to calculate the stresses everywhere around a well bore except very near the bottom or the top." The "shielded zone" allows the concrete to be poured and to cure at least partially, before full ground stresses are applied. This zone of stress shielding advances with the sinking of the shaft. Galle and Wilhoit also show a zone of elastically higher stress below the shaft bottom. This higher stress zone extends approximately the same distance below the shaft bottom.

The short length of the elastic shield zone supports the traditional assumption that the influence of the shaft bottom stress deviations can be ignored in shaft lining design. Measurement results from the Straight Creek pilot bore (Abel, 1967) give a vastly different picture. Ground stabilization occurred at an average distance behind the tunnel face in excess of 40 radii. Abel and Lee (1973) reported the onset of stress ahead of an advancing tunnel in excess of 14 radii. In contrast to the elastic predictions, the response of a rock mass to driving a tunnel or sinking a shaft is apparently non-elastic, as shown by the greater influence distances in rock.

The sequence of loading for shaft linin at the Mt. Taylor Mine of Gulf Mineral Resources Company near Grants, New Mexico, indicated a progressive loading of the linin which related to the incremental deepening

ferences and illustrations at end of paper.

of the shaft and advance of the stress shielded zone. Figure 1 presents an idealized representation of the progressive development of ultimate tangential stress in the rock mass adjacent to the shaft wall as the shaft is deepened. This representation has been inferred from measurements of the progressive increase in concrete lining stress. It has been assumed that the overburden stress acts uniformly on any horizontal plane.

## LINING PRESSURE PREDICTION

Steel sets are blocked against the rock at a low loading condition and concrete is poured against the rock under no load. In both cases the rock mass has to deform against the support before significant support loads develop. A flexible support capable of yielding when subject to the deformation of the rock adjacent to the shaft need only be designed to resist the active pressure of the rock mass. A rigid support resists the elastic deformation as well as the active pressure of the rock mass. For instance at Mt. Taylor the approximate cured concrete stiffness is 4,000,000 psi, whereas the rock stiffness is between 600,000 and 1,000,000 psi. As such the concrete lining represents a stiff inclusion within the rock. The stiffer concrete resists the elastic deformation of the rock toward the shaft. A stiff concrete lining literally draws load from the rock and this additional lining load must be accommodated in concrete shaft lining design.

The traditional methods of estimating rock pressure on a shaft lining (Terzaghi, 1943 and Talobre, 1957) assume a rigid (non-yielding) lining. The properties required to predict the external pressure (Pi) exerted on a rigid concrete lining by a rock mass are angle of internal friction, rock mass compression strength and cohesion. The horizontal ground stress is also necessary, since it is the driving stress. The horizontal load that was carried by the rock prior to shaft excavation must be supported by the composite structure of the shaft lining and the adjacent rock.

Terzaghi (1943) presented the following prediction equation for the lining pressure on a rigid lining in plastic (yielding) rock:

$$Pi = \frac{2}{(\text{Tan}\beta + 1)} \left\{ \sigma_H + \frac{\sigma_o}{(\text{Tan}\beta - 1)} \right\} \left(\frac{r}{R}\right)^{(\text{Tan}\beta - 1)} - \frac{\sigma_o}{(\text{Tan}\beta - 1)} \qquad (1)$$

Pi = radial stress applied to outside of lining

$\text{Tan}\beta$ = passive pressure coefficient

$$\text{Tan}\beta = \frac{1 + \text{Sin}\,\phi}{1 - \text{Sin}\,\phi}$$

$\phi$ = angle of friction

$\sigma_H$ = horizontal ground stress (assumed uniform

$\sigma_o$ = rock mass uniaxial compression strength

r = excavation radius

R = relaxed zone radius

Talobre (1957) developed a similar equation for clastic (brittle) rock, as follows:

$$Pi = \left\{ \frac{c}{\text{Tan}\,\phi} + \sigma_H (1 - \text{Sin}\,\phi) \right\} \left(\frac{r}{R}\right)^{(\text{Tan}\beta - 1)} - \frac{c}{\text{Tan}\,\phi} \qquad (2)$$

c = rock mass cohesion

The properties of a rock mass are not readily measurable. The angle of friction ($\phi$) can be either the angle of internal friction if the potential failure of the rock is through intact rock (Fig. 2) or the angle of surface friction if the failure would occur along weaknesses in the rock mass. However, once the concrete is in place only the angle of internal friction need be considered. Hobbs (1970) demonstrated that the angle of friction for British coal measure rock was the same for triaxially confined intact rock as for broken rock.

The uniaxial compression strength of rock mass ($\sigma_o$) cannot be determined from specimen tests, unless the specimens are very large. Table I presents several indications of the decrease in rock strength with increase in size. The reported decrease in uniaxial compression strength from NX(2-in.) cores specimens to large blocks of rock ranges from over seven times to about four times. Wilson (1972) recommended the use of specimen cohesion for rock mass compression. Obert, et. al. (1) suggest dividing specimen strength by 2 or 4 to obtain a design compression strength for the rock mass.

The rock mass cohesion (c) can be calculated from the measured angle of internal friction and the estimate of rock mass compression strength, as follows:

$$c = \frac{\sigma_o}{2\sqrt{\text{Tan}\beta}} \qquad (3)$$

The excavation radius is tied to the internal lining radius as determined by production and use requirements of the shaft and by the required thickness of the lining. Lining thickness must be determined by iterative solution, involving first the selection of a trial lining thickness and secondly calculating the resulting lining safety factor. This process is repeated until the desired safety factor is obtained. The lining thickness is designed to carry the lining pressure which develops after sinking

:LE I. Uniaxial compression strength decrease with increasing specimen size.

| COAL (Bieniawski, 1968) | | QUARTZ DIORITE (Pratt and others, 1972) | |
|---|---|---|---|
| Side Length (in.) | Strength (psi) | Side Length (in.) | Strength (psi) |
| 0.75 | 4260 | 3.18 | 4420 |
| 1 | 4760 | 4.24 | 4530 |
| 2 | 4880 | 4.5 | 4860 |
| 2.7 | 4575 | 8 | 3340 |
| 3 | 4070 | 12 | 1980 |
| 6 | 1850 | 18 | 1400 |
| 12 | 1158 | 24 | 1660 |
| 18 | 910 | 36 | 1080 |
| 24 | 800 | 72 | 1330 |
| 28 | 774 | 108 | 990 |
| 36 | 709 | Increase | Decrease |
| 48 | 650 | 34 times | 78% |
| 60 | 644 | | |
| Increase | Decrease | | |
| 10 times | 85% | | |

as removed the stress shield. Above the shielded zone the design tangential rock stress ( $\sigma_t$) and the maximum lining pressure (Pi) are present.

In the typical case where the elastic tangential stress, as well as overburden stress, exceeds the uniaxial compression strength of the rock mass the rock near the shaft wall relaxes, or unloads, to a stress that can be supported. The relaxation of a zone of overstressed rock behind the concrete lining results in partial failure of the rock (Fig. 3).

The radius of the relaxed, or overstressed, rock zone (R) adjacent to the shaft has traditionally been estimated with the Mohr-Coulomb strength criteria. Rock strength increases outward from the shaft wall as the radial confining stress ($\sigma_r$) increases. The elastic tangential stress in the rock is a maximum at the shaft wall, and decreases outward into the rock (Fig. 3).

Within the relaxed zone, rock failure results in expansion of the rock mass which is resisted by the concrete lining. Rock failure cannot be permitted until the concrete has gained sufficient strength to resist the radial expansion stress which equals the lining pressure (Pi). The partially relaxed rock adjacent to unsupported shafts and tunnels or in pillars can frequently be seen as splits in the rock when looking into a borehole drilled into the rib or wall. Figure 4 presents schematically this partial failure of the rock in the relaxed zone. The lower half of Figure 5 presents the associated Mohr-Coulomb predicted stable stress distribution outward from the concrete lining at the 3032-ft depth in the Mt. Taylor shaft. In the unlined portion of the shaft, near the shaft bottom, the stresses are limited to the rock mass compression strength ( $\sigma_o$). The actual tangential and vertical stresses may well be less because this portion of the shaft is within the "shielded zone". The stresses in the shielded zone increase upward. In weak ground this limits the length of pour in order to prevent sloughing and caving of the exposed rock.

The Mohr-Coulomb strength criteria predicts the extent of the relaxed zone outward from the shaft wall ($\ell$). The boundary of the relaxed zone is the point where the radial stress ( $\sigma_r$) is just sufficient to triaxially reinforce the rock mass to carry the overburden ( $\sigma_v$) or tangential stress ( $\sigma_t$), whichever is greater.

$$\sigma_r = \sigma_H \left(1 - \frac{r^2}{(r+\ell)^2}\right) \quad (4)$$

$$\text{Failure Strength} = \sigma_o + \text{Tan}\beta\ \sigma_r \quad (5)$$

$$\sigma_t = \sigma_H \left(1 + \frac{r^2}{(r+\ell)^2}\right) \quad (6)$$

Figure 5 shows the predicted radial and tangential stress distributions adjacent to the shafts at the 3032-ft depth at Mt. Taylor. The elastic stress distributions are also shown. Figure 5 also indicates the transfer of tangential stress from the overstressed rock near the shaft (Area I) to the triaxially confined rock beyond the boundary of the relaxed zone (Area II).

The radial stress ( $\sigma_r$) increases from zero to Pi from the shaft bottom to the top of the shielded zone. The lining pressure, calculated from Talobre's clastic equation, is 507 psi (See Figs. 4 & 5). The unconfined compression strength ( $\sigma_o$) of the rock mass must decrease as the overstressed rock near the shaft relaxes (partially fails) against the lining. The unconfined compression strength of the partially failed rock directly against the lining is conservatively assumed to be zero. The triaxial strength of the rock adjacent to the lining is not zero, however, because it is confined by the 507 psi lining pressure. Its strength is:

$$\text{Failure Strength (psi)} = \sigma_o + \text{Tan}\beta\ (\text{Pi}) \quad (7)$$

$$\text{Failure Strength (psi)} = 0 + 2.90\ (507)$$

$$= \underline{1469\ \text{psi}}$$

based on the Mohr-Coulomb strength criteria and the properties of the Upper Westwater sandstone. The uniaxial compression strength ( $\sigma_o$) is assumed to rise across the relaxed zone, reaching 500 psi at the overstressed zone/elastic rock boundary. The failure strength curve shown on Figure 5 indicates the tangential and radial stress distribution adjacent to the shaft. Their elastic distributions are also shown, although the overstressed rock near the shaft wall will of course not be responding elastically. The area, desig-

nated Area I on Figure 5, below the elastic tangential stress curve and the failure strength curve represents the load that cannot be carried by the overstressed rock. This load must be transferred to the stronger confined rock in the elastic zone, indicated as Area II on Figure 5.

The Mohr-Coulomb strength criteria ignores the effect of the intermediate stress. Mogi (1967) indicated that "10 to 50% differences of strength are associated with the influence of the intermediate principal stress." Ostrowski (1972) applied the strain energy of distortion theory of failure to predict the thickness of the relaxed zone adjacent to the shaft wall while taking into consideration the intermediate stress. The assumptions are simple, (Seely and Smith, 1952), namely (1) volumetric strain from hydrostatic stress does not result in failure, and (2) rocks yield or fail only under sufficiently large differential 3-dimensional stress conditions. The critical indicator of failure is the shear stress invariant (t):

$$t = \frac{1}{3}\sqrt{(\sigma_1-\sigma_2)^2+(\sigma_1-\sigma_3)^2+(\sigma_2-\sigma_3)^2} \qquad (8)$$

$\sigma_1$, $\sigma_2$, $\sigma_3$ = Principal stresses

Near the shaft the principal stresses are the tangential stress ( $\sigma_t$), the radial stress ( $\sigma_r$) and the vertical stress ( $\sigma_v$). Failure is predicted when the shear stress invariant (t) reaches the critical value for the associated volumetric stress invariant (s):

$$s = \frac{\sigma_1 + \sigma_2 + \sigma_3}{3} \qquad (9)$$

The critical "t" value for associated "s" values can be defined by applying equations 8 and 9 to the same triaxial strength tests used for the Mohr-Coulomb strength criteria, as shown on Figure 6 for the 3032-ft depth at Mt. Taylor. At a specific shaft depth the elastic volumetric stress invariant adjacent to a circular shaft is a constant, since $\sigma_t$ plus $\sigma_r$ equals twice the assumed uniform horizontal stress and the vertical overburden stress is assumed uniform. The thickness of the relaxed zone ( $\ell$ ) is determined by finding the thickness which produces a shear stress invariant just under the strength, or failure, line.

## MT. TAYLOR CASE STUDY

The concrete lining in the 14-ft I.D. shaft at the Mt. Taylor Project of Gulf Mineral Resources Co. was instrumented with Carlson strain cells at three depths; 940 ft, 2030 ft and 3032 ft. The measured concrete strains were converted to concrete stress ( $\sigma_{tc}$) and then the lining pressures (Pi) calculated. The Lame' thick walled cylinder equation was employed:

$$Pi = \frac{\sigma_{tc}}{\left(\frac{r^2}{r^2-a^2}\right)\left(1+\frac{a^2}{x^2}\right)} \qquad (10)$$

r = excavation radius
a = shaft lining radius
x = instrument radius
(See Figure 3)

Table II presents the results of the instrumentation program. The scatter of the calculated lining pressures can be seen on Figure 7. This scatter may be the result of the irregular shaft wall.

Statistical regression curves were fitted to the calculated lining pressures, as shown on Figure 7. It is interesting to note that the lining pressure predicted for the 3032-ft depth from the 940-ft and 2030-ft depth data was reasonably close, even though the rock types changed, as noted on Table III.

The in situ stress conditions and rock mass properties are two elements in predicting pressure on a shaft lining. The formations were hydrofractured at 1106 and 2390 ft. A horizontal stress equal to 0.7 times the vertical stress was indicated by these tests. The vertical stress was assumed to be the result of the overburden load. The average rock density of 138 lb/ft$^3$ resulted in estimated in situ stresses shown in Table III. The physical properties employed in the analysis are also presented on Table III. The estimated rock mass compression strengths of 1000 psi for the Mancos shale and 500 psi for the Upper Westwater were obtained by decreasing the specimen strength of the Mancos by over 7 times and the Upper Westwater over 5 times. These reductions were inferred from the fissile nature of the Mancos, similar to Bieniawski's (1968) cleated coal, and from the massiveness of the Upper Westwater, similar to Pratt's (1972) quartz diorite. Figures 8 and 9 present the triaxial test results for the Mancos shale and the Upper Westwater Canyon member of the Morrison Formation, respectively.

## SAMPLE CALCULATIONS FOR 3032-FT DEPTH

The first step in calculating the pressure on the lining involves calculating the thickness of the relaxed zone ( $\ell$ ) at the 3032-ft depth. An iterative process was employed which yielded a relaxed zone thickness of 0.353 times the excavation radius, as follows:

$$\sigma_r = \sigma_H\left(1 - \frac{r^2}{(r+\ell)^2}\right) \qquad (11)$$

$$\sigma_r = 2150\left(1 - \frac{r^2}{(r+0.353\ r)^2}\right) = 975 \text{ psi}$$

The triaxial compression strength under psi of confinement is (Mohr-Coulomb strength criteria):

$$\text{Fail} = \sigma_o + \text{Tan}\beta(\sigma_r) = 500 + 2.90(975) = 3300 \text{ psi} \quad (12)$$

The triaxial compression strength just exceeds the elastic tangential stress ( $\sigma_t$) for the relaxed zone equal to 0.353r, as follows:

$$\sigma_t = \sigma_H \left( 1 + \frac{r^2}{(r+\ell)^2} \right) \quad (13)$$

$$\sigma_t = 2150 \left( 1 + \frac{r^2}{(r+0.353r)^2} \right) = 3320 \text{ psi}$$

The tangential stress ($\sigma_t$) value is used for comparison to the failure strength ( $\sigma_{Fail}$) because the overburden stress is only 2906 psi.

The predictions of lining pressure for the above relaxed zone thickness at 3032-ft depth are presented on Table IV. One additional lining stress prediction is included on Table IV, the no cohesion clastic modification of Talobre's (1957) equation presented by Rabcewicz (1964). Similar results for the 940-ft and 2030-ft depths are also on Table IV. Factors of safety for all three instrumented depths are presented on Table V. The design concrete strength is 5000 psi. Lamé's thick walled cylinder equation provides the solution, as given below:

$$FS = \frac{f'_c}{\frac{\left(\frac{t}{a} + 1\right)^2}{2\,Pi}} \quad (14)$$

t = lining thickness (in.)
a = shaft lining inside radius (84-in.)
$f'_c$ = concrete design strength (5000 psi)
Pi = lining pressure

The distortion energy method predicts the thickness of the relaxed zone ( $\ell$ ) at the 3032-ft depth as 0.113 times the excavation radius. This is shown on Table VI and Figure 6 for the value of "$\ell$" in terms of "r" where the strength and stress invariant values are equal. With Terzaghi's equation the predicted plastic lining pressure is 854 psi. The Rabcewicz no cohesion clastic lining stress prediction is 899 psi and the Talobre prediction is 850 psi. These lining pressures are greatly in excess of the maximum 548 psi calculated from the strain cell instrumentation. See Table IV for comparisons. The assumption that the critical shear stress invariant (t) determined from triaxial tests can predict strength under polyaxial stress conditions does not appear to be valid.

## CONCRETE CONSIDERATIONS

The assumption that concrete acts as a rigid shaft lining is conservative. The elastic deformation of the shaft lining as it is progressively loaded reduces the radial stress imposed. Similarly the tendency of concrete to shrink, and to creep under stress will also reduce the radial stress.

The maximum rigid lining stress for the 3032-ft depth in the 14-ft I.D. shaft indicated by the field measurements was (Lamé thick-walled cylinder equation):

$$\sigma_{tc} = 2Pi \left( \frac{r^2}{r^2 - a^2} \right) \quad (15)$$

$$\sigma_{tc} = 2(548) \left( \frac{108^2}{108^2 - 84^2} \right) = 2740 \text{ psi}$$

The minimum safety factor for the 24-in thick concrete lining is 1.82 for the 5000+ psi concrete.

The elastic decrease in shaft diameter for the 24-in concrete lining at the 3032-ft depth, when subjected to the average 420 psi exterior lining pressure is 0.090 in., calculated as follows:

Average lining stress $\overline{\sigma_{tc}} = \frac{420(216)}{48} = 1890$ psi

Stiffness of the concrete (E) from American Concrete Institute (ACI),(1977):

$$E = 57000 \sqrt{f'c} \quad (16)$$

$f'c$ = concrete strength

$$\text{Average lining strain} = \frac{\overline{\sigma_{tc}}}{E} = \frac{1890}{4{,}030{,}000} = 0.000469 \text{ in./in.} \quad (17)$$

Average lining circumference C = $2\pi(96) = 603$ in.

Shortening of circumference $\Delta C = C\epsilon = 603(0.000469) = 0.283$ in.

Deformed shaft diameter $d_{new} = (C - \Delta C)/\pi = 191.91$ in.

Decrease in shaft I.D. $\Delta d = 0.09$ in.

The elastic decrease in shaft lining diameter will decrease the radial stress acting on the supposed rigid lining. This decrease will be in direct relation to the diameter decrease of the elastic deformation of the shaft if unlined, calculated from Obert and Duvall (1967) as

$$U = \frac{4r\,\sigma_H}{E_r} \quad (18)$$

U = elastic decrease in shaft diameter (in.)
r = excavation radius (108-in.)
$E_r$ = elastic rock modulus (600,000 psi)
$\sigma_H$ = horizontal ground stress (2150 psi)

$$U = \frac{4(108)2150}{600{,}000} = 1.55 \text{ in.}$$

The resulting decrease in lining pressure (Pi) from elastic deformation of the shaft lining is:

$\frac{0.09}{1.55}$ (100) = 5.8% increase in lining pressure (Pi) due to elastic lining response.

This may not be a significant decrease, but it is in the right direction, conservative.

Concrete undergoes non-elastic shrinkage in the course of curing. If the moisture content of the concrete is held constant this shrinkage amounts to about 0.07% for a rich 7 sack mix. If the concrete is exposed to air drying, which was not the case for the wet Mt. Taylor shaft, shrinkage is tripled to 0.21% for Type I cement and more than tripled to 0.23% for Type III cement (Troxel, and others, 1968).

Shrinkage will further decrease the diameter of the shaft lining and thereby reduce the predicted lining stress, as follows:

0.07% strain = 0.000700 in./in.
$\Delta C$ = 603(0.000700) = 0.422 in.
$d_{new}$ = 191.87 in.
$\Delta d$ = 0.13 in.
$\frac{0.13}{1.55}$ (100) = 8.4% decrease in lining pressure due to shrinkage alone.

Troxell, et. al. (1968) state, "that the rate of creep is relatively rapid at early ages." "Roughly, about one-fourth of the ultimate creep occurs within the first month and three-fourths within the first year." The rate of shaft sinking will partially determine how soon the concrete lining will be fully loaded: therefore, how much creep will occur. Troxell, et. al. (1968) describe non-elastic creep under sustained stress partly through "viscous flow of the cement/water paste, closure of internal voids, and crystalline flow of aggregates, but it is believed that the major portion is caused by seepage into internal voids of colloidal (absorbed) water from the gel that formed by hydration of the cement."

The magnitude of creep depends on several factors relating to the quality of the concrete, as well as to the stress applied and to how early in the curing process the concrete is loaded. The ultimate magnitude of concrete creep under stress "is usually about 1 millionth per unit of length, per unit stress (psi)" (Troxell, and others, 1968). The non-elastic concrete/rock interaction is complex and difficult to predict. However, if no other factor were to decrease the lining pressure the estimated creep related stress decrease would be approximately:
Circumferential creep strain $\epsilon$ = 0.000001 (1890) = 0.001890 in./in.

$\Delta C$ = 603(0.001890) = 1.14 in.
$d_{new}$ = 191.64 in.
$\Delta d$ = 0.36-in.
$\frac{0.36}{1.55}$ (100) = 23.4% decrease in lining pressure (Pi) due to creep alone.

The composite effect of the non-linear elastic response of the concrete lining, shrinkage of the concrete, and the creep which is governed by the stress and load history appear to prevent a precise assessment of these effects on shaft lining. It is possible to state that each of these factors increase the effectiveness of a concrete shaft lining.

## OVERBREAK

Overbreak is another factor that influences the stability of a concrete shaft lining. Overbreak is rock excavation beyond the pay-line. The concrete placed beyond this design line is considered to be at the contractor's expense. Overbreak is allowed because neither the owner nor the contractor wants to excavate tights before placing the lining. The approximate overbreak, in terms of design concrete yardage, at the three instrumented levels at Mt. Taylor was 16.3% at the 940-ft depth, 8.1% at 2030-ft and 7.5% at 3032-ft. This compares quite favorably with the results of an extensive study of tunnel overbreak which indicated an average of about 12% over several tens of miles of tunneling.

## SUMMARY AND CONCLUSIONS

The prediction of the pressure imposed on a concrete shaft lining is the critical item in designing a concrete shaft. The level of confidence is directly related to the confidence in the rock properties and the in situ stress field used in the prediction.

The Talobre (1957) equation for predicting lining pressure produced values which most closely approximated the measured results at Mt. Taylor. Talobre's [illegible] is for clastic (brittle) rock, whereas Terzaghi's model was for plastic (yielding) rock. The rocks through which the Mt. Taylor shafts were sunk are relatively low-strength shales and sandstones, apparently not subject to significant time dependent plastic deformation. The shale and sandstone have very similar physical properties which made the regression prediction of lining pressure possible at Mt. Taylor. The Mancos shale is actually stronger under unconfined compression than the Upper Westwater sandstone. We initially thought the high montmorillonite content of the Mancos shale might permit it to respond plastically. Shaft sinkers in the Grants area expect and achieve high advance rates in the Mancos. This implies that it is not pliable and viscous but a rock which can be blasted, loaded and supported efficiently, similar to more brittle rock.

ACKNOWLEDGEMENTS

The authors are indebted to Sam Smith, Larry Fischer and Jim Hanley who installed and read the instruments. Without their efforts this paper would be of little value. We also acknowledge the generous permission of Gulf Mineral Resources Company to use the field data.

REFERENCES

Abel, J.F., Jr., 1967, Tunnel mechanics, Quart. CSM, v. 62, n. 2, Colo. School of Mines, Golden, 88 p.

Abel, J.F., Jr., and Lee, F.T., 1973, Stress changes ahead of an advancing tunnel, Intl. Jour. of Rock Mech. and Min. Sciences, v. 10, n. 6, pp 673-697.

American Concrete Institute, 1977, Building code requirements for reinforced concrete, ACI Pub 318-77.

Bieniawski, Z.T., 1968, The effect of specimen size on compressive strength of coal, Intl. Jour. of Rock Mech. and Min. Sciences, v. 5, n. 4, pp 325-326.

Bieniawski, Z.T. and Van Heerden, W.L., 1975, The significance of in situ tests on large rock specimens, Intl. Jour. of Rock Mech. and Min. Sciences and Geomechanics Abstracts, v. 12, n. 4, pp 101-114.

Dowis, J.E., 1971, Shaft sinking cost analysis, unpublished M.S., University of Arizona, Dept. of Min. and Geol. Engrg., 145 p.

Galle, E.M. and Wilhoit, J.C., Jr., 1962, Stresses around a wellbore due to internal pressure and non-symmetrical geostatic stresses, Soc. Petroleum Engineers Jour., v. 2, n. 2, p. 145-155.

Hobbs, D.W., 1970, The behavior of broken rock under triaxial compression, Intl. Jour. of Rock Mech. and Min. Sciences, v. 7, n. 2, pp 125-148.

Lane, K.S., 1957, Effect of lining stiffness on tunnel loading, Proc. 4th Int'l. Conf. on Soil Mech. and Fnd. Eng., v. 2, pp 223-227.

Metcalf, J.R., 1966, Angle of repose and internal friction, Intl. Jour. of Rock Mech. and Min. Sciences, v. 3, n. 2, pp 155-162.

Mogi, K., 1967, Effect of intermediate principal stress on rock failure, Jour. of Geop. Res., v. 72, n. 20, pp 5117-5131.

Obert, L., Duvall, W.I. and Merrill, R.H., 1960, Design of underground openings in competent rock, USBM Bul. 587, 36 p.

Obert, L. and Duvall, W.I., 1967, Rock mechanics and the design of structures in rock, Wiley, New York, 650 p.

Ostrowski, W.J.S., 1972, Design considerations for modern shaft linings, Trans. CIM, v. 75, pp 184-198.

Pratt, H.R. et. al., 1972, The effect of specimen size on the mechanical properties of unjointed diorite, Intl. Jour. of Rock Mech. and Min. Sciences, v. 9, n. 4, pp 513-529.

Rabcewicz, L.V., 1964, The new Austrian tunnelling method, Water Power, v. 16, n. 11, pp 453-458.

Richards, D.P. and Abel, J.F., Jr., 1979, Shaft lining design in rock, AIME Annual Mtg., 7 p.

Seely, F.B. and Smith, J.O., 1952, Advanced mechanics of materials, 2nd Ed., Wiley, New York, 690 p.

Talobre, J., 1957, La mechanique des roches Dunod, Paris, 444 p.

Terzaghi, K., 1943, Theoretical soil mechanics, Wiley, New York.

Troxell, G.E., Davis, H.E. and Kelly, J.W., 1968, Composition and properties of concrete, 2nd Ed. McGraw-Hill, 527 p.

Wilson, A.H., 1972, Research into the determination of pillar size, Part I. An hypothesis concerning pillar stability The Mining Engineer, v. 131, n. 141, pp 409-417.

TABLE II

Shaft lining pressure calculation for 14-ft diameter shaft.

| Depth (ft) H | Excavation Radius (in.) r | Instrument Radius (in.) x | Tangential Stress (psi) $\sigma_{tc}$ | Cell Location | Calculated Lining pressure (psi) Pi |
|---|---|---|---|---|---|
| 0 | -- | -- | 0 | -- | 0 |
| 940 | 114.0 | 99.5 | 400 | NE | 107 |
| | 113.0 | 98.5 | 400 | NW | 104 |
| | 106.5 | 95.0 | 400 | SW | 85 |
| | 106.5 | 95.0 | 370 | SE | 78 |
| 2030 | 105.0 | 94.5 | 350 | NE | 70 |
| | 106.0 | 95.0 | 950 | NW | 198 |
| | 106.0 | 95.0 | 1500 | SW | 313 |
| | 106.0 | 95.0 | 1500 | SE | 313 |
| 3032 | -- | -- | -- | N | No Reading |
| | 110.0 | 97.0 | 2300 | W | 548 |
| | 108.0 | 96.0 | 1360 | S | 304 |
| | 117.0 | 106.0 | 1360 | E | 405 |

TABLE III

In situ stresses and physical properties at shaft instrumentation depths.

| Depth (ft) | Vertical Stress (psi) | Horizontal Stress (psi) | Angle of Internal Friction | Passive Pressure Coefficient | Rock Mass Compression Strength | Bed |
|---|---|---|---|---|---|---|
| H | $\sigma_v$ | $\sigma_H$ | $\phi$ | $\tan^2\beta$ | $\sigma_o$ | |
| 940 | 901 | 667 | 32.1° | 3.27 | 1000 | Mancos Shale |
| 2030 | 1945 | 1440 | 32.1° | 3.27 | 1000 | Mancos Shale |
| 3032 | 2906 | 2150 | 29.2° | 2.90 | 500 | Upper Westwater Sandstone |

TABLE IV

Lining pressure on Mt. Taylor shaft, 14-ft diameter shaft.

| Depth (ft) | Estimated Horizontal Ground Stress (psi) | Mohr-Coulomb Relaxed Zone Thickness (xr) | Lining Pressure (psi) Maximum Measured | Terzaghi Plastic Predicted | Rabcewicz No Cohesion Predicted | Talobre Clastic Predicted |
|---|---|---|---|---|---|---|
| 940 | 667 | 0.0642r | 107 | 10 | 654 | 213 |
| 2030 | 1440 | 0.200r | 313 | 142 | 737 | 297 |
| 3032 | 2150 | 0.353r | 548 | 434 | 769 | 506 |

TABLE V

Lining thicknesses and resulting factors of safety, Mt. Taylor 14-ft shaft.

| Depth (ft) | Lining Thickness | | Factor of Safety for Minimum Measured Lining Thickness | Factors of Safety for Design Lining Thickness | | |
|---|---|---|---|---|---|---|
| | Minimum Measured* (in.) | Design (in.) | | Terzaghi Plastic Predicted | Rabcewicz No Cohesion Predicted | Talobre Clastic Predicted |
| 940 | 22.5 | 18 | 7.52 | >30 | 1.23 | 3.78 |
| 2030 | 21.0 | 18 | 2.57 | 5.67 | 1.09 | 2.71 |
| 3032 | 24.0 | 24 | 2.28 | 2.28 | 1.28 | 1.95 |

*Note: Refer to TABLE II, minimum measured lining thickness is the minimum excavation radius minus the inside radius of the shaft lining (84 in.). TABLE IV presents the measured and predicted lining pressures (Pi). Refer to equation 11 for method of calculating the factor of safety for the minimum measured and design lining thicknesses.

TABLE VI

Distortion energy lining pressure prediction, 3032-ft depth as plotted in Figure 6.

(A) Triaxial test strength line

| Confining Stress ($\sigma_2=\sigma_3$) (psi) | Failure Stress ($\sigma_1$) (psi) | Volumetric Stress Invariant - s (psi) | Shear Stress Invariant - t (psi) |
|---|---|---|---|
| 100* | 790 | 330 | 325 |
| 500 | 1950 | 983 | 684 |
| 1000 | 3400 | 1800 | 1131 |
| 1368.5---cross | 4469 | over---2402---point--- | 1461.5 |
| 1500 | 4850 | 2617 | 1579 |
| 2000 | 6300 | 3433 | 2027 |

(B) Evaluation of polyaxial stresses to find critical shear stress invariant (t) at predicted failure.

| Relaxed Zone Thickness (in terms of r) | Volumetric Stress Invariant - s (psi) | Shear Stress Invariant (psi) |
|---|---|---|
| 0.00r | 2402 | 1791 |
| 0.05r | 2402 | 1632 |
| 0.10r | 2402 | 1494 |
| 0.1129r---cross over----- | 2402 | -----point----- 1461.5 |
| 0.15r | 2402 | 1374 |
| 0.20r | 2402 | 1270 |
| 0.25r | 2402 | 1179 |
| 0.30r | 2402 | 1098 |

Note: Confining stress in triaxial tests is uniform around the test specimen. Therefore, $\sigma_2=\sigma_3$ in the volumetric and shear stress invariant equations.

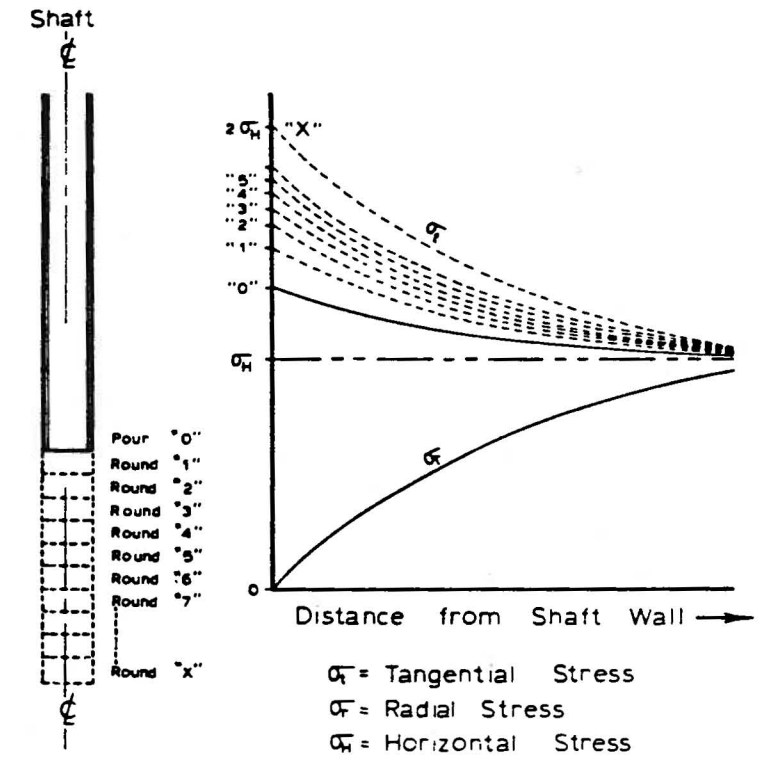


FIG. 1 - PROGRESSIVE INCREASE IN ELASTIC TANGENTIAL STRESS AROUND SHAFT AT POUR "0" AS EACH SHAFT ROUND IS EXCAVATED.

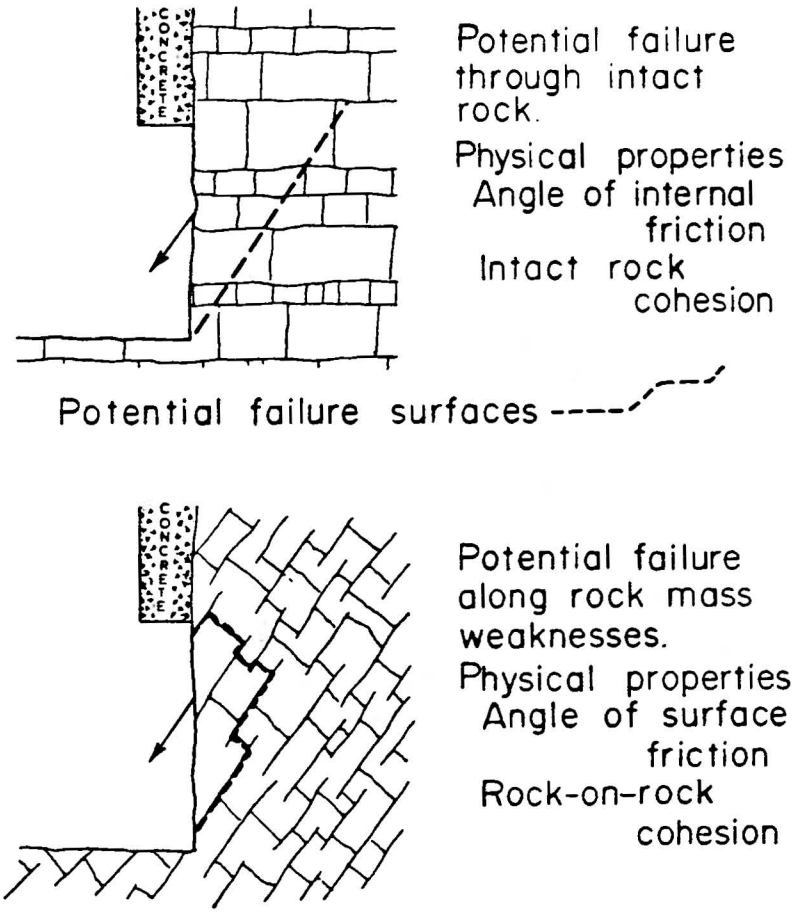


FIG. 2 - POTENTIAL FAILURE OF ROCK.

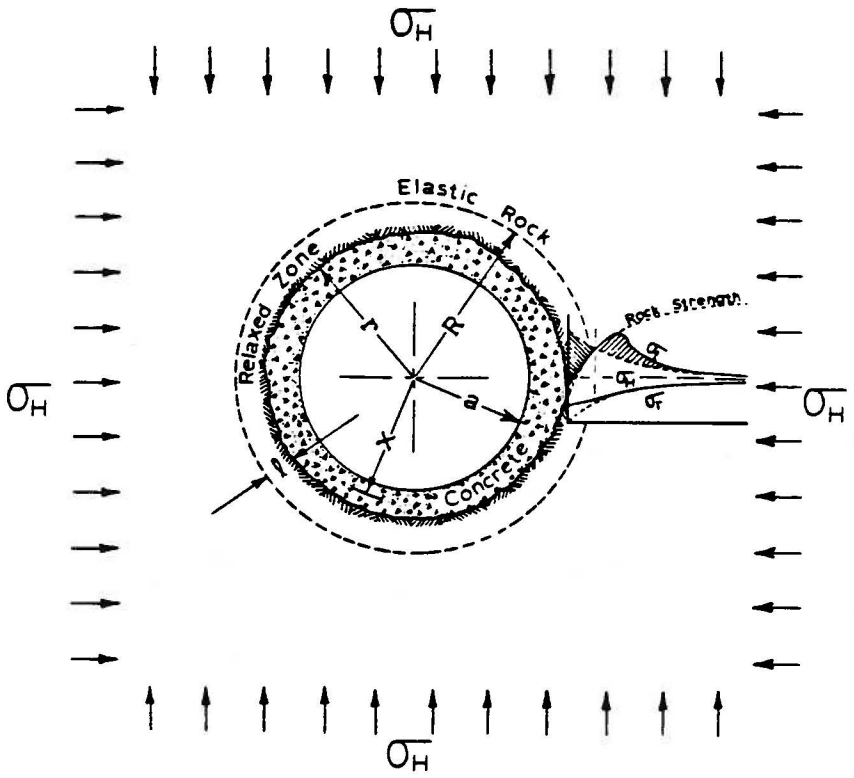


FIG. 3 - SHAFT LAYOUT.

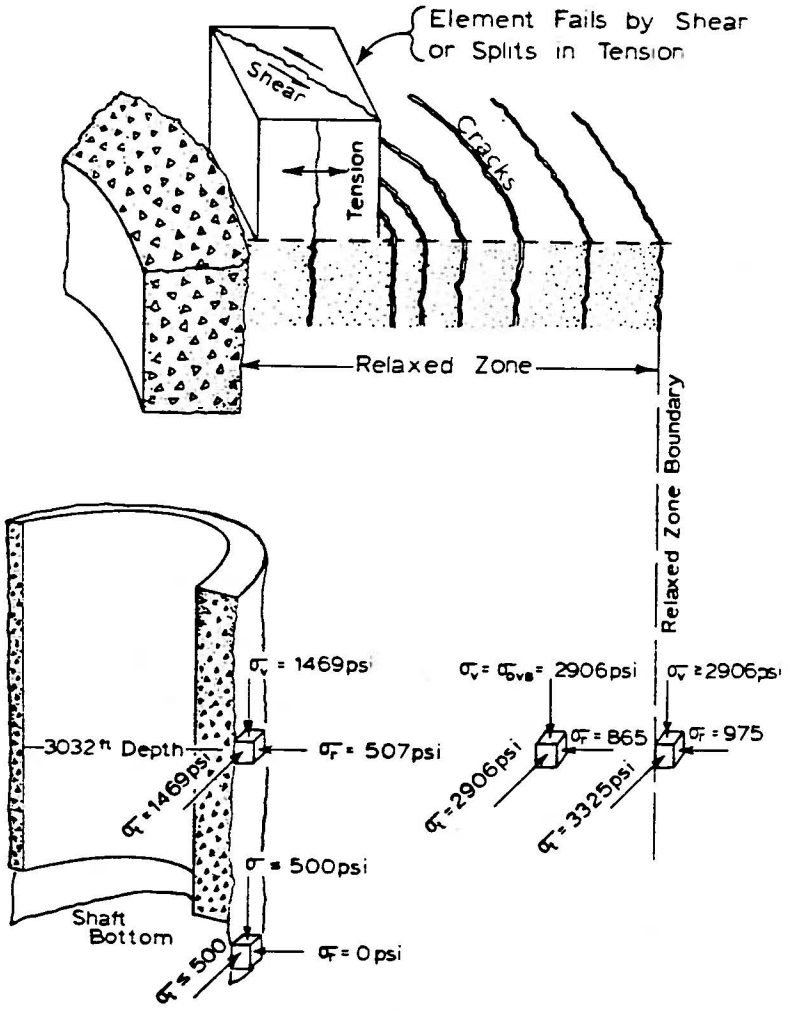


FIG. 4 - CRACKING IN RELAXED ZONE AND MOHR-COULOMB CALCULATED STRESS DISTRIBUTION, 3032-FT DEPTH.

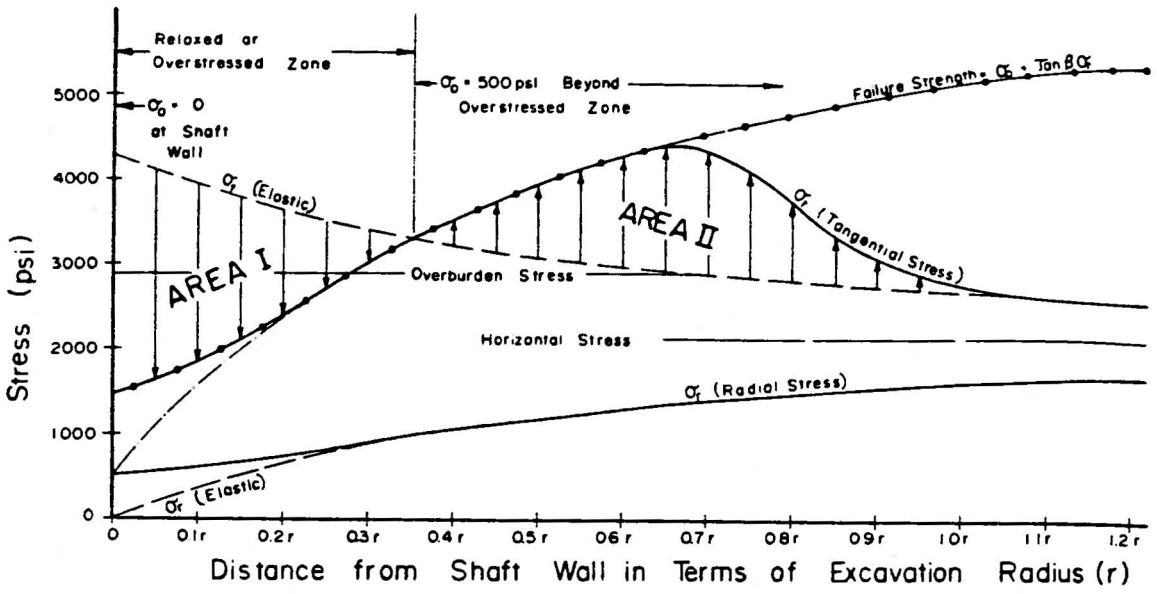


FIG. 5 - TANGENTIAL AND RADIAL STRESS DISTRIBUTION OUTWARD FROM SHAFT WALL, 3032-FT DEPTH, MOHR-COULOMB STRENGTH CRITERIA AND TALOBRE PRESSURE PREDICTION.

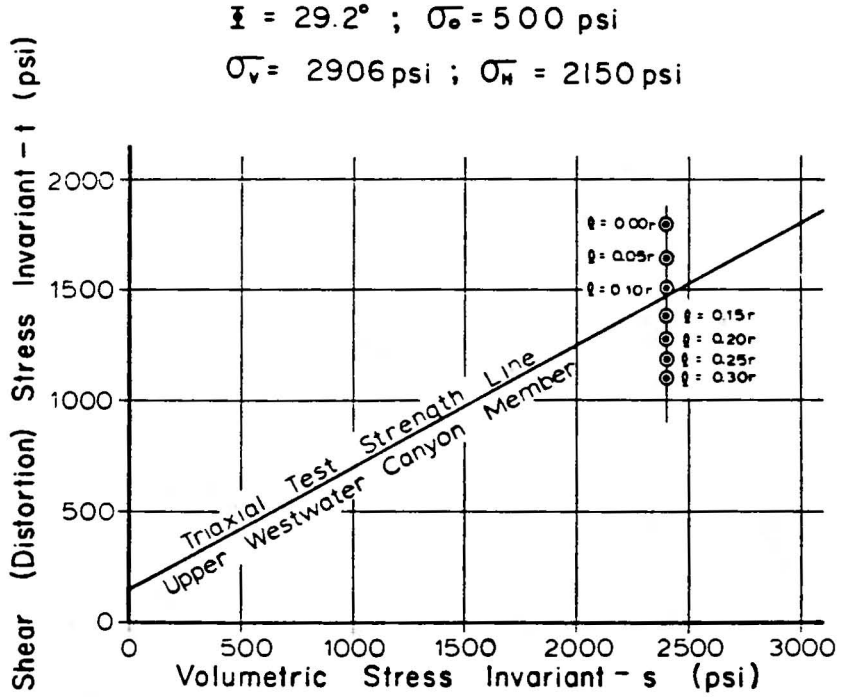


FIG. 6 - DISTORTION ENERGY ESTIMATE OF RELAXED ZONE THICKNESS, 3032-FT DEPTH.

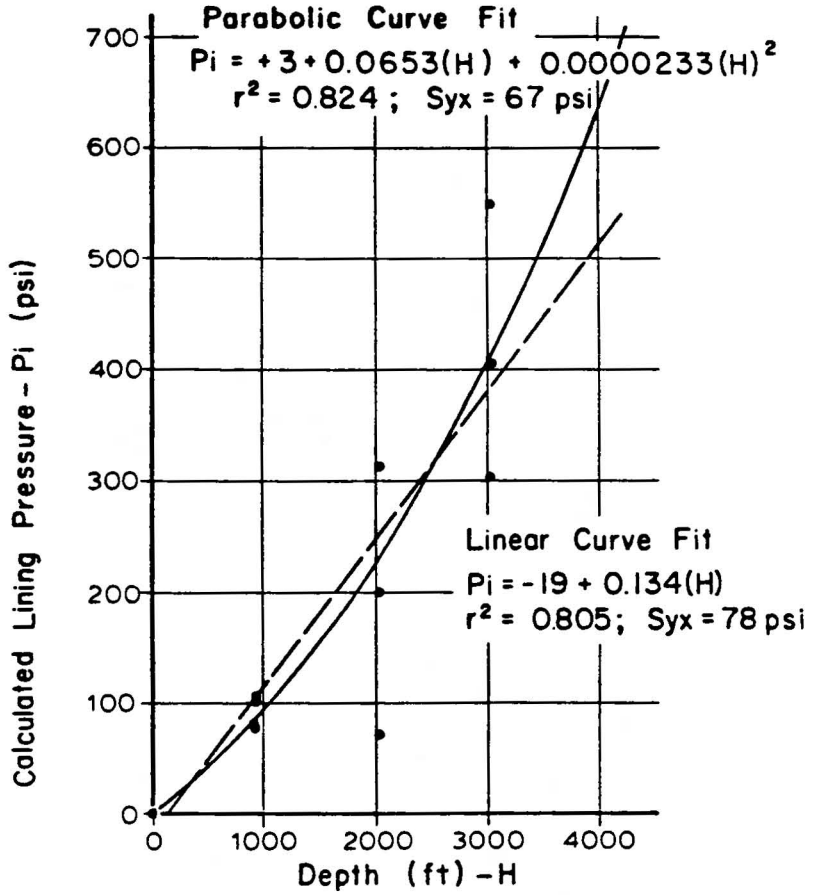


FIG. 7 - SHAFT LINING PRESSURE MEASUREMENTS AND REGRESSION CURVE FITS.

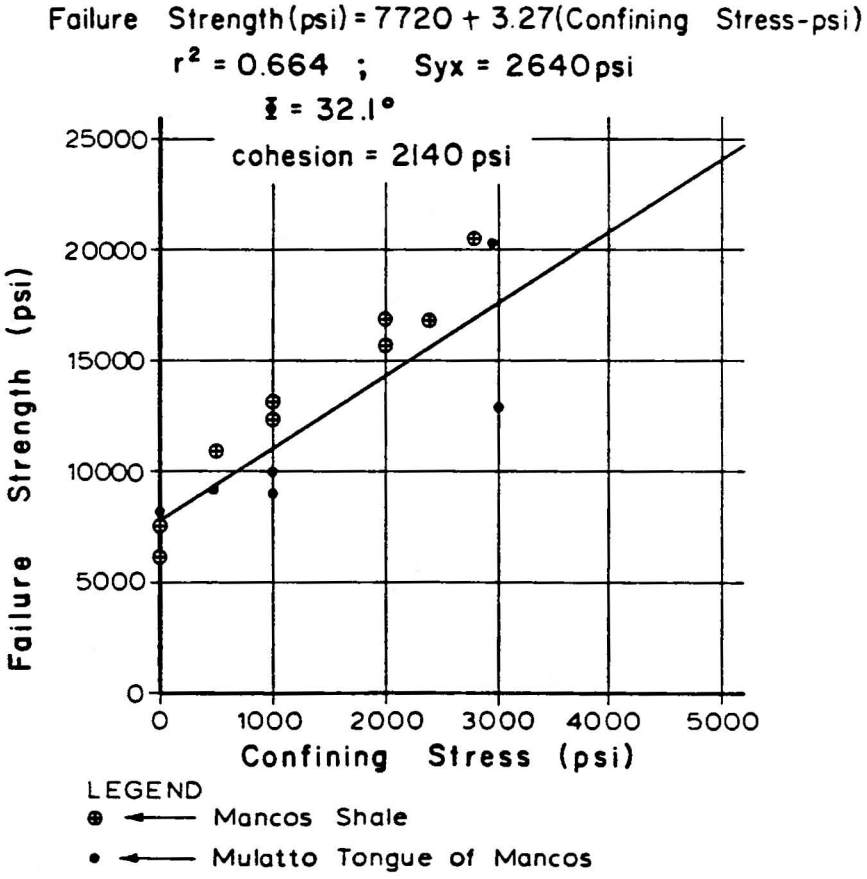


FIG. 8 - TRIAXIAL COMPRESSION TEST RESULTS, MANCOS SHALE FORMATION.

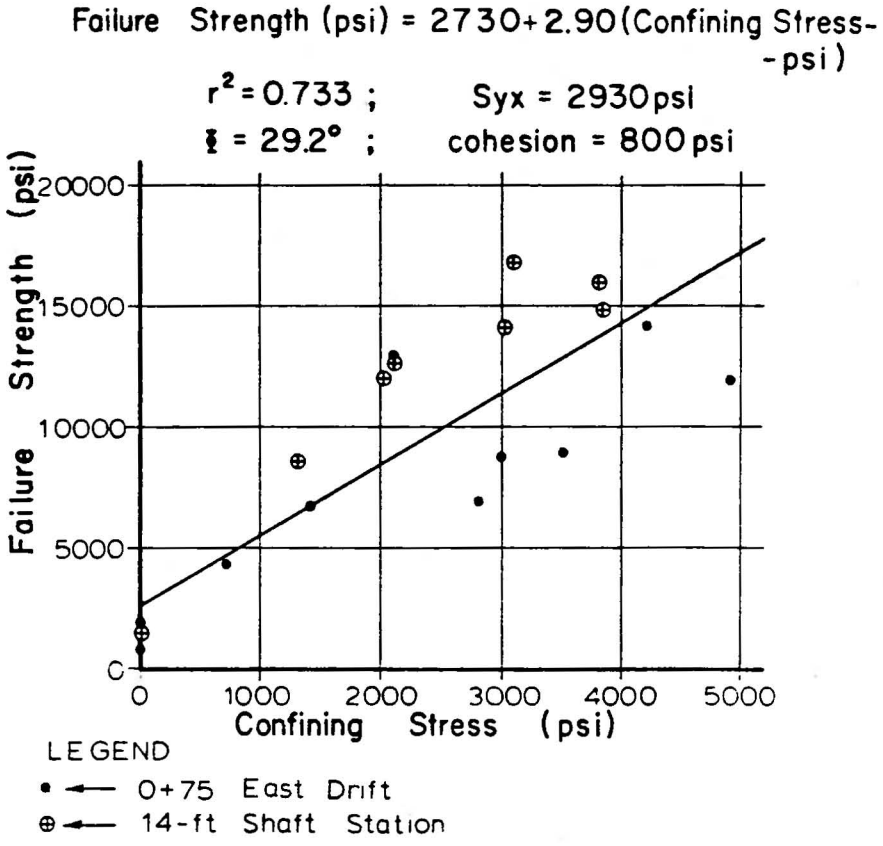


FIG. 9 - TRIAXIAL COMPRESSION TEST RESULTS, UPPER WESTWATER CANYON MEMBER OF THE MORRISON FORMATION.

## CONVERGENCE CONFINEMENT METHOD (after McCreath)

Example from Mc Creath Thesis

| | | | | | |
|---|---|---|---|---|---|
| MASS DENSITY | | (g) | | kN | |
| DEPTH | | (Z) | | m | |
| TUNNEL RADIUS | | (a) | 1 | m | |
| FRICTION ANGLE | | (fi) | 35 | deg | 0.611 rad |
| PLASTIC FRICTION ANGLE | | (fip) | 30 | | 0.524 rad |
| COHESION | | (c) | 0.13 | kPa | |
| PLASTIC COHESION | | (cp) | 0.01 | | |
| COEFF. OF LATERAL STRESS | | (K) | 1 | | K=n/(1-n) |
| ELASTIC MODULI | GROUND | (E) | 100 | kPa | |
| POISON RATIO | GROUND | (n) | 0.3 | | |
| DILATANCY COEFF. | | (AL) | | deg | |
| UNCONFINED STRENGTH | | (Sc) | 0.5 | kPa | Sc=2*c*tan(45*asin(1)/90+fi) |
| RATIO PEAK/RESID STRENGTH | | (s) | | | 1.4745 |
| | | | | | 0.0746 |
| SHEAR MODULUS | | (G) | | kPa | |
| G=E/(2*(n+1)) | | | | | |
| COEFF.OF PASSIVE PRESS. | | (m) | | | |
| m=(1+SIN(fi))/(1-SIN(fi)) | | | | | |
| VERTICAL STRESS | | (Po) | 1 | kPa | |
| Po=Z*g | | | | | |
| LAMBDA e | | (lame) | | | |
| lame=1/(1+m)*(m-1+Sc/Po) | | | | | |

| | | | | |
|---|---|---|---|---|
| Coefficient Mc | | | | |
| Mc=(1+(lam-1)*Po/Sc)/(lam+1) | | (Mc) | 1.3604 | |
| Plastic dilation | | | | |
| ev=(2*(U1/R)*(R/a)^2)/(((R/a)^2-1)*(1+1/rc)) | | (ev) | | |
| Parameter rc | | | | |
| Thin Plastic zone | rc=2*(-sin(fi))*ln(R/a) | (rc) | R/a < (3)^0.5 | |
| Thick Plastic zone | rc=1.1*(-sin(fi)) | (rc) | R/a > (3)^0.5 | |
| Deformat. at the boundary of Plast.zoi | | (U1) | | |
| U1=(1+n)/E*(Mc*Sc)*R | | | | |
| Coeff.of Passive Pressure | | (lam) | 3.6902 | |
| lam=(1+sin(fi))/(1-sin(fi)) | | | | |
| lamp=(1+sin(fip))/(1-sin(fip)) | | (lamp) | 3 | |
| Parameter A | | | | |
| A=(2*U1/R-ev)*(R/a)^2 | | | | |

## ELASTO-PLASTIC DISPL. IN GROUND

| | | | |
|---|---|---|---|
| Press. at the boundary of Plast.zone | (P1) | | kPa |
| P1=Po*(1-sin(fi))-c*cos(fi) | | | |
| RADIUS OF PLASTIC ZONE | (R) | | m |
| R=a*((Po+cp/tan(fi)-Mc*Sc)/(Ps+cp/tan(fi)))^(1/(lam-1)) | | | |
| ELASTIC DISPL | (Ue) | | m |
| Ue=U1*R/a | | | |
| ELASTO-PLASTIC DISPL | (U(e+p)) | | m |
| U(e+p)=a*(1-((1-ev)/(1+A))^0.5) | | | |

(3)^0.5= 1.7321

| Ps kPa | lams =1-Ps/Po | Ps/Po | U1 m | R m | R/a | rc | ev | A | U(e+p) m | U(e+p) mm |
|---|---|---|---|---|---|---|---|---|---|---|
| 1 | 0 | 1 | 0.0050749 | 0.573929 | 0.5739 | 0.637 | -0.0034 | 0.0069 | 0.00177 | 1.7686 |
| 0.9 | 0.1 | 0.9 | 0.0053452 | 0.604502 | 0.6045 | 0.5774 | -0.0037 | 0.0078 | 0.00203 | 2.03458 |
| 0.8 | 0.2 | 0.8 | 0.0056639 | 0.640546 | 0.6405 | 0.511 | -0.0042 | 0.009 | 0.00238 | 2.38261 |
| 0.7 | 0.3 | 0.7 | 0.0060474 | 0.683916 | 0.6839 | 0.4358 | -0.0047 | 0.0105 | 0.00285 | 2.85474 |
| 0.6 | 0.4 | 0.6 | 0.0065211 | 0.737486 | 0.7375 | 0.3493 | -0.0055 | 0.0126 | 0.00353 | 3.52611 |
| 0.5 | 0.5 | 0.5 | 0.007127 | 0.806004 | 0.806 | 0.2474 | -0.0065 | 0.0157 | 0.00454 | 4.54415 |
| 0.4 | 0.6 | 0.4 | 0.0079407 | 0.898028 | 0.898 | 0.1234 | -0.0081 | 0.0208 | 0.00624 | 6.23796 |
| 0.3 | 0.7 | 0.3 | 0.0091169 | 1.031047 | 1.031 | -0.035 | -0.0108 | 0.0303 | 0.0095 | 9.50007 |
| 0.2 | 0.8 | 0.2 | 0.0110411 | 1.248663 | 1.2487 | -0.255 | -0.0169 | 0.0539 | 0.01771 | 17.7109 |
| 0.1 | 0.9 | 0.1 | 0.0151188 | 1.709818 | 1.7098 | -0.615 | -0.043 | 0.1774 | 0.0588 | 58.8037 |
| 0 | 1 | 0 | 0.0427681 | 4.836721 | 4.8367 | -0.631 | -0.0316 | 1.1526 | 0.30773 | 307.732 |

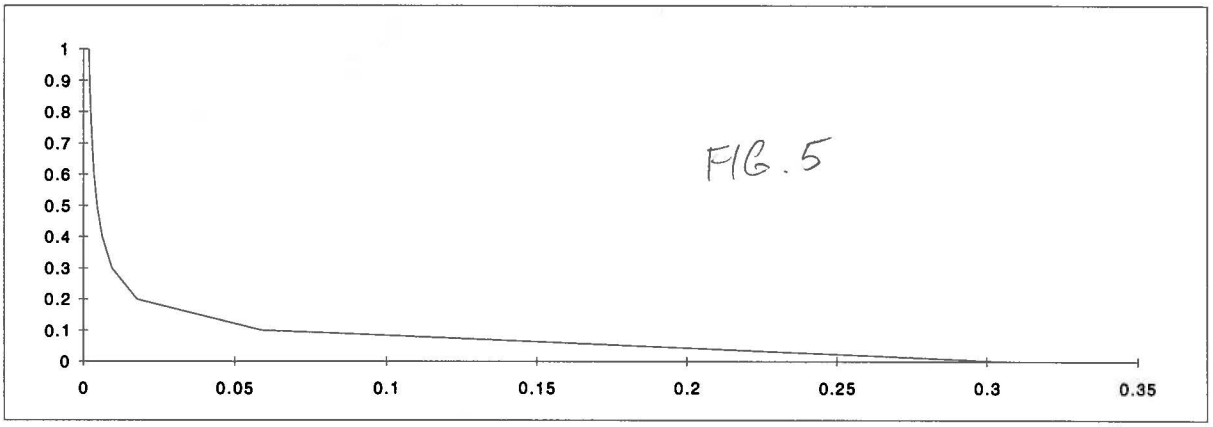


FIG. 5

## CONVERGENCE CONFINEMENT METHOD (after McCreath)

EXAMPLE from McCreath Thesis

| | | | | | |
|---|---|---|---|---|---|
| MASS DENSITY | | (g) | | | |
| DEPTH | | (Z) | | | |
| TUNNEL RADIUS | | (a) | 17.36 | in | 7 |
| FRICTION ANGLE | | (fi) | 29 | deg | 0.506 rad |
| PLASTIC FRICTION ANGLE | | (fip) | 29 | deg | 0.506 rad |
| COHESION | | (c) | | | |
| PLASTIC COHESION | | (cp) | 73.168 | psi | |
| COEFF. OF LATERAL STRESS | | (K) | 1 | | K=n/(1-n) |
| ELASTIC MODULI | GROUND | (E) | 60000 | psi | |
| POISON RATIO | GROUND | (n) | 0.2 | | |
| DILATANCY COEFF. | | (AL) | | | |
| UNCONFINED STRENGTH | | (Sc) | 500 | psi | Sc=2*c*tan(45*asin(1)/90+fi) |
| RATIO PEAK/RESID STRENGTH | | (s) | | | |
| | 73.1687948 | | | | 510.33 |

| | | | |
|---|---|---|---|
| SHEAR MODULUS | (G) | | |
| G=E/(2*(n+1)) | | | |
| COEFF.OF PASSIVE PRESS. | (m) | | |
| m=(1+SIN(fi))/(1-SIN(fi)) | | | |
| VERTICAL STRESS | (Po) | 2150 | psi |
| Po=Z*g | | | |
| LAMBDA e | (lame) | | |
| lame=1/(1+m)*(m-1+Sc/Po) | | | |

| | | | | |
|---|---|---|---|---|
| Coefficient Mc | | | | |
| Mc=(1+(lam-1)*Po/Sc)/(lam+1) | | (Mc) | 2.3423 | |
| Plastic dilation | | | | |
| ev=(2*(U1/R)*(R/a)^2)/(((R/a)^2-1)*(1+1/rc)) | | (ev) | | |
| Parameter rc | | | | |
| Thin Plastic zone | rc=2*(-sin(fi))*ln(R/a) | (rc) | R/a < | (3)^0.5 |
| Thick Plastic zone | rc=1.1*(-sin(fi)) | (rc) | R/a > | (3)^0.5 |
| Deformat. at the boundary of Plast.zoi | | (U1) | | |
| U1=(1+n)/E*(Mc*Sc)*R | | | | |
| Coeff.of Passive Pressure | | (lam) | 2.8821 | |
| lam=(1+sin(fi))/(1-sin(fi)) | | | | |
| lamp=(1+sin(fip))/(1-sin(fip)) | | (lamp) | 2.8821 | |
| Parameter A | | | | |
| A=(2*U1/R-ev)*(R/a)^2 | | | | |

## ELASTO-PLASTIC DISPL. IN GROUND

| | | |
|---|---|---|
| Press. at the boundary of Plast.zone | (P1) | |
| P1=Po*(1-sin(fi))-c*cos(fi) | | |
| RADIUS OF PLASTIC ZONE | (R) | |
| R=a*((Po+cp/tan(fi)-Mc*Sc)/(Ps+cp/tan(fi)))^(1/(lam-1)) | | |
| ELASTIC DISPL | (Ue) | |
| Ue=U1*R/a | | |
| ELASTO-PLASTIC DISPL | (U(e+p)) | |
| U(e+p)=a*(1-((1-ev)/(1+A))^0.5) | | |

(3)^0.5= 1.7321

| Ps psi | lams =1-Ps/Po | Ps/Po | U1 in | R in | R/a | rc | ev | A | U(e+p) in | U(e+p) mm |
|---|---|---|---|---|---|---|---|---|---|---|
| 2150 | 0 | 1 | 0.2773726 | 11.84201 | 0.6821 | 0.3709 | -0.011 | 0.0269 | 0.13492 | 134.923 |
| 1935 | 0.1 | 0.9 | 0.2923464 | 12.48129 | 0.719 | 0.3199 | -0.0121 | 0.0305 | 0.15523 | 155.225 |
| 1720 | 0.2 | 0.8 | 0.3099146 | 13.23134 | 0.7622 | 0.2633 | -0.0135 | 0.0351 | 0.18159 | 181.587 |
| 1505 | 0.3 | 0.7 | 0.3309157 | 14.12795 | 0.8138 | 0.1998 | -0.0153 | 0.0412 | 0.21695 | 216.95 |
| 1290 | 0.4 | 0.6 | 0.3566218 | 15.22544 | 0.877 | 0.1272 | -0.0176 | 0.0496 | 0.26641 | 266.408 |
| 1075 | 0.5 | 0.5 | 0.3890763 | 16.61103 | 0.9569 | 0.0428 | -0.0208 | 0.062 | 0.33951 | 339.511 |
| 860 | 0.6 | 0.4 | 0.4318193 | 18.43588 | 1.062 | -0.058 | -0.0256 | 0.0817 | 0.45619 | 456.187 |
| 645 | 0.7 | 0.3 | 0.4916676 | 20.99101 | 1.2092 | -0.184 | -0.0335 | 0.1174 | 0.66486 | 664.863 |
| 430 | 0.8 | 0.2 | 0.5840125 | 24.93354 | 1.4363 | -0.351 | -0.0492 | 0.1981 | 1.11461 | 1114.61 |
| 215 | 0.9 | 0.1 | 0.7545485 | 32.21432 | 1.8557 | -0.533 | -0.0754 | 0.4211 | 2.25802 | 2258.02 |
| 0 | 1 | 0 | 1.2610101 | 53.83694 | 3.1012 | -0.533 | -0.0597 | 1.0251 | 4.80179 | 4801.79 |

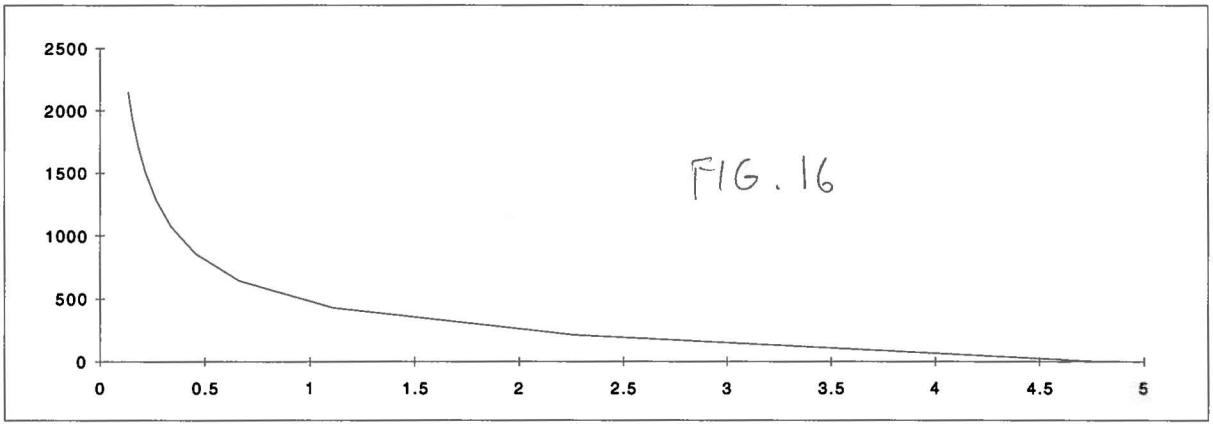


FIG. 16